CHARACTERIZATION OF RESIDUE FROM DIRECT COAL LIQUEFACTION AND DETERMINATION OF ITS POTENTIAL APPLICABILITY AS A SOURCE OF FUEL

by

Nitya Arunachalam Iyer

A thesis submitted in partial fulfillment of the requirements for the degree of

Master of Science

in

Chemical Engineering

Department of Chemical and Materials Engineering
University of Alberta

Abstract

Direct coal liquefaction is a technology for producing liquid products from coal. One of the by-products from this process is coal liquefaction residue, which is remaining coal that was not converted to liquid products during the liquefaction process. The residue is enriched in mineral matter and the organic content is more refractory. The objective of our work was to characterize the residue produced under different DCL operating conditions and to evaluate the performance of the residue as a feed for gasification and combustion.

The feed to the direct coal liquefaction process was Canadian sub-bituminous Coal Valley (CV) coal. The industrial solvents employed were hydrotreated (under N_2 and H_2) and non-hydrotreated poly-aromatic hydrocarbons (under N_2). Different residues were obtained from the process, conducted at four different temperatures ranging from 300-450 °C in an autoclave reactor (0.25 L) at an initial pressure of 20 bar. Coal liquid yields obtained for liquefaction using hydrotreated solvent were found to be much better, under the same operating conditions. Thus, effect of solvent and temperature in coal liquefaction is discussed briefly. The residues were further characterized for their mineral composition, organic content and particle sizes using various standard techniques: Thermogravimetic analyser (TGA), elemental analyser, mastersizer, FTIR spectrometer, X-ray fluorescence, surface area analyser. A great deal of variation in the chemical and physical composition of the residues were observed and found to be closely related to the efficiency of the process.

In order to further investigate the potential applicability of liquefaction residues as a feedstock for boilers and gasifiers, the residues from the Coal Valley sub-bituminous coal liquefaction in hydrotreated solvent (N_2) were gasified in a TGA. This proved to be a useful platform for comparison of the reactivity of the residues with that of raw coal. The kinetic parameters for the process were also determined under isothermal gasification conditions at temperatures 800 °C, 950 °C and 1000 °C under O_2 and at 950 °C, 1000 °C and 1100 °C under CO_2. Further, in order to determine the practical applicability of the coal residues as boiler feed, an entrained flow reactor (drop tube furnace) was employed to test the conversion efficiency of the residues. Though higher carbon conversion were found for residues, compared to raw coal, similar concerns due to ash-slagging would be prevalent for both cases.

Dedicated to
Amma, Appa and Rammu

Appa, you will always be my role model. This could not have been possible without your love, support and faith in me. We've made it!
Love you all

"Believe in yourself and follow your heart, it would eventually lead you where you wish to belong"

Acknowledgements

This thesis embodies the work I conducted during the two beautiful and enriching years of my life in University of Alberta. This little piece of contribution in the branch of the coal liquefaction science, would not have been possible without the support and encouragement of my supervisors, Dr. Rajender Gupta and Dr. Arno de Klerk, research mentors, friends and family.

I would like to extend my profound gratitude to Dr. Rajender Gupta for his constant guidance and continued motivation. His mentorship has been extremely helpful in shaping my capabilities towards being an independent researcher. The liberty to work in the direction that interested me the most was a great advantage under his supervision, which helped me learn and explore different dimensions of approach to a problem. I am highly indebted to him for providing me the opportunity to be a part of his research team.

Well, I vividly remember the first day when I met Dr. Arno de Klerk, a very warm, modest individual with a remarkable personality. He has always been a source of inspiration and encouragement. His innovative approach towards problem-solving has been highly motivating. His valuable comments and suggestions during the course of my project are gratefully acknowledged.

I highly appreciate the help and assistance of Dr. Moshfiqur Rahman during all the experiments undertaken in the laboratory. I would like to thank him for all the support and guidance he provided during my hard times, particularly after the unpleasant incident in the lab during one of the experiments. I would like to express my appreciation towards the entire safety team, especially Dr. Gord Winkel for extending his valuable time to help and support us as a team in approaching the post-incident HAZOP study and communicating with the EHS and the necessary departments. I am also thankful to Andrew Worthington and James Dickie from Swagelok for their assistance. Many thanks to Dr. Deepak for his co-operation during equipment allotments. I am grateful to Vinoj for assisting me in the Entrained flow reactor experiments, Pramod for taking time out to help me during the BET tests and Mehdi for his pre-assistance during particle size analyses. I have been blessed to have a wonderful research team. Many thanks to Shiraz Merali for conducting XRD and XRF analysis of the samples; Jeremiah Bryska (from the IOSI team), Jim Skwarok (Oilsands group), Shihong and Dimitre (ACSES) to have trained me to use their facility to carry out various analysis of my samples.

I have also had the opportunity to make great friends who helped me build

beautiful memories, that I would cherish throughout my life. Pankhu, I could not have imagined these two years without you! Thank you for staying up all during those late night work days. You have been a great moral support. Rohan and roomies, Raghu, Pops, Shivam, Deepesh, Pripads, your place has been like my second home. You guys rock! Thank you for all those yummy late night paranthas Anu di. Well, my stay in Edmonton has definitely been enriched by Guru Ashwin Iyer's carnatic lessons, Kala aunty and Iyer uncle's warmth, Edmonton Taata-Paati's blessings and all the lovely people I got acquainted to, through them. I am also thankful towards the team CMEGSA, Energy club and AWA. You have helped me learn the importance of team work and been of great value towards nurturing my leadership skills. My entire gang of friends at the university - Loki Anna, Prateek Anna, Yathi, Rosi, Navjot, Prakash, Siri, Talat, Abdul, Bhainaa, Hirak, Tolu, Kody, Obinna, Madhu di, Tinu (well, the list is endless. Sorry if I missed anyone) and also everyone back home. Thank you for all your support and love.

Finally, I would like to thank the most important people in my life, my entire family, especially Rajesh maama, Mammama, Moonamai for their blessings. Paati, words are no match to say how thankful I am towards all that you have done for me. The values you have ingrained in me are priceless and have given me the strength and courage to walk through each milestone in life. Taatha, I have been very lucky to have your aashirvadam. Amma, Appa and Rammu, this could not have been possible without your constant support, encouragement, belief in me and the sacrifices made towards this success. Late Mammama Taatha and Late Balu Periappa, I am sure you would have been proud of me!

Table of Contents

List of Tables

List of Figures

Chapter 1

INTRODUCTION

As the nations all over the globe grow towards being developed countries, it is expected that there would be a rise in the energy demand of around 33% beyond current demand by 2035 on a global scale [1]. This necessitates the advancement of a highly diverse energy supply base ranging from petroleum resources and unconventional hydrocarbons (oil sands, shale gas, natural gas from coal) to alternatives (solar, wind, nuclear, hydro) [2], [3]. Increasing energy demand combined with the supply limitations and ongoing political as well as environmental issues, make it imperative to develop economical, efficient and sustainable alternatives for producing clean liquid transportation fuels and chemicals [1]. It would thus be of benefit to supplement petroleum-based liquid fuels with those from alternative sources, such as coal, natural gas, oil shale and biomass [4], [5].

Coal is one of most abundant and plentiful fuels in the family of fossil fuels, with hydrogen to carbon (H/C) atomic ratio of about 0.8 as compared to 1.5 for petroleum (crude) and 4 for natural gas [6]. Surge in oil prices in 1973 and 1978 led to the rise of commercial development of coal liquefaction technology [1]. And from then on, there has been a huge expansion of coal liquefaction projects and plants all over the world [7], [8], [9]. This trend abruptly ended in 1986 with the collapse of the crude oil price.

Each run of liquefaction process generates around 25-30 wt.% of residual waste constituting unreacted coal, mineral matter and valuable industrial liquefaction catalyst, as depicted in Fig. 1.1. There is a general consensus in the literature that one of the most important problems to be resolved in the commercial development of direct coal liquefaction processes is the separation of solids from valuable coal liquids and utilization of the residue stream. The effective use of the residue is directly linked to the economy of the entire liquefaction process [10]. It is thus im-

perative to consider the environmental implications and management of these highly carbonaceous residual wastes.

Thus, the main objective of this research project deals with resolving the issues associated with the big picture concerning coal liquefaction waste management as listed below:

1. Characterization of the residual wastes
2. Investigate a robust pathway of upgrading of the residues.

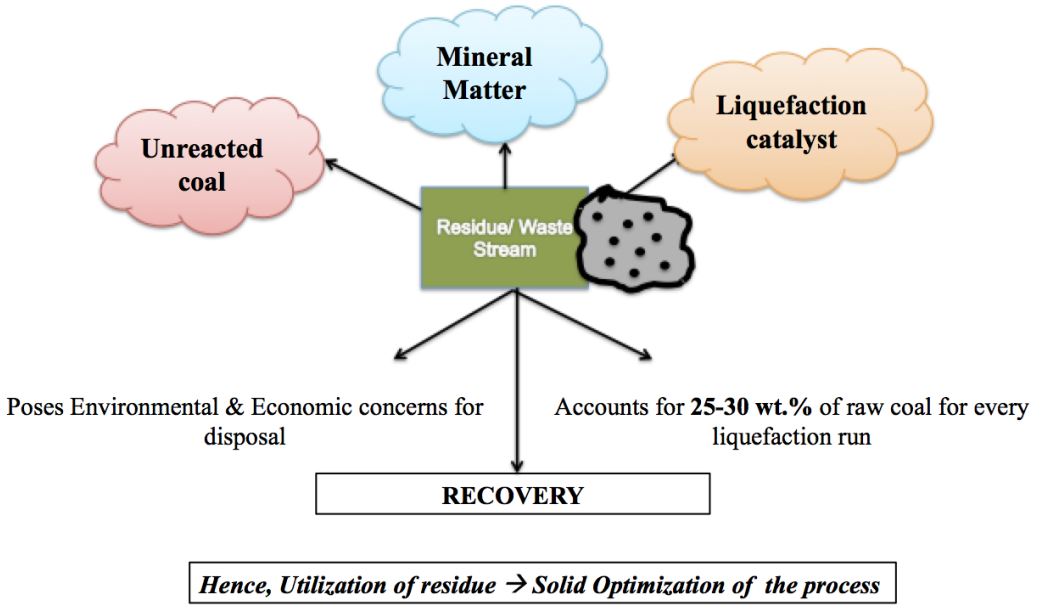

Figure 1.1: Concerns towards residue utilization

For the upgrading of the residue or its utilization as raw material for an industrial process, a thorough understanding of it's chemical and physical properties is highly essential. Hence, characterization studies formed a major part of this project. Further, a very brief kinetic study was undertaken for residue gasification using CO_2 and air as the gasifying agents. Thus, the scope of the project is as outlined below:

1. Study of the effect of temperature and solvent properties on coal residue properties.
2. Characterization of residues obtained from the various liquefaction processes.
3. Conducting a brief kinetic study of residue in presence of CO_2 and air.
4. Determination of the efficiency of the residue as a boiler fuel.

Chapter 2

LITERATURE REVIEW

2.1 OVERVIEW OF COAL LIQUEFACTION PROCESS

A prolonged investigation on conversion of coal to synthetic fuels by Friedrich Bergius [11], which was later patented as the Bergius process in 1913, formed the foundation of catalytic direct coal liquefaction. A schematic representation of a typical coal liquefaction process is depicted in Fig. 2.1. To get a clear understanding of the mechanism of the process, it was found important to have specific knowledge about the structure of coal. Various theories on coal structure have been stated in literature [12], [13], [14]. Simply put, coal could be thought of a combination of dense network of organic species, linked with heteroatoms and mineral matter. Depending upon the grade the composition of these species might vary. A coal liquefaction process involves the process of conversion of coal to liquid fuels [10] under reductive pyrolysis conditions [1]. "Coal liquids" could be thought to represent the soluble portion of the products derived from the complex organic matrix of coal by employing suitable solvents. From an economic viewpoint, the coal liquefaction process aims towards production of petroleum substitutes with a composition that would require the least of further processing including removal of heteroatoms, addition of H_2 and more [15].

Whitehurst et al. [15] suggest a simple three-step process for coal liquefaction to occur consisting solubilization, defunctionalization of coal and lastly hydrogen transfer and rehydrogenation of the solvent. Thus, the effect of solvent during the liquefaction process can be highly influential towards the product distribution. A solvent has a physical as well as chemical role to play during liquefaction [1]. Physically, it acts as a medium for transport of coal. Chemically, the solvent depending upon the path taken towards product formation could be defined as, H-donor sol-

vent, Solubilizing solvent and H-shuttling solvent [15], [16]. When the bond is cleaved, three different pathways are available for the generation of products, which could undergo H-abstraction, H-addition or rearrangement and elimination, addition reaction to form aromatics. It was found that recycle solvents generally initiate char formation by promoting heavy aromatic compound generation [15]. This is also closely associated with the solubility parameter of the resins suggested by Teas [17], which is applicable to the solvents-in-use based on the total cohesive energy (hydrogen bonding, dipole and dispersion) [15]. Based on these, various expressions for solvent swelling and solvent interaction have been suggested in literature [18].

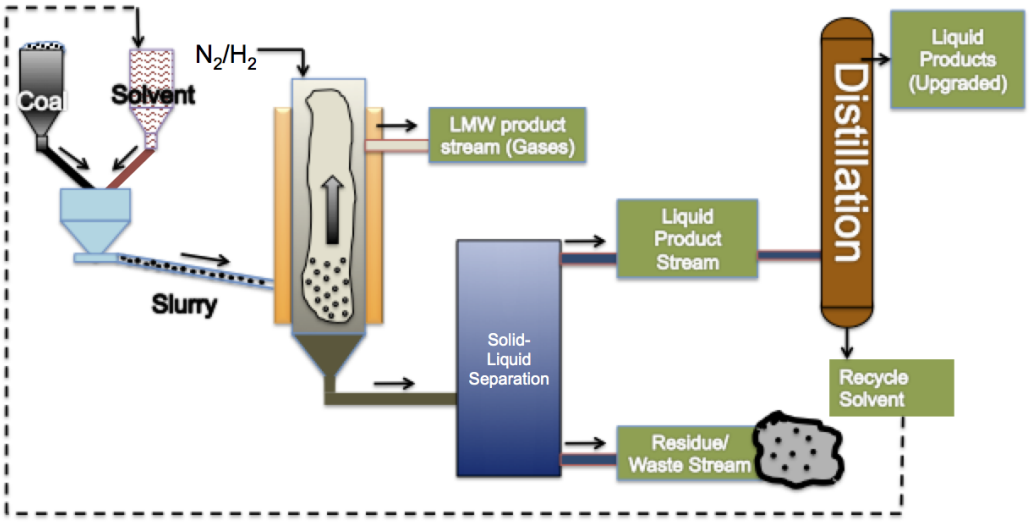

Figure 2.1: Direct Coal Liquefaction Process

The residence time and temperature are also two other major influential factors as they dictates the conversion rates to a large extent. High temperatures and pressure conditions favour the liquefaction process [11]. At temperatures above 400 °C-450 °C and pressures close to 15-20 bar, the feed coals are considered to be substantially dissolved [1]. Also, increasing the temperature tends to accelerate the reaction thus consuming H_2, causing a shift in the equilibrium towards aromatics. Temperature-programmed studies have also proven the retrogressive reactions at high temperatures [19]. However, the aromatics at temperatures above 400 °C have been found to be lower and almost consistent after 425 °C due to the supply of sufficient thermal energy for the rupture of bonds [20]. Thus, gaseous products are favoured at high temperatures. Short residence time can lead to incomplete conversion and promotes products aromatic in nature with large heteroatomic groups

attached to it. They favour breakage of weaker bonds leaving behind a large chunk of fused aromatic compounds [13]. Thus, longer residence time favours better conversion rates [6]. It also aids in the reduction of the viscosity of the generated solid wastes from low rank coal liquefaction. Further, long contact times and sever liquefaction conditions would increase the char formation [15].

2.2 COAL RESIDUE CHARACTERISATION

Before discussing about the competent progresses made in the field of characterization of residues, it is very important to realize that different coal ranks produce coal residues depending on the pathway employed for coal liquefaction. Also, the definition of a direct coal liquefaction residue varies broadly in literature. Hence, the material relevant to our study on THFIS (tetrahydrofuran insolubles) is largely discussed here.

Determination of the volatile, ash content and H/C ratio through proximate and ultimate analysis respectively have been the largely used methods for characterization of the residues. Table 2.1 lists few of the characterization results reported in literature.

The information on liquefaction chemistry was largely obtained from the studies of model compounds and product analysis, until 1970s. Very little attention had been given to the characterization studies of liquefaction residues or derive conclusive results about the mechanistic pathways of coal liquefaction studies. This has been largely associated with the lack of suitable analytical techniques for structural characterization of carbonaceous solids [21]. However, with the growth and advancement of techniques such as solid state ^{13}C NMR in the late 1970s, it became possible to define the organic framework in the coal liquefaction residues in an improved way.

Barron et al. [22] carried out the first ^{13}C-NMR of the liquefaction residue obtained from Lindell bituminous coal liquefaction at 360 °C-400 °C. It was found that increase in the hydrogenation time yields more aromatic products and decreased aliphatic components in the residual mixture. By this, it was concluded that the aliphatic material in the liquid or in the gaseous product stream at one time during conversion represents the fraction of that of the organic material in the residue. Also, a model structure of the residue was predicted from the NMR studies, of a core made of highly aromatic content resistant to hydrogenation surrounded by aliphatic material which could be available for further conversion. At the petrographic level, the core could be thought to be made of inertinite surrounded by vitrinite and exitinite, susceptible to hydrogenation [22]. This work was further developed by

Wilson et al. [20] by incorporating CP-MASS with NMR techniques to report more accurate results by overcoming the discrepancies that might have resulted due to the overlap of signals due to chemical anisotropy. Also, the residues obtained at higher liquefaction temperatures above 400 °C upto 650 °C were investigated using this technique. The aromaticity of the residues was always found to be higher at 400 °C than that of residues obtained from 425 °C liquefaction temperature. This proved that the increased thermal energy had been supportive towards the rupture of aromatic bonds. Also, slight decrease in the aliphatic content was also concluded on the same grounds [20].

Many researchers have worked on, to understand the effect of mineral matter during coal liquefaction [23], [24], [25]. In order to comment upon the effects of mineral matter during coal liquefaction, they realized the need to analyse the minerals in the wastes generated during a liquefaction process. Through application of scanning electron microscopy and X-ray diffraction techniques, Russel [26] reported the presence of wollastonite, calcium silicate form ($CaSiO_3$) in small quantities in the residue. Also, presence was pyrrhotite was evident as they occurred typically in the form of aggregates in the residues [26], [27]. Calcite and quartz, originally present in the coal were found to remain unaltered during the process. Dehydration of mineral matter during liquefaction was also reported by Jenkins and Walker Jr [27]. A microscopic analysis of the coal liquefaction residue was carried out by Derbyshire et al. [28]. The residues derived from the sub-bituminous coal liquefaction showed no traces of plastic behaviour of the parent coal and had tattered skeletons of the structure as those in the parent coal it was derived from. Also, higher vitrinte content was reported, on the basis of reflectance, in the residues compared to the parent coal. Also, particle disintegration was predominant in the sub-bituminous residues proving the absence of plastic behaviour of that coal.

Hower et al. [39] carried out studies to investigate the effect of residence time and temperatures on the coal macerals during liquefaction based on petrographic results of the residual material. With increasing severity of the liquefaction conditions and at high residence time, the semifusinite material all got transformed into vitroplast and further into anisotropic semicoke in the residues. The liptinite was found in the form of alginite in the residues with increase in the concentration of granular residue. Further, Hower et al. [40] carried out petrographic studies of the liquefaction residues obtained from Beulah-Zap lignite, Stockton bituminous coal and low volatile Pocahontas coals. The material recognition of the residues were influenced by the initial feed size of the parent coal. More vitroplast containing unreacted mineral material was observed in the residues obtained from the bituminous coal types, while

Table 2.1: Proximate and Ultimate Analysis during residue studies[a]

Residue Samples	Proximate Analysis		Ultimate Analysis					Refs.
	Volatile	Ash	C	H	N	S	O	
Texaco gasifier residue	32-46	17-33	3.5-5.4	1.1-1.5	1.0-2.6			[29]
Shenhua residue	40.80	16.37	82.24	4.62	9.46	1.24	2.44	[30]
Hydro-treatment residue	19.37	29.78	84.70	4.64	4.45	1.25	4.96	[31]
ShenmuFugu residue	37.71	14.12	85.86	4.61	1.01	1.64		[32]
IEP extract	27.82	27.64	81.91	3.57	0.58	2.66		[32]
Viscosity studies								[33]
Sample 1	41.65	16.80	90.37	5.47	1.91 (N+O)	2.25		
Sample 2	48.79	13.31	89.78	5.79	2.68 (N+O)	1.75		
Sample 3	40.42	16.70	90.64	5.52	1.49 (N+O)	2.35		
Shenfu residue	38.93	22.86	85.86	4.61	1.01	3.39	4.55	[34]
Shengli residue	71.07	46.35	78.97	6.85	1.71	3.17	6.57	[34]
Demineralized residue								[34]
Shenfu residue	32.77	4.81	86.24	5.27	0.97	3.27	4.07	
Shengli residue	39.84	4.02	80.76	5.68	1.45	2.14	9.87	
Residue(steam gasification)	47.69	11.59	84.42	6.40	1.46	0.20	7.52	[35]
Kashima pilot plant residue		24.1	85.0	6.2	1.2		7.6	[36]
Material for CMF	31.37	21.17	84.08	6.40	1.46	3.07	4.99	[37]
Material with ionic liquids	24.0	33.9	84.1	6.40	0.91	3.07	4.97	[38]

[a] All values are expressed as wt.%

Table 2.2: Ash analysis of residues

Sample	SiO_2	Al_2O_3	Fe_2O_3	CaO	MgO	SO_3	K_2O	Na_2O
Shenhua residue	16.76	6.62	31.40	22.07	2.61	15.10	0.18	2.07
Residue for CMF	11.1	6.66	32.18	20.94	1.76	17.84	0.28	2.75

partially reacted macerals and slightly vitroplast materials were obtained from those of lignite and Pocahontas coals. Due to the highly plastic behaviour of the residues, it was difficult to differentiate between the granular residue and vitroplast material. Also the granular residue had a higher particle size compared to the parent coal.

FTIR, NMR and pyrolysis-GC-MS analysis of the residue samples were also reported by Song et al. [19] and exhibited a good platform for comparison of the coal and residue's structural morphological during their studies on the effect of drying and oxidative pre-treatment on coal liquefaction. The THF-insolubles of the residue were the subjects of characterization studies. They were washed with acetone and then with pentane to ensure complete removal of all THF prior to vacuum drying under 110 °C for 6 hours. The NMR spectra revealed the increase in the aromatization of residues with increasing liquefaction temperatures above 300 °C for Wyodak sub-bituminous coal liquefaction. Phenolic, carboxyl and carbonyl structures are absent in the residue with the severity of the liquefaction process. The degree of protonation of aromatic carbons was found to be related with the conversion of the coal liquefaction process. This revealed that more bridgehead aromatic carbons were present in the residues derived at high temperatures. A general expression co-relating the NMR data of the residue with the reaction temeprature has also been given by Song et al. [19] by equation 2.1. Here, T is the temperature of liquefaction, α and β are the constants with no physical meaning, C_i and f_i stand for the specific carbon content in the residue and parent coal respectively, while 'i' stands for specific carbon type.

$$\mathrm{C_i} = \alpha \mathrm{f_i} + \beta \mathrm{T} \tag{2.1}$$

With increasing efforts to obtain higher oil yield, a stable discharge of the residual material was found to be necessary. Thus, fluidity characteristics of the coal liquefaction residue was studied by Tomoyuki et al. [41]. The viscosity of the organic entity of the residue was calculated by the Mori-Ototake's equation. The increase in the viscosity of the organic species had a direct co-relation with the carbon content of the sample. Also, the ash content in the material dramatically increased the viscosity of the material. Similar investigative studies was undertaken by Masumi et al. [42] and Ying-jie et al. [33]. It was found that the apparent viscosity of the residue being highly dependant on temperature, did not exhibit any peak and decreased rapidly with increase in temperature [33]. Ying-jie et al. [33] proposed an expression to strike a relationship between apparent viscosity and temperature given by Arrhenius equation 2.2. Three different residues in this study

were obtained from Shenhua direct coal liquefaction plants.

$$\nu = \mathrm{Ae}^{\frac{\mathrm{E}_\nu}{\mathrm{RT}}} \tag{2.2}$$

The gasification studies of residue in steam involved characterization of residue using proximate and ultimate analysis followed by BET characterization under N_2. The residues exhibited lower surface areas and micro-pore areas almost half of that of raw coal [35]. On the same lines, characterization of residue was also under taken by Xu et al. [30] using the Shenhua direact coal liquefaction residues. It is defined as the heavy fraction of the coal liquid consisting heavy oils, preashphaltene, asphaltene and tetrahydrofuran insolubles(THFIS). The THFIS makes up almost 38.9 ± 3.68 wt.% of the residue. The variation in the fractions is due to the difference in the solid-liquid separation methods and source of the parent coal. The FTIR of the residues had five characteristic peaks. The stretching of -OH functional groups was evident at 3400 cm^{-1}, followed by aromatic $C-H$ stretching at 3000-3100 cm^{-1}. The symmetric and asymmetric stretching vibrations of aliphatic $C-H$ bond was prominent in the 2800-3000 cm^{-1}. Similar results were obtained for the THFIS peaks for the FTIR studies carried out by Li et al. [31], indicating high aromatic content.

Li et al. [32] carried out sequential extraction of the residue obtained from the liquefaction of sub-bituminous coal at 19MPa of H_2 at 455 °C. the sequential extraction was carried out at reflux temperatures ranging from 37 °C - 68 °C, with petroleum ether, cyclohexane, methanol, acetone, carbon disulfide and isometric CDS/acetone mixture (ICDSAM). The residual material insoluble in ICDSAM was termed as inextractable portion(IEP). The IEP is rich in mineral matter and has lower H/C ratios compared to other extracts. Almost complete extraction of the residual material was confirmed from the comparative studies of the H/C ratios of the extracts and the residue material. The FTIR studies reveal higher aromatic condensates, mineral matter and catalyst presence in the IEP.

Not much work has been reported on particle size distribution of the residues, though few conclusive reports from the scanning electron microscope analysis of liquefaction residues analysed for change in particle size by Whitehurst et al. [15] have been referred to during our analyses (Section 4.5.6).

2.3 COAL LIQUEFACTION RESIDUE CONVERSION

With the growth and expansion of coal liquefaction projects globally, upgrading of coal liquefaction residue became more crucial.

The concept of partial liquefaction of coal proposed by Liu and Yang [43] presented a novel idea which insists on reduction of hydrogen consumption by reduction in the severity of the liquefaction conditions. The carbon reject thus generated from the process was further utilized for production of O_2.

The expansion of a continuous coal liquefaction plant in Kashima, Japan (1996) incorporating NEDOL process, saw the need to upgrade the residual material (defined as materials having $\geq$811 K boiling points and high softening temperature (423 K-443 K)) [9]. On these lines, Sugano et al. [36] studied the efficiency of hydrogenolysis of residues as a pathway towards utilization of coal liquefaction residue. The residue was pretreated with hydrogen peroxide at 50 °C for a period of 6 hours. This led to oxidation of the mineral matter in the residue yielding iron sulphate which enriched the reaction as Fenton's reagent in presence of hydrogen peroxide. Further, the hydrogenolysis reaction was supported under thermal liquefaction conditions, employing tetralin as the solvent at 420 °C under H_2 atmosphere. The residual material was filtered with acetone and further with n-hexane to calculate the yield of the process. The yield of the n-hexane solubles, as desired, was found to be higher and thus this method proved to be highly beneficial towards residue upgrading. Similarly, residues pretreated with tire wastes were also found to yield higher n-hexane solubles after hydrogenolysis with tetralin [8].

Attempts to pyrolyse the residue with supercritical fluids was carried out in 2002 [44]. Supercritical methanol and water were employed as the solvents. Successful extraction of hexane solubles and acetone insolubles were obtained at 300 °C-400 °C in presence of supercritical methanol, while more volatiles yield were higher at temperatures above 400 °C. Increase in pressure during pyrolysis upto 26.47 MPa caused reduction in the polymerization reactions. This attracted use of ionic liquids towards extraction of organic components from the coal liquefaction residue [38], [45], [46], [47]. The extraction of organic matrix from the residues was the aim of the process. The ionic liquid mixture was made of 1-butyl-3-methylimidazolium chloride and n-methyl pyrrolidinone. This organic precursor was the raw material required for generation of carbon fibers. A strong rupture of the aromatic bonds and high extraction yield with the use of n-methyl pyrrolidinone was reported by Li et al. [47]. The mechanism of the extraction process was attributed to the swelling of fixed carbon in the residue and further rupture of bonds triggered by the ionic liquid. The ash content of the extract was undetermined and was reported to be rather inert to the liquid [47].

Wang et al. [34] conducted microwave-assisted hydroconversion of the residues obtained from Shenfu and Shengli coals using methanol and ethanol as extraction

and reaction solvents. The residues obtained from liquefaction under 19 MPa H_2 at 455 °C was pulverized and passed through a 200-mesh screen and vacuum dried for a 24 hour period. To avoid the mineral effects during hydroconversion, the residues were demineralized using a technique reported by Silbernagel et al. [48]. Though the ash contents of the samples decreased largely, the volatile content was also found to be lower which was addressed to be associated witht he dissolution of volatile matter into the water phase [49]. Application of nickel catalyst enhanced the microwave irradiation process by improved solubility of the residue at low temperatures. This was confirmed by the FTIR studies of the extracts, where hydrogenation of the aromatic rings and presence of aliphatic species were detected. The GC-MS analysis was useful in the confirmation of the aliphatic species and reported presence of alkanes, arenes, octathiocane and organosulphurs. Better solubilities were reported with methanol at 130 °C under 0.7 MPa of initial hydrogen pressure.

Li et al. [31] performed hydro-treatment of direct coal liquefaction residue to investigate its potential in delivering for oil yield. This was carried out at similar conditions of a typical coal liquefaction process, in presence of hydrogen at temperatures ranging from 250 °C - 450 °C in presence of an iron-based catalyst. FTIR studies of the product derived from THFIS (tetrahydrofuran insoluble) fraction proves 30 wt.% conversion into lighter products in presence of H_2. The study confirms the presence of aliphatic C-H and shows no trace of aromatic C-H, with decrease in the oxygen content in its products.

Attempts to produce carbon microfibers (CMFs) from coal residue have been made by Zhou et al. [37]. The method employed arc-jet plasma at atmospheric pressure using a direct current upto 240 A and 140-150 V. SEM and EDX analysis of the CMFs revealed that the composition of CMF was dominated by carbon alone. The mechanism of the formation of the CMF was, however, not clear. Though, it is speculated that presence of Fe aids in the reaction and enhances the growth of the CMFs [37]. On similar grounds, carbon nanotubes have also been synthesized using catalytic chemical vapor deposition (CCVD) by Xiao et al. [50]. Further, the conversion of the aromatics in the residual material to soluble carboxylic acid functional group compounds was studied by Li et al. [32]. Efforts to carry out combustion of coal liquefaction residue as blends with biomass was also undertaken by Zhou et al. [51] to investigate the effects of sulphur emissions during the process.

2.4 GASIFICATION OF WASTE

The coal liquefaction residue, being a derivative of raw coal from the liquefaction process, was found to have calorific values comparable to that of raw coal [52]. Hence, gasification towards production of syngas (CO + H_2) and pyrolysis characteristics of residue have been under investigation recently [29], [30], [35], [52] - [53].

Earlier in the 1960's residues were defined as the undissolved coal slurry containing the liquefaction solvent. These were treated for solvent extraction under conditions to recover about 70% by weight of the moisture and ash-free coal. This extract was further separated from the residue by filtration technique and hydrotreated. The thick high-boiling residue was then used as boiler fuel [54]. However,it was found that particular residues have valuable components [54]. Hence, low temperature carbonization of the residues in the temperature range 425 °C-760 °C towards production of hydrogen was undertaken. However, with increasing difficulty in the application of this method due to agglomeration of the solids in the reactor tubes, this method was only suited for residues obtained from low efficiency liquefaction process.

Thus, in order to satisfy the technological as well as the environmental requirements, a Texaco coal gasifier capable of handling higher gasification temperature and pressure conditions was tested for gasification of residue-water slurry at 1200 °C - 1400 °C and about 24 bar pressure for the production of syngas [29]. However, this method was not effective against high ash-concentrated residues (41 wt.%) since it generated very low yield of syngas. Also, due to higher sulphur content (7 wt.%) in the residues, undesirable side reactions to produce H_2S and COS [53] in turn induced additional costs for sulphur stripping of the product gas stream.

Efforts to solve these issues through simulation studies of the Texaco downflow entrainment pilot plant to employ coal liquefaction residues as feedstock was studied by Wen and Chaung [55]. The hydrodynamics of the gasifier, the kinetics of the reaction and the material and energy balances formed the basis of their computation. A study to understand better the performance of the gasifier under different operating conditions was carried out. This definitely proved beneficial as an elementary study required to determine the necessary parameters for the gasification of the residue. However, much refinement and study of its applicability with different coal types was needed to validate the model. Work on the similar area was carried out by Govind and Shah [56].

Integrated coking and gasification of solid carbonaceous waste with coal by addition of ammonia or its precursor was suggested by Carr and Schmid [57]. Further

suggestions to improve gasification by blending the residual material with coal pyrolysis wastes for production of syngas and synthetic crude oil from the volatiles was made by Richardson [58]. This was supported through the work carried out by Taki et al. [59] in carrying out a gasification test in pilot plants of the residual wastes. Though production of syngas was appreciated, a considerable amount of capital investment was required for installation of a separate unit for cleaning the highly sulphurous by-products.

By the end of 1999, plans for construction of China's largest liquefaction plant was announced. Initially, Shenua's DCL project separated the heavy residual bottoms by the fractionation process. The heavy oil fractions with high boiling points about 524 °C were sent to the partial oxidation unit for production of hydrogen [7]. This process still presented drawbacks due to generation of ash, which now necessitated the need for a robust research for residual waste utilization. It was realized that utilization of the residual waste would present as a solid optimization technique of the direct coal liquefaction project [35].

Along with the research advancement in the use of ash-free coal, solvent-mediated H_2 transfer and catalytic hydrocracking [6] towards reduction of wastes, steam [35] and CO_2 gasification and H_2 production from the residual wastes [60] was also explored.

Three years after the proposal of the concept of partial liquefaction [43], Hong et al. [60] investigated the potential of the coal liquefaction residue to produce hydrogen. It was found that due to the presence of the coal liquefaction catalyst and high mineral content, the residue exhibited good reactivity.

Zhou et al. [61] studied the combustion of the Shenhua coal liquefaction residues in the TGA and calculated the kinetic parameters based on the Free-Caroll method. However, the reactivity and other parametric calculations were not clearly defined in this study.

Chu et al. [35] used steam as the agent for residue gasification in a quartz tube reactor. Also, the demineralization effects on the reactivity of residual chars and that of the residual waste obtained from the liquefaction of the residue was also studied. Chu et al. [35] found increased catalytic activity of the mineral content in the residue during gasification. The contribution towards catalysis by the liquefaction catalyst was found to be almost nil. This was in contradiction to the study of sulphur transfers from the residue to the syngas in the formation of H_2S and COS [62]. Complete reaction of the iron based liquefaction catalyst with steam was proved from the X-ray diffraction studies which exhibited peaks for formation of Fe_3O_4. They also concluded that CO_2 gasification led to higher concentration of COS

compared to H_2S, while during steam gasification due to stronger reducibility to form H_2S, it was higher in concentration than CO.

Pyrolysis studies to gather the preliminary data required to determine the effect of temperature on yield and product properties was initiated by Peng et al. [63]. This was useful in predicting the potential of the recycle of residues in the liquefaction plant. Further pyrolysis studies have been carried out by Xu et al. [30] to determine the kinetic parameters using the DAEM (distributed activation energy model). The mean activation energy was found to be 87.6 kJ/mol. They reported graphitization of the char samples with the severity of pyrolysis conditions (above 600 °C). This was proved from the absence of -CH_3 peaks in the tar at 600 °C compared to those sharply evident in the residue and tar at 400 °C pyrolysis. The catalytic effect of the mineral matter was also found to be prevalent during the pyrolysis of the residue. The SEM analysis of the chars revealed the porous structure of the char after the pyrolysis under N_2. Co-gasification studies with petcoke yields high reactivity in presence of CO_2 thus proving as a potential gasifier feed. The reactivity is enhanced due to the catalytic activity of the mineral content in the residue material [64].

Chapter 3

EFFECT OF OPERATING CONDITIONS ON RESIDUE FORMATION

3.1 INTRODUCTION

A batch reactor system was employed for the solvent extraction of coal to produce coal liquefaction residue with a known antecedence. The reactor was operated in such a way that it resembled an environment that closely represents an industrial coal liquefaction process. This we believe would help generate products and solid wastes with properties similar to those generated in the industry.

In order to do so, two different types of industrial solvents and the Coal Valley sub-bituminous coal were selected to carry out solvent extraction of coal at various temperatures. The coal liquid product yield was calculated for the processes, thus providing us data on extraction efficiency of solvents and indicating the degree of refractory material which has been dealt with.

Increasing the severity of the liquefaction conditions is speculated to yield larger coal liquid yields, which may in turn be effective in reduction of residue formation. Also, since a coal liquefaction process is considered to proceed through a radical formation mechanism, where the fate of the product stream is dictated by hydrogen capping, liquefaction under H_2 using HT solvent may be expected to curb residue formation. Experiments are, thus, conducted to study the effect of these liquefaction conditions on the rejects generated during the process.

3.2 EXPERIMENTAL METHOD

3.2.1 RAW MATERIALS

Sub-bituminous coal (Coal Valley coal) of Canadian origin from Sherritt International Corporation has been used throughout for our study. The washed and crushed coal was grounded using a ball mill, sieved ($\leq$ 150 μm) and vacuum dried for 12 hours at 80 °C. The proximate analysis (Table 3.1) and ultimate analysis (Table 3.2) of the dried coal were performed using the standard test methods ASTM D7582-12 [65] and ASTM D3176-09 [66], respectively. The as received coal contained 8.7 wt.% moisture. The maceral composition (Table 3.3) was determined by CSIRO Brisbane using automated reflectance microscopy.

Table 3.1: Proximate analysis of Canadian Coal Valley sub-bituminous

Proximate analysis (wt.%)[a]				
Composition	Moisture	Volatile Matter[b]	Ash[b]	Fixed Carbon[b]
x	5.02	36.13	21.33	37.52
s	0.07	0.24	0.99	0.75

[a]Averages (x) and sample standard deviations (s) of triplicate analyses
[b]The calculations are on a moisture-free basis. Calculation of the fixed carbon is by difference.

Table 3.2: Ultimate Analysis of the Canadian Coal Valley sub-bituminous, HT and NHT coal tar distillates employed as the solvent

Ultimate Analysis (wt.%) [a]						
	CV sub-bituminous		HT solvent		NHT solvent	
Element	x	s	x	s	x	s
Carbon	62.199	0.563	91.960	0.036	91.601	0.102
Hydrogen	3.801	0.033	6.273	0.010	5.822	0.014
Nitrogen	0.860	0.007	0.701	0.017	0.893	0.001
Sulphur	0.127	0.005	0.074	0.021	0.523	0.130
Oxygen	33.013	0.608	0.992	0.020	1.161	0.171

Industrial hydrotreated (HT) and non-hydrotreated (NHT) coal tar distillates, supplied by Sherritt International Corp. were employed as the solvents for solvent extraction of the sub-bituminous coal. The boiling point of HT solvent and NHT was measured as 161.6 - 506.54 °C and 161.45 - 506.35 °C by Rahman et al. [67]

by the ASTM D2887 method [68]. The ultimate analysis of the solvent is reported in (Table 3.2). ICP-MS analysis of the solvents were also performed reporting trace metal impurities present as Al (27.2 ppm), Ca (435 ppm) and Fe (47.1 ppm) for NHT solvent and Al (20.3 ppm), Ca (190 ppm) and Fe (34.0 ppm) for HT solvent, respectively. This table is thus indicative of the metals that may be incorporated in the waste from the solvent stream during the coal liquefaction process.

Table 3.3: Maceral composition of Canadian Coal Valley sub-bituminous

Maceral Composition (wt.%) [a]					
Composition	Vitrinite	Inertinite	Liptinite	Bright minerals	Dark minerals
x	67.8	19.5	7.5	17.9	6.8

[a] The maceral composition includes associated minerals.

Table 3.4: ICP-MS analysis of the HT and NHT coal tar distillate

Trace Elements (ppm)											
Solvent	Na	Mg	Al	K	Ca	Ti	V	Fe	Zn	P	As
HT	1.1	4	20.3	$\leq$6	190	5.40	1.91	34.0	5.60	13.0	2.56
NHT	2.8	3	27.2	$\leq$6	435	9.24	4.25	47.1	6.04	26.0	21.3

3.2.2 EQUIPMENTS

PARR AUTOCLAVE REACTOR SYSTEM

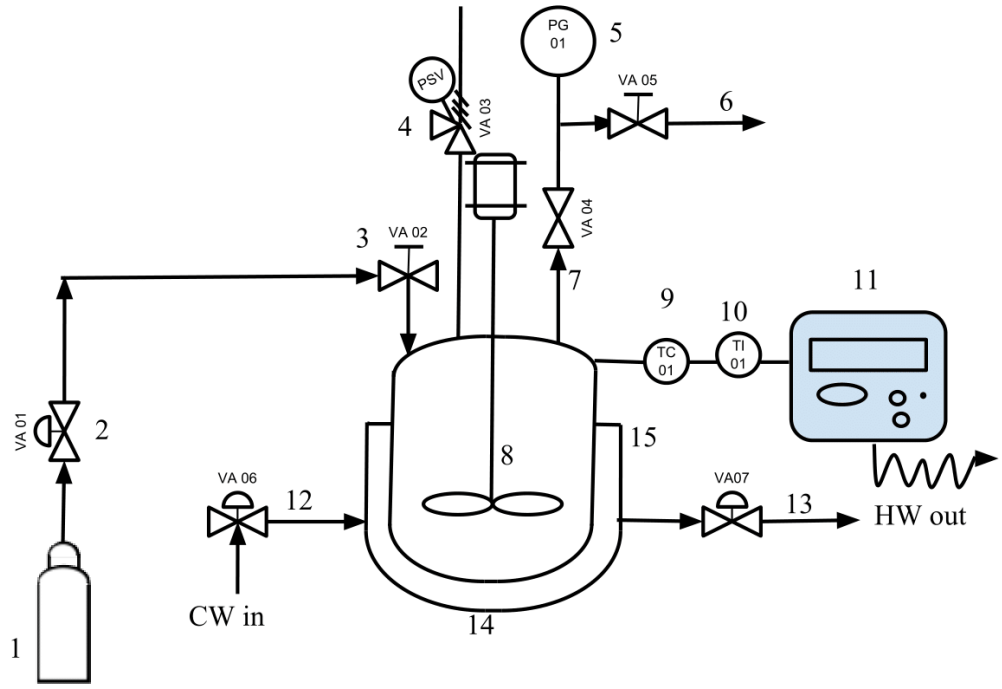

1. Gas cylinder
2. Outlet valve for cylinder
3. Inlet valve - Autoclave
4. Pressure Relief Valve
5. Pressure gauge
6. Outlet valve - Autoclave
7. Block valve - Autoclave
8. Motorized stirrer
9. Thermocouple
10. Temperature indicator
11. Control system connected to computer
12. Cold water inlet
13. Hot water outlet
14. Autoclave reactor system
15. Jacketed heater - Autoclave

Figure 3.1: Laboratory DCL process setup

A 250 ml 4576A (fixed head) High Pressure/High Temperature series bench top autoclave reactor manufactured by Parr Instruments, USA was engaged to carry out the DCL process. A P& ID representation of the autoclave set up is as shown in Fig. 3.1. The maximum pressure of the system for the DCL process was observed to be 34473.79 kPa (5000 psi is the maximum allowable working pressure for the system) at a maximum temperature of 450 °C. The specifications of the set up, as obtained from the manual provided by Parr Instruments are indicated in Table 3.5.

Table 3.5: Specifications of 4576A HP/HT autoclave reactor

Model No.	4576A
Reactor mounting	Bench top
Size,ml	250
Maximum Working Pressure	5000 psi (345 bar)
Maximum Temperature with FG Flat gasket	500 °C
Vessel Details	
Magnetic stirrer Model No.	A1120HC
Maximum torque	16 inch-pounds
4-blade impeller	1.38 diameter
Temperature measurement	Thermowell
Thermocouple type	K-type
Heater style	Ceramic
Heater power, Watts	1000
Stirrer motor, variable speed	1/8 hp
Volts, AC	230
Vessel dimensions	
Inside diameter, inches	2.5
Inside depth, inches	3.2
Weight of movable vessel, pounds	29
Reactor dimensions	
Moveable width x Depth x Height, in.	17 x 24 x 41
Moveable weight w/Controller, pounds	120
Spare parts kit	4579D

VACUUM DRYER

Yamato, USA's DP43 vacuum drying oven operates by a decompressed chamber direct heating and cooling system, over temperature ranges 5 °C-200 °C. The temperature of the oven is regulated with a PID control by microprocessors and double sensor K-type thermocouple. A digital display with a Up/Down setting key for functional modifications is set below the dryer's single swing door. The system is capable of handling pressures starting from 101.32 kPa-1.33 kPa. A 2.25 kW mica heater with a triac zero-cross heater circuit control system is incorporated in the device. The dryer's interior material is made of stainless steel (SUS 304) and exterior is a cold rolled steel plate with baked-on melamine resin finish.

3.2.3 PROCEDURE

NOTE: All runs were carried out in triplicates to check the reproducibility of the results.

SAMPLE PREPARATION

About 100 grams of raw coal was set for vacuum drying in the DP43 oven for a period of 12 hours at 80 °C. A vacuum close to 0.067 kPa was maintained for the process. This step is critical in ensuring moisture removal from the sample before its introduction in the autoclave reactor for the liquefaction process.

DIRECT COAL LIQUEFACTION PROCESS

Dry, pulverized coal of 20 grams was placed in a 250 ml stirred tank, bench top autoclave reactor (4575/76A HP/HT series Parr Instruments, USA) and mixed with 100 ml (∼100 g) of solvent, maintaining a coal to solvent ratio of 1:5. This slurry was then heated to the desired temperature (our study deals with liquefaction at 300 °C, 350 °C, 400 °C and 450 °C) in presence of N_2/ H_2 and agitated constantly with the stirrer. The initial pressure in the vessel for the process was 20 bar. A constant heating rate of 6 °C/min was maintained, following which a soak time of 60 minutes at isothermal conditions was maintained. The system was cooled manually by initiating the cold water supply to the heater system. This process takes upto 90 minutes to reach temperatures close to 90 °C, due to a manual procedure. This was followed by vacuum hot filtration of the product slurry at 80 °C-90 °C using a 0.1 μm Whatman microfiber filter. The remaining solid residual waste was washed thoroughly with tetrahydrofuran (THF) in order to recover residual coal liquids and solvent from the residue. The residue was further sent to a DP43 vacuum drying oven to remove any residual solvents from the sample material.

3.3 RESULTS & DISCUSSION

3.3.1 RESIDUE GENERATED

The DCL was thus, successfully conducted to observe the effects on the residue under three parametric variations:

1. Temperature of liquefaction process (300 °C, 350 °C, 400 °C, 450 °C)
2. Solvent for solvent extraction (Industrial solvent - Non-hydrotreated, Hydrotreated)
3. Liquefaction atmosphere (N_2 and H_2)

The properties of the residual waste are directly correlated with the efficiency of extraction of organic matrix of coal during the liquefaction process. Thus, determining the competency of the DCL process in terms of the ash content left in the

Table 3.6: Weight% residue generated

Solvent	Atmosphere	Temperature	Wt%	s[b]
HT	N_2	300	37.054	0.230
		350	25.456	0.038
		400	25.225	0.122
		450	28.007	0.283
HT	H_2	300	60.325	0.495
		350	47.515	0.097
		400	30.624	0.178
		450	29.760	0.215
NHT	N_2	300	54.916	0.031
		350	34.904	0.030
		400	36.584	0.025
		450	47.848	0.024

[b] Sample standard deviations (s) of triplicate analyses

residual material to calculate the coal yield [67], was the method employed in our study.

The chemistry governing the liquefaction of coal describes residue formation. A typical direct coal liquefaction reaction is believed to proceed by the mechanism representation in Fig. 3.3.

Here, the hypothetical coal molecule undergoes thermal pyrolysis to give intermediate radical compounds [69]. These radicals further undergo termination reaction with Hydrogen generated from the solvents employed for liquefaction to yield the liquid products. Further,the pathway of hydrogen exchange which may occur either by radical disproportionation reaction,primarily, or the radical hydrogen transfer [70] is very selective upon the type of products formed and may thus, dictate the residue formation.

Another theory behind the process was the "Coal Gel" theory [71], [72] where, the coal is also conceptualized as a gel matrix holding the soluble material by Vander-Waals forces. The swelling of coal when dissolved in the solvent results in relaxation of its steric requirement [71] and overcomes the Vanderwaals forces [69]. Thus, the gel matrix is disintegrated into the solvent and the coal exhibits fluid properties [72].

Thus, in all theories presented, hydrogen capping from the solvent or the gas feed is crucial step in reduction of fusion of radicals towards the formation of char. As the major portion of the soluble matrix is stabilized and extracted by the solvent, more complex is the heterogeneity of the waste produced.

Table 3.7: Residue weight% on a dry and ash free basis

Solvent	Atmosphere	Temperature	Wt%	s[b]
HT	N_2	300	74.11	0.518
		350	54.87	0.384
		400	51.17	0.358
		450	68.96	0.482
HT	H_2	300	83.14	0.344
		350	74.23	0.808
		400	56.19	1.77
		450	55.36	0.740
NHT	N_2	300	81.22	2.56
		350	78.12	0.673
		400	70.01	0.281
		450	79.14	0.668

[b] Sample standard deviations (s) of triplicate analyses

Residue wt.% obtained during the liquefaction process is calculated with respect to that of the parent coal. This is inclusive of the ash content of both the materials. Thus, representation of residual wt.% on a dry and ash free basis would help in the estimation of the remaining organic material in the residues, as shown in Table 3.7. Values obtained above are indicative of the parametric effect of solvent, residence time and temperature which is discussed further.

The residues can thus be defined as the unconverted portion of the coal which failed to metamorphose into product liquid or gases. The failure to metamorphose could be attributed to three major factors :

1. Residence Time
2. Temperature of liquefaction
3. Solvent solubility

3.3.2 EFFECT OF TEMPERATURE & RESIDENCE TIME ON COAL RESIDUE FORMATION

From Table 3.1 we observe very high liquid yield for temperatures in the range 350 ° C- 400 °C. Similarly, irrespective of the solvent employed, there is a definitive

increase in the residue generated (Table 3.6) at elevated temperatures.

$$\text{Yield of coal liquid} = \frac{\text{Weight of raw coal (daf basis)} \; - \; \text{Weight of residue (daf basis)}}{\text{Weight of raw coal (daf basis)}} * 100 \tag{3.1}$$

where, daf = dry and ash-free basis

Thus, the coal liquid yields for liquefaction at temperatures 300 °C, 350 °C, 400 °C, 450 °C thus calculated are,

Table 3.8: Coal Liquid Yield from DCL process(daf)[a]

Solvent	Atmosphere	Temperature (°C)	x[b]	s[b]
HT	N_2	300	71.716	0.106
		350	80.296	0.013
		400	83.171	0.084
		450	74.522	0.054
HT	H_2	300	25.678	0.021
		350	55.166	0.027
		400	78.127	0.034
		450	79.057	0.042
NHT	H_2	300	47.158	0.050
		350	65.576	0.039
		400	67.661	0.029
		450	52.153	0.038

[a] daf= dry ash-free basis
[b] Averages (x) and sample standard deviations (s) of triplicate analyses

Temperatures, play a very crucial role in thermal cleavage of the C-C bonds in a liquefaction reaction [73]. The generation of radicals is a highly endothermic reaction, requiring elevated temperatures. The weak VanderWaals forces are readily overcome by the coal matrix generating the minimal product yields depending on the solvent solubility at the lowest temperature of liquefaction, in our study, 300 °C. Now, further increase in temperature increases the reaction rate, following the principle of Arrhenius law and thus, radical formation is increased. The increase in temperature targets the thermal rupture of weak chemical bonds, thus reducing the viscosity of the generated material, yielding more gaseous products. The cracking of aliphatic side chains on aromatic ring compounds is a very rapid reaction. The intermediates (radicals) formed, thus, tend to stabilize to lower activation energies following the shortest mechanistic pathway. Due to this recurring phenomena, a condition of deprivation of hydrogen is reached leading to polymerisation and con-

densation reactions generating residual waste at 350 °C, 400 °C and 450 °C. This is insensitive to the type of initial gas supplied for the liquefaction process as seen from the Table 3.8.

Coal liquefaction reactions occurs on the threshold temperature of cracking of aliphatic bonds. Thus, residence time is crucial for higher product yields and residue formation. A standard maintenance of a 60 min period residence time was provided for all the liquefaction runs to investigate its influence. Low coal liquid yields at 300 °C and 350 °C for liquefaction under H_2 in presence of a hydrogen-donor solvent (HT solvent) are due to the adduction reaction between solvent and coal at residence times higher than the optimum. Further increase in temperature, helped to overcome the adduction effects. Similar phenomena was observed by Cronauer et al. [74] for experiments carried out under 0, 10, 30 and 60 min residence times in presence of H_2 and labelled tetralin solvent.

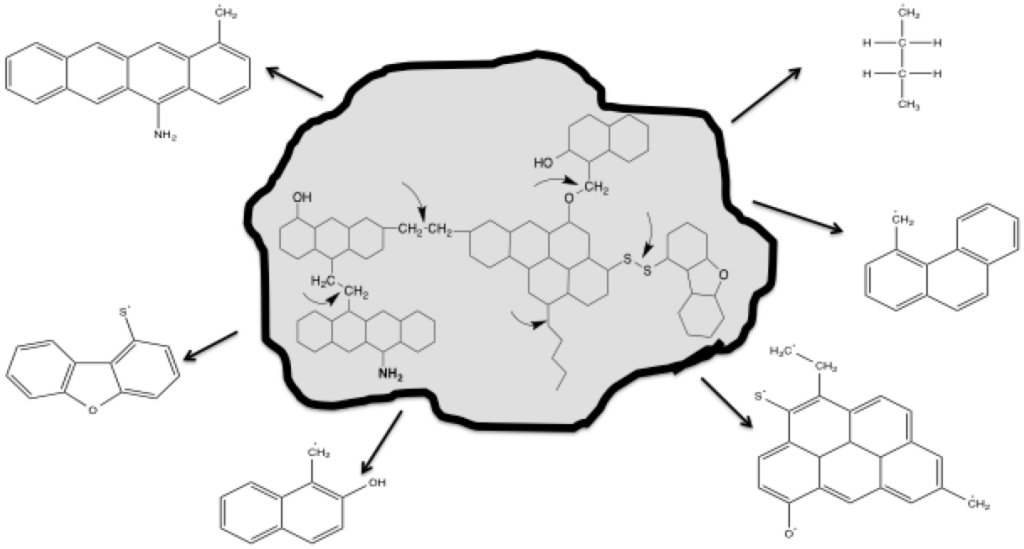

Figure 3.2: Radical formation during direct coal liquefaction process

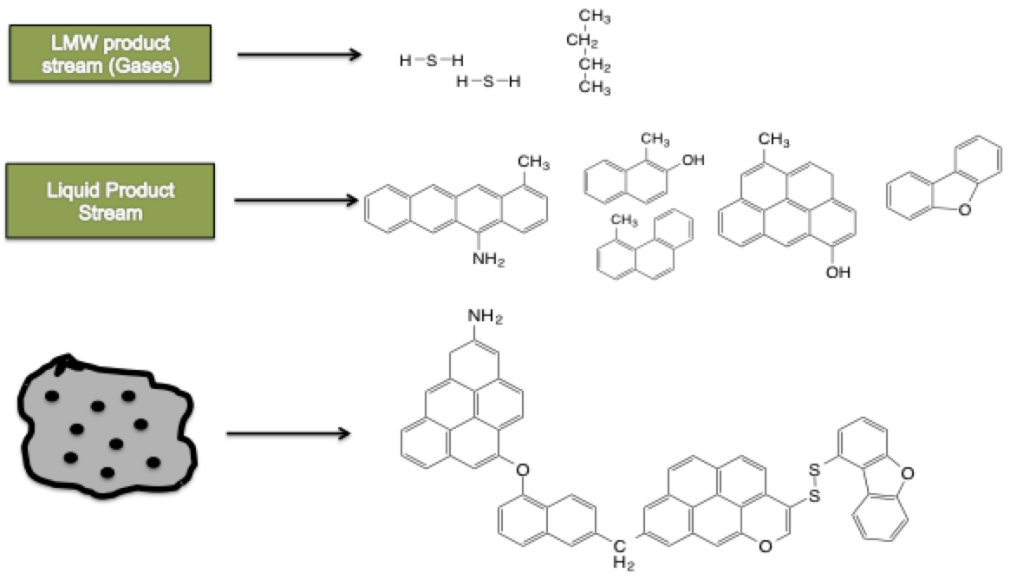

Figure 3.3: Product and residue streams generated from a direct coal liquefaction process

Another factor to be noted is the effect of temperature on the pressure of the system. At temperatures above that of the optimum liquefaction yield, an acute increase in the reactor pressure from approx. 75-80 bar (observed at 350 °C-400 °C) to 130 bar (at 450 °C). This rise in the system pressure which was observed with increased temperature of liquefaction cannot be completely attributed partially to the existing system pressure and escaping of solvent to the vapour phase (which is minimal considering a very high system pressure). Hence, the major contributing factor is the gaseous product formation with increasing temperatures of liquefaction. This is associated with the thermodynamics that do not favour the retention of cyclic aliphatic structures thus, increasing the production of light hydrocarbon by-products with increase in temperature [15].

Considering two hypothetical intermediates during the course of the reaction as shown in Fig. 3.2, a schematic representation of the product (hypothetical) poly-condensation reactions occurring during the reaction is represented in Fig. 3.3.

3.3.3 EFFECT OF SOLVENT ON COAL LIQUID YIELD

Now, in order to generate residual waste with properties similar to those originating during an industrial liquefaction process, industrial solvents were employed. The solvents chosen during our study were specifically for improved solubility parameters aimed towards increasing the extraction of the organic matrix in coal.

The solvent properties need to be such that the retrogressive reactions during the progress of the reaction are prevented and dealt with by acting as an efficient hydrogen donor and/or shuttler [73]. Also, the solubility factor and elemental content such as H/C ratio and S/C, in particular, determine the efficacy of the solvent in extraction of the organic matrix in coal and can help in disruption of the reversible cross-linking reactions prevalent at high temperatures [1]. Solomon et al. [75] have reported that the rate and extent of cross-linking was found to be lower in donor-solvent liquefaction due to the capping of the cross-link sites with the hydrogen from the donor-solvent. This is clearly evident from our results as mentioned in Table 3.2.1.

The solvents employed are particularly of the PAH (polyaromatic hydrocarbon) type. PAH solvents are generally follow the radical hydrogen transfer mechanistic pathway , i.e. transfer of hydrogen from solvent derived radicals to the closed species of raw coal at low temperatures and high aromatic content. It may also be favoured by cleavage of free H-atoms at lower concentrations. The thermolysis at high temperature liquefaction, generates coal radicals which are highly reactive in nature. Generation of residual material is highly dependent on availability of hydrogen for this case which may prevent condensation reaction. In the presence of hydrogen availability of hydrogen from the donor solvent, penetration into the coal structure is easier, thus proceeding to solvent hydrogen and aromatic coal equilibrium reactions. In our case, the HT solvents exhibited higher H/C ratio of 0.82 (Table 3.2) as compared to that of NHT solvents. This explains, the plausible reason for the extraction of coal liquid yields being higher for HT solvents compared to that of NHT solvents. The role of interactions of coal surface with solvents play a very crucial role as well [76]. Various types of solvents could be chosen, based on their effects on coal. The solvents chosen during our study were specifically for improved solubility parameters aimed towards increasing the extraction of the organic matrix in coal.

HT solvent has very low sulphur contents (0.074) (Section 3.2.1) as against 0.76 for NHT with comparatively large sulphur values (0.523), thus exhibiting better hydrogen donor abilities than NHT solvent. In such case, the sulphur is transferred to the products and create an increase in the hydrogen requirement. Also, the "vulcanizing" property of sulphur may dominate leading to creation of a coal matrix which is more and more susceptible to solvent extraction [77], producing more residual waste in NHT solvent products. Thus, with reference to the above discussed solvent properties and its co-relation with our data, better yields were obtained under similar conditions, for CV sub-bituminous using HT solvent.

3.4 GENERAL DISCUSSIONS

This study thus presents a detailed information about the three main parameters (temperature, solvent and liquefaction atmosphere) necessary to be accounted for, during a direct coal liquefaction process. The operating parameters under consideration in our study are depicted in Fig. 3.4.

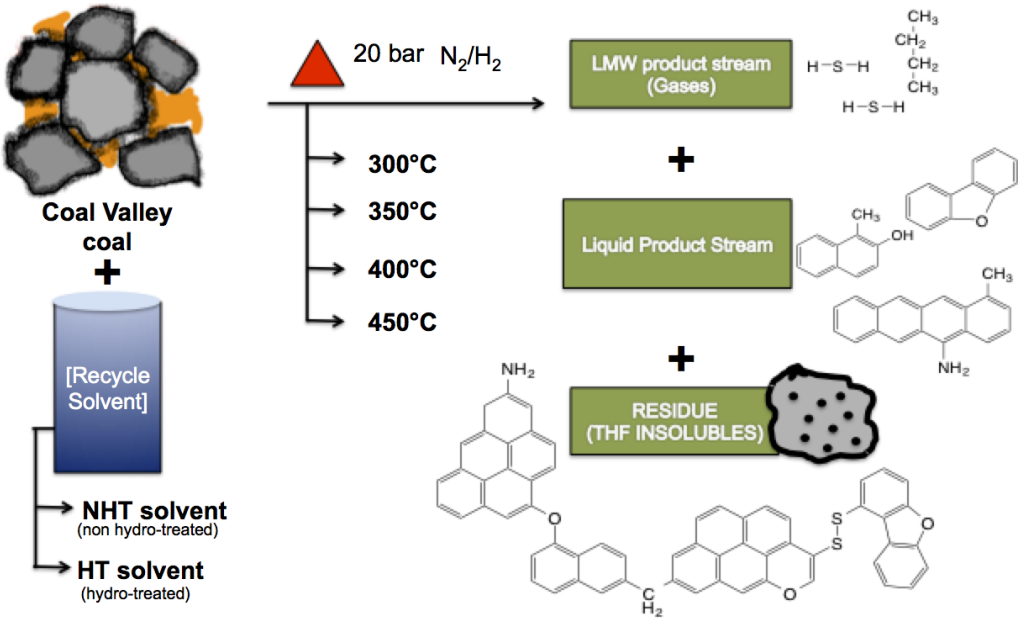

Figure 3.4: Operating parameters under the scope of our study

Industrial recycle solvents and pulverized coal from Sherritt Intl. Ltd. were the raw materials employed under conditions that resembled a real-time liquefaction process to draw conclusive implications that would be of relevance to the industries. These residual material account for almost 30 wt.% of the raw coal for each run of the liquefaction process and contained the liquefaction catalyst, unreacted coal and mineral matter (Fig. 1.1). The amount of organics in the waste stream is calculated from the weight of the residue on moisture and ash free basis, mentioned in Table 3.7. Thus solvent properties influence the conversion of the organic material in coal independent of the atmosphere of liquefaction. Liquefaction under H_2 at residence time of 60 minutes in low temperatures was found to yield low conversions and hence the prevalent organic in the waste associated with the adduction reactions, as seen in Fig. 3.5. The anomalously low organic matter conversion under hydrogen atmosphere could not be explained. The measured and calculated values of yield percentages of desired products and unconverted organics, still prevalent in the

waste stream, dictate the design parameters of the reactor for execution of a robust liquefaction process.

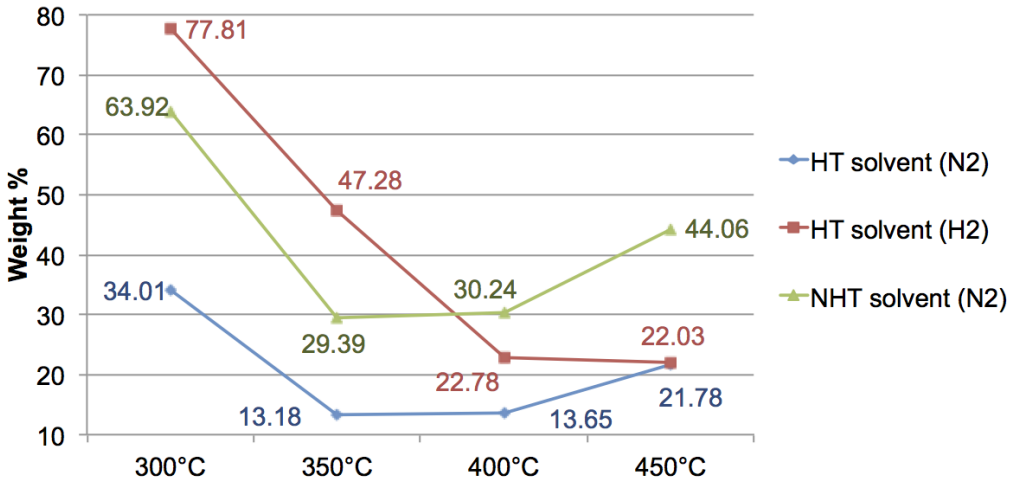

Figure 3.5: Organic matter in the coal that remained in the residual waste

3.5 CONCLUSIONS

The experiments were conducted at four different operating temperatures 300 °C, 350 °C, 400 °C and 450 °C under N_2 or H_2 employing HT and NHT industrial solvents. The experiments aimed to investigate the effect of these operating parameters on the product yield i.e. coal liquid and also the amount of the residues generated. The conclusions can be summarized as follows:

1. Better yields of liquid products were derived from the HT solvent (84%) compared to NHT solvent (68%) owing to improved solubility and H-donor ability of the solvent.

2. Liquefaction at 300 °C generated a major reject stream with residues upto 78 wt.% organic (daf basis). Further increase in the liquefaction temperature increased the organic conversion of the coal upto 400 °C. However, due to conditions leading to unavailability of H_2 at very high liquefaction temperatures (450 °C), the organic conversion reduces to yield upto 44 wt.% C (daf basis) in the waste stream.

3. Comparatively higher coal liquid yields (83%) were observed for liquefaction under HT solvent under N_2. The highest value of liquid yield for liquefaction under NHT solvent was 68%.

4. Liquefaction under H_2 at induction/residence time of 60 min, had a negative impact on the yield of the liquid products. It is speculated that this could due to adduction reactions generating upto 55 wt.% residual stream at low temperatures (300 °C). Further increase in temperature, increases the conversion percentage and reduces the percentage of organic in the residual stream to 30 wt.% C at 350 °C and 400 °C. Further increase in temperature to 450 °C, results in very slight increase (about 1 wt.%) in the yield of coal liquid products.

Chapter 4

CHARACTERIZATION OF COAL LIQUEFACTION RESIDUE

4.1 INTRODUCTION

This project was initiated with a vision of upgrading of the coal liquefaction waste/residue. This requires an understanding of the structure and the elemental composition of the waste.

Thus, the analysis of the coal liquefaction residues slowly progresses from the morphological effects of the solvent extraction process by comparing the raw coal with residues at different temperatures to their chemical composition and functional group analysis using Fourier Transform Infrared Spectroscopy methods. We would see how a simple carbon material undergoes its transitions from a raw coal to being what we have termed, as "waste", which could be still a potential source of fuel. The following sections, thus explore the physical as well as chemical properties of the residues through extensive analytical techniques.

A solvent with lower heteroatoms is expected to yield liquid products of superior quality which do not require extensive hydro-processing towards heteroatom removal. Increasing severity of liquefaction could in turn reduce the particle size of the coal particles during the process. Also, with increasing conversion of the organic matrix of coal, a large chunk of the bulky mineral material could be suspected in the residual waste stream. Thus, analysis of the residues have been conducted to determine the morphology, mineral composition, particle size distribution, surface area, elemental composition and presence of the type of functional groups.

4.2 EXPERIMENTAL

4.2.1 RAW MATERIALS

The waste generated during the direct coal liquefaction process and the raw coal from the process are two main raw materials for the analytical characterization of the residue. The raw coal characteristics can be found in the Section 3.2.1 in Chapter 3. The properties of the residue would be stated in the proceeding sections.

4.3 EQUIPMENTS

The various analytical instruments used for characterization are discussed here.

SCANNING ELECTRON MICROSCOPY

Tescan, Czech Republic's Vega 3 Scanning Electron Microscope featuring Energy-dispersive X-ray spectroscopy for elemental analysis of the samples was employed to study the morphology of the residues. The object is displayed by the projection of thin electron probe (beam). The column forms the beam and sweeps it on to the examined specimen on the chamber of the microscope. The microscope's electron gun has an electron source capacity to emit upto 30 keV electron energy and brightness upto 10^6 A/cm^2 and emission current upto 300 μA. At the highest image brightness the gun is correctly centred.The stigmator in the microscope help compensate for the astigmatism in all displaying modes. Demagnification of the virtual source are conducted by a pair of strong magnetic lenses C1 and C2. Vega 3 has five modes of display namely, Resolution mode, Wide field mode, Depth mode, Field mode and Channelling mode based on the focal depth and resolution required. Samples can also be analysed in various pressures, ranging from 0.005 Pa-2000 Pa.

PROXIMATE ANALYSIS

A quantitative analysis of the moisture, volatiles, ash and fixed carbon in the samples was performed using TGA 701 from LECO Corporation, USA. A simultaneous analysis of upto 19 samples could be performed using this instrument. It complies with the ASTM D7582 method required to analyse the sample using the standard techniques. The instrument has a maximum allowable temperature upto 1000 °C with a maximum sample size of 5 mg. Three major ports for N_2, air and O_2 at a calibrated pressure as mentioned in 4.1. The maximum allowable sample size for this system is $\leq$ 250 μm. Thermocouples are installed to help monitor and control the

Table 4.1: Proximate Analysis: Gas Specifications

Gas	Product Grade	MSDS reference	Inlet Pressure, kPa
Nitrogen	5.0	P-4631	241.32
Oxygen	4.8	P-4574	241.32
Air	Ultra zero Ambient Monitoring	P-4560	310.264

temperature inside the furnace. The instrument is connected to a computer which runs an easy-to-follow menu-drive Windows-based software program of TGA 701 LECO software. This allows the analysis methods to be tailored to satisfy most applications. The samples are indexed automatically to the position above the balance pan. The instrument finally measures a weight loss as a function of temperature in a controlled environment. Ceramic crucible of density 3 g/cm^3 are used for sample introduction into the furnace. The standard density for the loaded samples are set at 1.5 g/cm^3.

4.3.1 ULTIMATE ANALYSIS

C, H, N and S analysis was carried out by employing vario MICRO cube (Elementar Analysensysteme GmbH). The system has a capacity of 120 sampling carousels. Also, the sample feed could weigh anywhere from a micron to 800 mg feed. The sample is injected with a jet flow of oxygen to lower gas consumption. High heating temperatures of the furnace upto 1800 °C are capable of 100% recovery of samples which are difficult to combust. The analysis is fast, simple and efficient without the use of any toxic gases. H_2 and O_2 of 99.995% purity (Ar optional) of 3 litres and 0.05 litres are consumed per analysis. Analysis of each sample for CHNS takes upto 10 minutes for completion.

4.3.2 FTIR

An ABB Inc. (Quebec, Canada) MB3000 Fourier Transform Infrared Spectrometer with a doped triglycine sulphate (DTGS) detector working in the spectral range of 485 to 8,500 cm^{-1} was employed to analyse the IR spectra of raw coal and the residues. It features a non-hygroscopic beam splitter material (ZnSe) with a 3 point kinematic adjustable sample compartment. The operating temperature for this device ranges from 10 °C-35 °C. The instrument is connected to a computer operating the Horizon software interface to control the functions required to perform the necessary procedural or desired steps using the spectrometer.

4.3.3 PARTICLE SIZE ANALYZER

A Mastersizer 3000, Malvern Instruments was employed. This incorporates expert engineering and application know-how into every stage of its design. It works on the principle of laser light scattering, where the laser beam illuminates the particles. A detector series then accurately measure the intensity of light scattered by the particles within the sample for both red and blue light wavelengths, over a wide range of angles. It has a typical measurement time less than 10 minutes. Particle sizes ranging form 0.01 μm to 3500 μm can be analysed under the data acquisition speed of 10kHz. It consists of a Hydro LV which is the wet dispersion unit where the sample is placed.

4.3.4 SURFACE AREA ANALYSIS

An autosorbiQ-MP by Quantachrome Instruments USA was employed for carrying out the the surface area analysis for raw coal as well as residues. This is equipped with three physisorption analysis ports for surface area and pore size analysis. Each analysis zone contains a cell consisting a tube for sample introduction, insulation pad to a maintain the sample temperature and a sample holder. Low pressure micro-pore analysis can also be carried out in these systems using a 13.33 Pa transducer. Low leak rates are achievable due to vacuum coupling radiation(VCR) gasket fittings. Two major gas input ports are available with the model, one of each is connected to He and N_2/CO_2. Liquid Nitrogen port is equipped in a standard cryogen dewar with a capacity of 1 litre. Physisorption station is equipped with a high temperature furnace, capable of heating upto 1100 °C for chemisorption. A level sensor helps in maintaining the liquid level of liquid coolant (ice and cold water slurry at about 2 °C-3 °C) thus ensuring the zone is constantly at the desired set temperature. The equipment is connected to a computer program running the iQ interface to help initiate the desired set of functions to the equipment.

4.4 PROCEDURE

4.4.1 SEM ANALYSIS

The sample preparation step involves coating the conductive raw coal and residue samples with Au (gold) to prevent image disruptions due to conductance during analysis of the samples in the presence of secondary electron gun beam. The device is first vented to stabilize the column pressure close to that of atmospheric pressure. The stubs with sample mounts are then screwed tightly onto the the sample

holder stem of the SEM. The device is now de-pressurized and a vacuum ≤ 3 Pa is maintained in the system. The high voltage (HV) switch is now set to 20 kV and auto-signal is selected. The SEM scanning page now displays a section of the samples, and the desired area of the sample can be analysed by selecting the appropriate magnification.

4.4.2 PROXIMATE ANALYSIS

A list of standard procedures are maintained for carrying out proximate analysis of the samples using ASTM D7582-12 [65]. All the gas cylinders (N_2, Air and O_2) are checked for the standard pressure requirements. The TGA and the computer system connected to its controls is turned on to open the LECO interface. A thorough system check is conducted to review errors in the system, if any. About 1g of samples are loaded one, each at a time (when prompted) along with an empty reference crucible to calculate the weights of the actual loaded material into the TGA. The following three steps form the basis of analysis:

1. Moisture analysis: A baking oven mode furnace is heated from ambient to 104 °C steadily at a rate of 6 °C/minute. Isothermal conditions are maintained until the weights of all the loaded samples are consistent or reach stability. The final amount of moisture is calculated as,

$$\text{Moisture} = \frac{\text{weight of used sample } - \text{ weight of sample after heating}}{\text{weight of used sample}} * 100 \tag{4.1}$$

2. Volatile matter analysis: The crucibles are closed with the cover to calculate the volatile mass. The samples are then heated rapidly at 50 °C/min to 950 °C. isothermal conditions are maintained for 7 minutes. The final volatile content is calculated as,

$$\text{Volatile matter} = \frac{\text{Moisture mass } - \text{ Volatile mass}}{\text{weight of used sample}} * 100 \tag{4.2}$$

   On a dry basis,

$$\text{Volatile matter\%} = \frac{100}{100 - moisture} * Volatile \tag{4.3}$$

3. Ash analysis: The samples are further cooled upto 600 °C and heated slowly at roughly 10 °C/min to 750 °C for raw coal and up to 950 °C for residue

samples. Isothermal conditions are maintained for 25 minutes. The final ash content is calculated as,

$$\text{Ash content\%} = \frac{\text{Ash mass}}{\text{weight of used sample}} * 100 \tag{4.4}$$

On dry basis,

$$\text{Ash content\%} = \frac{100}{100 - moisture} * Ash \tag{4.5}$$

4. Fixed Carbon: This represents the solid residual combustible material content of the sample. It is calculated on a differential basis as follows,

$$\text{Fixed Carbon content\%} = 100 - [Moisture - Volatile\ matter - Ash\ content] \tag{4.6}$$

4.4.3 ULTIMATE ANALYSIS

About 2.5-3.5 mg of the sample was weighed and placed into a small aluminium pan. The pan is well sealed and placed onto the tin vessel for measurement. The samples are then loaded into the integrated carousels. The sample now travels into the combustion tube through a ball valve.The samples are now flushed with inert gases such as Ar, to remove atmospheric N_2. This is followed by combustion at 1200 °C. The combustion are now passed to the second furnace chamber where they are reduced in presence of hot Cu. Now, the formed gases, N_2, CO_2, H_2O and SO_2 remain in the He carrier gas stream. The gas mixture is separated by a temperature programmed desorption (TPD) technique and then led through the electronic gas flow controller to the thermal conductivity detector (TCD). The computer connected to the device computes the elemental concentration from the detector signal on the basis of the calibrated values fed into the system.

4.4.4 FTIR ANALYSIS

Once, the communication between the instrument and the Horizon's MB interface is established, spectra were recorded by adding 120 scans at a resolution of 4 cm^{-1} for empty reference cell. A pinch of the sample is then placed on the Pike MIRacle Single Reflection ATR. This procedure is repeated for the sample, maintaining a detector gain value of 81.

4.4.5 PARTICLE SIZE ANALYSIS

The instrument is initialized by repetitive cleaning of the stirrer with water and dispersant. The sample introduction tank is now filled with deionized (DI) water. This is followed by degassing the tank and cell to remove the air bubbles in the tank, if any. The instrument is then auto-aligned with the tank cell. A laser then runs to check the dark background using blue light. This is done to eliminate the background light effects to consider the laser obscuration by the particle alone. The dark background laser obscuration is about 76.45% for all cases. Sample properties are then included in the toolbox before sample introduction into the DI water tank. An optimum stirrer speed is maintained to initiate effective mixing of the sample particles with the DI water to prepare a slurry mixture, until an optimum obscuration range (3- 12%) is achieved. The obscuration for all samples was maintained in the range of 6.5% - 12%. A stirrer speed of 2700 rpm was maintained.

4.4.6 SURFACE AREA ANALYSIS

Surface area analysis of coal has a specific standard operating procedure. The analysis is carried out in two major steps as indicated below:

1. Degassing stage
2. Physisorption stage

A sample of about 800 g is introduced in the cell for degassing the sample. This stage helps in removal of the volatiles and moisture from the sample. The sample is heated upto 200 °C under vacuum. A cold trap liquid nitrogen. The cryogen dewar is filled with 950 ml liquid nitrogen forms the cold trap for the released volatiles and other gases. After this step, the remaining sample is re-weighed and introduced in the physisorption section maintained at the temperatures close to 0 °C with the help of a ice-water slurry. The CO_2 is employed as the adsorption-desorption gaseous medium. The pressure is varied from 0-2 bar and each stage takes a period of 10 hours for completion.

4.5 RESULTS & DISCUSSIONS

4.5.1 SEM ANALYSIS

SEM analysis carried out for the residue samples obtained at different temperatures and compared with that of raw coal (Figs. 4.1, 4.3, 4.5, 4.7 and 4.9). These

figures represent the back scattered electron (BSE) images of raw coal and the residue. Since elements with higher atomic number back scatter strongly compared to elements having lower atomic weight number [78], detection of mineral matter based on reflectance was analysed. The residue, thus, exhibits higher mineral matter compared to that of raw coal. This conclusion is made based on the high reflectance of the ash material compared to carbon. Also, this is confirmed from the proximate and ultimate analysis, explained in the Section 4.5.2 and 4.5.3 in our study.

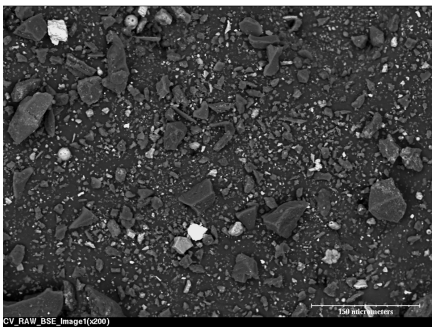

Figure 4.1: BSE image: CV coal (200x magnification)

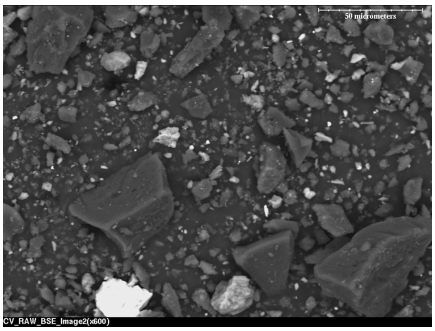

Figure 4.2: BSE image: CV coal (600x magnification)

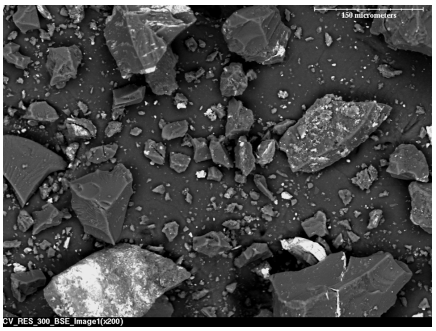

Figure 4.3: BSE image: residue from 300 °C liquefaction (200x magnification)

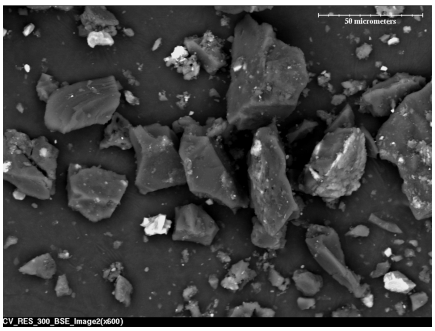

Figure 4.4: BSE image: residue from 300 °C liquefaction (600x magnification)

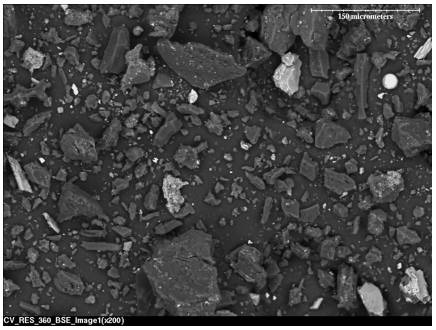

Figure 4.5: BSE image: residue from 350 °C liquefaction (200x magnification)

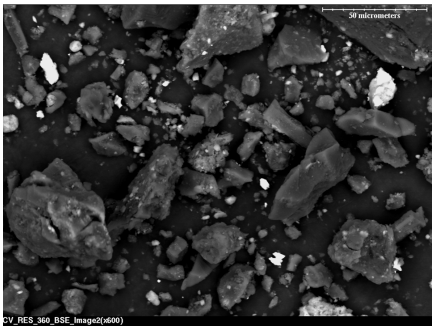

Figure 4.6: BSE image: residue from 350 °C liquefaction (600x magnification)

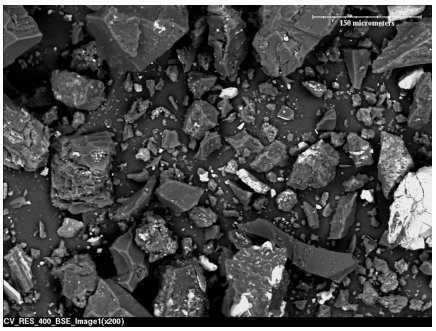

Figure 4.7: BSE image: residue from 400 °C liquefaction (200x magnification)

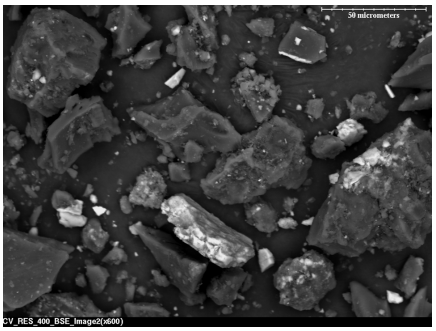

Figure 4.8: BSE image: residue from 400 °C liquefaction (600x magnification)

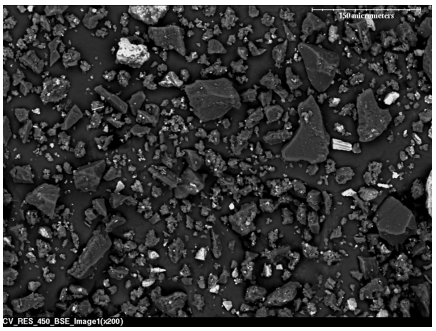

Figure 4.9: BSE image: residue from 450 °C liquefaction (200x magnification)

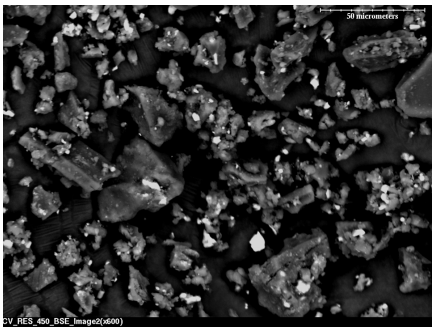

Figure 4.10: BSE image: residue from 450 °C liquefaction (600x magnification)

4.5.2 PROXIMATE ANALYSIS

The proximate analysis results of the residues derived form the liquefaction process are compared to that of raw coal, presented in Tables 4.2, 4.4 and 4.6. Also, the conversions of each component have been computed by using the proximate analysis data from Tables 3.1, 4.2, 4.4, 4.6 and weight of the residues after liquefaction (Table 3.6) using the equation below:

$$\text{Conversion of component } 'i' = 1 \; - \; \frac{Wt.\ of\ component\ 'i'\ in\ residue}{Wt.\ of\ component\ 'i'\ in\ coal} \qquad (4.7)$$

Here, component 'i' stands for moisture, ash, volatiles and fixed carbon. We assume that the ash remains as an inert component during the process and thus the weights are on an ash-free basis. Hence, it does not participate in the conversion. Thus, ash conversion would be 0% during each liquefaction run.

The residues still exhibit some amount to moisture and volatiles in the samples after liquefaction. The physical structure of coal consists complex organic and inorganic matrix embedded in the form of an extensive network of pores [79], with moisture as one of the elements present in it. Drying was reported to have a negative impact on liquefaction for sub-bituminous coal than bituminous feed [19]. Vacuum drying prior to its introduction into the autoclave, results in removal of about 60% moisture. However, this also leads to breakage of the pores [80] and affect the cross-link density of coal, thus making the further water loss more difficult and affecting the accessibility of coal structure [79], [81]. Thus, higher temperatures have been favourable for moisture removal (Tables 4.3, 4.5, 4.7). However, regardless of the solvent and gas employed during liquefaction, volatiles in the wastes steadily decreases as the liquefaction temperature conditions are increased.

The ash is computed as the material burnt-off after combustion of the residues at 950 °C in pure O_2 atmosphere [65]. De-ashing of the liquid products is much efficient for liquefaction using HT solvent. Also, ash removal efficiency can be reported to be slightly higher for higher liquefaction temperatures in HT solvent under H_2. The fixed carbon content is a precursor to the retrograde tar or coke [82]. This is largely effected by the availability of H_2 during the process, explained in Chapter 3. Thus, higher conversions of fixed carbonaceous material are reported for liquefaction under HT solvent than NHT solvent. Also, at lower temperatures of liquefaction (300 °C and 350 °C), the coke formation is comparatively higher in presence of H_2. Further, there is a decrease in the fixed carbon conversion above 400 °C of liquefactions under N_2, while there is a slow but a steady increase in the conversion under H_2,

which thus confirms the suppression of the cross-linking phenomena, as discussed in Chapter 3 due to retrograde reactions, over come under H_2, as depicted in Fig. 4.11. Thus, contribution of hydrogen transfer to the radicals towards product formation is dictated by the solvent than the atmosphere of liquefaction.

Table 4.2: Proximate Analysis for residues obtained from DCL under HT solvent in N_2

Proximate Analysis[a] [b]								
Sample	Moisture		Volatile		Ash		Fixed Carbon	
	x	s	x	s	x	s	x	s
CV RES 300	3.18	0.33	23.62	2.60	25.89	2.25	47.31	2.12
CV RES 350	1.65	0.69	19.47	0.95	45.13	1.93	33.75	0.69
CV RES 400	1.36	0.24	18.29	0.30	48.83	1.58	31.52	2.06
CV RES 450	1.51	0.18	15.00	2.16	31.04	0.60	52.45	2.57

[a]Averages (x) and sample standard deviations (s) of triplicate analyses
[b]The calculations are on a moisture-free basis. Calculation of the fixed carbon is by difference.

Table 4.3: Conversion for each component during direct coal liquefaction process under HT solvent in N_2

Proximate Analysis[a] [b]								
Sample	Moisture		Volatile		Ash		Fixed Carbon	
	x	s	x	s	x	s	x	s
CV RES 300	87.34	0.98	86.93	0.28	0.00	0.00	74.80	0.29
CV RES 350	97.75	0.77	96.31	0.08	0.00	0.00	93.83	0.03
CV RES 400	97.73	0.72	95.75	0.22	0.00	0.00	92.95	0.10
CV RES 450	97.19	0.64	96.13	0.07	0.00	0.00	86.96	0.07

[a]Averages (x) and sample standard deviations (s) of triplicate analyses
[b]The calculations are on a moisture-free basis. Calculation of the fixed carbon is by difference.

Table 4.4: Proximate Analysis for residues obtained from DCL under HT solvent in H_2

Proximate Analysis[a] [b]								
Sample	Moisture		Volatile		Ash		Fixed Carbon	
	x	s	x	s	x	s	x	s
CV RES 300	1.65	0.21	35.81	0.96	16.86	2.36	47.33	0.59
CV RES 350	0.92	0.48	35.50	1.81	25.79	0.69	38.93	1.98
CV RES 400	1.40	0.19	22.04	1.93	43.81	1.35	34.15	0.66
CV RES 450	0.84	0.08	18.39	2.34	44.64	0.97	30.97	1.14

[a]Averages (x) and sample standard deviations (s) of triplicate analyses
[b]The calculations are on a moisture-free basis. Calculation of the fixed carbon is by difference.

Table 4.5: Conversion for each component during direct coal liquefaction process under HT solvent in H_2

Proximate Analysis[a] [b]								
Sample	Moisture		Volatile		Ash		Fixed Carbon	
	x	s	x	s	x	s	x	s
CV RES 300	79.53	0.45	38.27	2.42	0.00	0.00	21.44	0.10
CV RES 350	93.90	0.54	67.30	1.07	0.00	0.00	65.46	0.16
CV RES 400	96.71	0.30	92.79	1.88	0.00	0.00	89.25	0.24
CV RES 450	98.21	0.12	94.55	1.26	0.00	0.00	91.16	0.34

[a]Averages (x) and sample standard deviations (s) of triplicate analyses
[b]The calculations are on a moisture-free basis. Calculation of the fixed carbon is by difference.

Table 4.6: Proximate Analysis for residues obtained from DCL under NHT solvent in N_2

Proximate Analysis[a] [b]								
Sample	Moisture		Volatile		Ash		Fixed Carbon	
	x	s	x	s	x	s	x	s
CV RES 300	1.81	0.47	30.36	0.16	18.16	0.88	51.59	0.565
CV RES 350	1.76	0.28	26.97	0.64	21.91	0.05	51.12	0.28
CV RES 400	1.96	0.03	19.50	1.09	30.02	0.03	50.49	0.36
CV RES 450	0.79	0.26	13.04	0.21	20.86	0.90	65.47	0.48

[a]Averages (x) and sample standard deviations (s) of triplicate analyses
[b]The calculations are on a moisture-free basis. Calculation of the fixed carbon is by difference.

Table 4.7: Conversion for each component during direct coal liquefaction process under NHT solvent in N_2

Proximate Analysis[a] [b]								
Sample	Moisture		Volatile		Ash		Fixed Carbon	
	x	s	x	s	x	s	x	s
CV RES 300	83.19	0.76	60.83	0.61	0.00	0.00	35.91	0.66
CV RES 350	95.29	0.84	89.98	0.08	0.00	0.00	81.71	0.98
CV RES 400	93.67	0.32	91.26	0.45	0.00	0.00	78.20	0.25
CV RES 450	94.22	0.41	86.76	0.92	0.00	0.00	35.97	0.87

[a]Averages (x) and sample standard deviations (s) of triplicate analyses
[b]The calculations are on a moisture-free basis. Calculation of the fixed carbon is by difference.

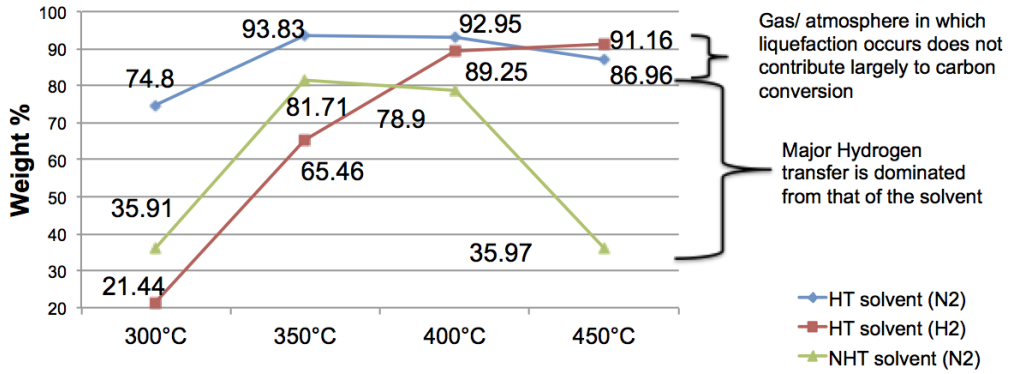

Figure 4.11: Fixed Carbon conversion during the direct coal liquefaction process

4.5.3 ULTIMATE ANALYSIS

After determining the fixed carbon , ash and volatiles of the residues, we look into the heteroatoms present in the residues. Removal of heteratoms is desired for the production of clean fuels with improved performance efficiency by reduction of NO_x and SO_x during combustion and formation of other undesirable by products during refining and distillary proceses.The percentage of carbon, hydrogen,sulphur and nitrogen was thus, obtained from the elemental analysis. The oxygen is calculated based on the ASTM D3176-09 method as follows:

$$\text{O \%} = 100 - \text{ C \%} - \text{ H \%} - \text{ N \%} - \text{ S \%} \tag{4.8}$$

The above method for determining the oxygen content is not accurate since it includes the cumulative errors inherent during elemental analysis and also in the

varying ash content in coal [83], [84]. It is however clear from the Tables 4.10, 4.8, 4.9 and 3.2 that oxygen is the most abundant heteroatom in coal and its presence in the coal residue is certain. A semi-quantitative analysis of the samples, yields higher oxygen values for residues obtained from liquefaction in NHT solvent, as compared against those from HT solvent. Since the plastic development of the western Canadian coal types are inhibited due the -OH substitution in the coal matrix [85], residues thus, having higher oxygen content do not exhibit properties of melting or those related to plastic character.

Table 4.8: Ultimate Analysis of the residue from HT solvent DCL process under N_2

	Ultimate Analysis (wt.%) [a]							
Element	CV Res 300		CV Res 350		CV Res 400		CV Res 450	
	x	s	x	s	x	s	x	s
Carbon	61.42	0.02	41.32	2.78	39.75	2.40	51.76	2.98
Hydrogen	3.51	0.35	2.34	0.65	1.83	0.15	2.30	0.37
Nitrogen	1.07	0.13	0.69	0.02	0.57	0.02	0.77	0.56
Sulphur	0.18	0.21	0.42	0.10	0.53	0.04	0.37	0.11
Oxygen	33.82	0.17	55.23	1.82	57.32	2.56	44.8	1.13

[a]Averages (x) and sample standard deviations (s) of triplicate analyses

Table 4.9: Ultimate Analysis of the residue from NHT solvent DCL process under N_2

	Ultimate Analysis (wt.%) [a]							
Element	CV Res 300		CV Res 350		CV Res 400		CV Res 450	
	x	s	x	s	x	s	x	s
Carbon	64.57	0.82	61.56	0.52	56.17	1.03	71.10	0.79
Hydrogen	3.38	0.08	3.11	0.32	2.51	0.66	2.81	0.37
Nitrogen	1.12	0.34	1.09	0.61	0.86	0.02	0.85	0.13
Sulphur	0.11	0.26	0.16	0.23	0.29	0.06	0.28	0.32
Oxygen	30.82	1.09	34.08	0.56	40.17	1.14	24.96	0.87

[a]Averages (x) and sample standard deviations (s) of triplicate analyses

Table 4.10: Ultimate Analysis of the residue from HT solvent DCL process under H_2

Ultimate Analysis (wt.%) [a]								
Element	CV Res 300		CV Res 350		CV Res 400		CV Res 450	
	x	s	x	s	x	s	x	s
Carbon	65.91	1.78	55.94	3.06	47.91	1.15	42.21	1.45
Hydrogen	4.02	0.42	3.09	0.21	2.40	0.66	1.82	0.42
Nitrogen	1.27	0.10	0.92	0.11	0.66	0.06	0.61	0.58
Sulphur	0.19	0.04	0.166	0.02	0.37	0.02	0.48	0.08
Oxygen	28.61	1.95	39.89	3.28	48.66	54.88	34.02	1.62

[a]Averages (x) and sample standard deviations (s) of triplicate analyses

During the DCL process, with the severity of liquefaction conditions, the demand for hydrogen increases.In presence of a hydrogen shuttler solvent, conditions close to those of pyrolysis prevails leading to insufficient transfer of hydrogen to products [77]. Hence, significantly lower values of H/C ratios are reported for residues from high liquefaction temperatures, as seen in Table 4.11. This is thus, indicative of the highly aromatic nature of the refractory material. Lower H/C ratios are preferable, also suggesting lower loss of hydrogen during the liquefaction process.

Table 4.11: H/C ratio for Residues

Residues (liquefaction temp.)	HT solvent N_2	NHT solvent N_2	HT solvent H_2
RES 300	0.0685	0.0628	0.0739
RES 350	0.0679	0.0606	0.0663
RES 400	0.0552	0.0536	0.0601
RES 450	0.0533	0.0474	0.0517

The efficiency of removal of nitrogen from the product stream during liquefaction is highly dependent on the solvent type employed i.e chemical character of the product is dictated much by the solvent employed [86]. Denitrogenation reactions are targeted for removal of nitrogen to produce pure hydrocarbons during the liquefaction process. At low liquefaction temperatures, this is easier to achieve since stable complexes of basic nitrogen compounds are formed during liquefaction in presence of metal salts from the mineral matter in coal [77]. These complexes have very low solubility and remain as THF-insoluble fractions. This accounts for higher N/C ratio (0.014-0.017) in the residues at 300 °C - 350 °C, irrespective of the solvent obtained from, as against 0.0119 for raw coal. The contribution of solvents towards N/C can be neglected due to the relatively low values of N/C ratios, 8.3e-03 for NHT solvent

and 6.6e-03 for HT solvent. However, with increase in temperature, the nitrogen complexes experience increased solubility in the solvent mixture and are transferred to the products [77]. This justifies the decrease in N/C ratio in residues with increase in temperature of liquefaction until 400 °C. Further increase in temperature forms heavy nitrogen complexes, which contributes to the increase in the N/C ratio. This phenomena may be hypothesized to occur in our case, which theoretically justifies for the increase in the nitrogen content in residues for HT solvents under N_2 and H_2 at 450 °C. Studies have shown the increased content of nitrogen in middle distillates [6]. Wu et al. [87] have reported the presence of sp-hybridised nitrogen compounds in residues.

The boiling point of the solvent is influential towards denitrogenation of the product stream. The N/C ratio of the residues definitely suggest the participation of the heterocyclic nitrogen present in the solvent. Studies have shown nitrogen content in the residue to be a function of the solvents' volumetric average boiling point. Increasing the volumetric average boiling point of the solvent decreased the nitrogen content in the residue [88]. This was explained by the increase in the soluble nitrogen content in the product slurry primarily due to presence of primary and secondary alkyl amide generation during liquefaction, which could be associated with the improved hydrogen donor capabilities of heteroaromatic solvents. To completely define this effect by use of NHT solvent, it would be necessary to analyse the types of nitrogen compounds present in the product stream qualitatively and quantitatively to equate it with the total nitrogen content in the feed stream. Losses if any, could then be associated with the gaseous products generated during the process. This could be a possible reason, that can be closely related to the decreasing nitrogen content of the residual waste for the case of NHT solvents, which is evident in the Table 4.12.

Table 4.12: N/C ratio for Residues

Residues (liquefaction temp.)	HT solvent N_2	NHT solvent N_2	HT solvent H_2
RES 300	0.0149	0.0149	0.0165
RES 350	0.0143	0.0152	0.0140
RES 400	0.0123	0.0131	0.0118
RES 450	0.0128	0.0102	0.0124

The sulphur plays a very interesting role during liquefaction process. Sulphur is present in the organic matrix as well as in the mineral matter in coal. The organic sulphur is bound to the matrix mainly in the form of thiophenes, thiols, sulfides and disulphides [89]. However, the increase in the S/C ratio suggests the

transfer of sulphur from the mineral matter of residue, which would be discussed more in Section 4.5.4. Determining the quantitative gas composition for H_2S and coal liquids for sulphur content would be effective to draw inferences on the lower S/C ratios for the residues from NHT runs.

Table 4.13: S/C ratio for Residues[a]

Residues (liquefaction temp.)	HT solvent N_2	NHT solvent N_2	HT solvent H_2
RES 300	1.09	0.64	1.08
RES 350	3.81	0.95	1.11
RES 400	5.00	1.91	2.90
RES 450	2.68	1.47	4.26

[a] The values are in the order of 10^{-3}

4.5.4 XRF & XRD ANALYSIS

Attempts have been made in the past to correlate the liquefaction reactivity to the mineral content in the coal liquefaction residue [23], [24]. Thus, the ash content in the residues forms a very important part of the characterization of residue. As observed in the images from the Scanning Electron Microscopy of raw coal and residue samples, the presence of high mineral matter in residue compared to that of raw coal is evident. Also, the proximate analysis proves this by providing us with the quantitative values for ash contents 4.5.2. With a curiosity to understand the composition of the ash in the residue and to investigate its contribution during the liquefaction reactions, an X-ray fluorescence (XRF) analysis of raw coal and residue was carried out.

XRF analysis is carried out by striking the sample surface with radiation energy above the ionization potential of the samples causing an empty inner orbital. This orbital is filled with the electron jump from a higher orbital, with a release of energy. The energy emitted during the process is characteristic of the element and further the intensity of the characteristic radiation is indicative of the amount of that element present in the sample. Hence, XRF is insensitive to elements with atomic numbers less than Na. The Fig. 4.12 represents the amount of the elements present in the CV raw coal and the residues. Si, Ca, Al, Fe and S were observed in the decreasing order as presented, for all the residues obtained. This is accounted for, from the material in the feedstock for liquefaction.

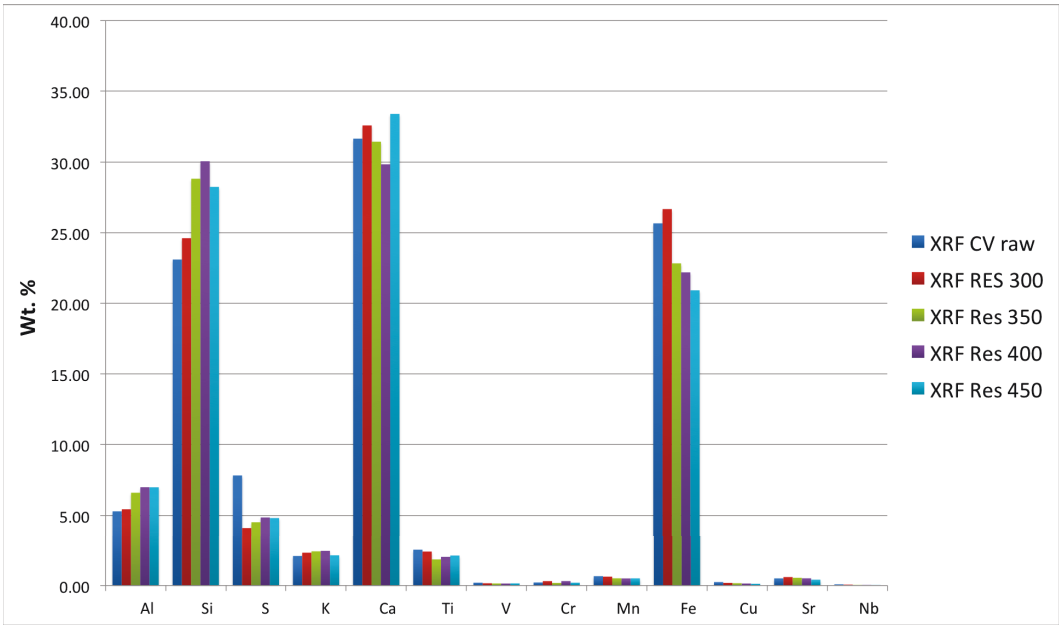

Figure 4.12: XRF of CV raw coal and residues

Iron and sulphur containing materials are available largely in the form of marcasite and pyrite in raw coal. At temperatures above 400 °C under vacuum, all of marcasite crystals readily undergo shift in the orthorhombic orientation pattern to transform to pyritic sulphur structure (cubic crytal) [90].

Table 4.14: S/Fe ratio in Residue Samples and CV sub-bituminous

Sample	S/Fe
Raw CV	0.533
Res 300	0.269
Res 350	0.269
Res 400	0.369
Res 450	0.441

At temperatures above 300 °C the pyritic sulphur tends to undergo reduction reaction to form pyrrhotite, a gold coloured mineral visualized as a golden sheen on the residue in Fig. 4.13. It is an endothermic reaction and requires temperatures as high as 900 °C for its complete conversion. This could be supported by formation of pyrrhotites at high liquefaction temperatures at and above 350 °C, as observed under Optical Microscope VHX-2000, Keyence Corp.4.13. Iron pyrites tend to follow the reaction pathway as mentioned below by equations 4.9 [91] and 4.10, where $0 < x \leq 0.22$. Also, Montano et al. [92] have deduced a rectilinear relation between the coal

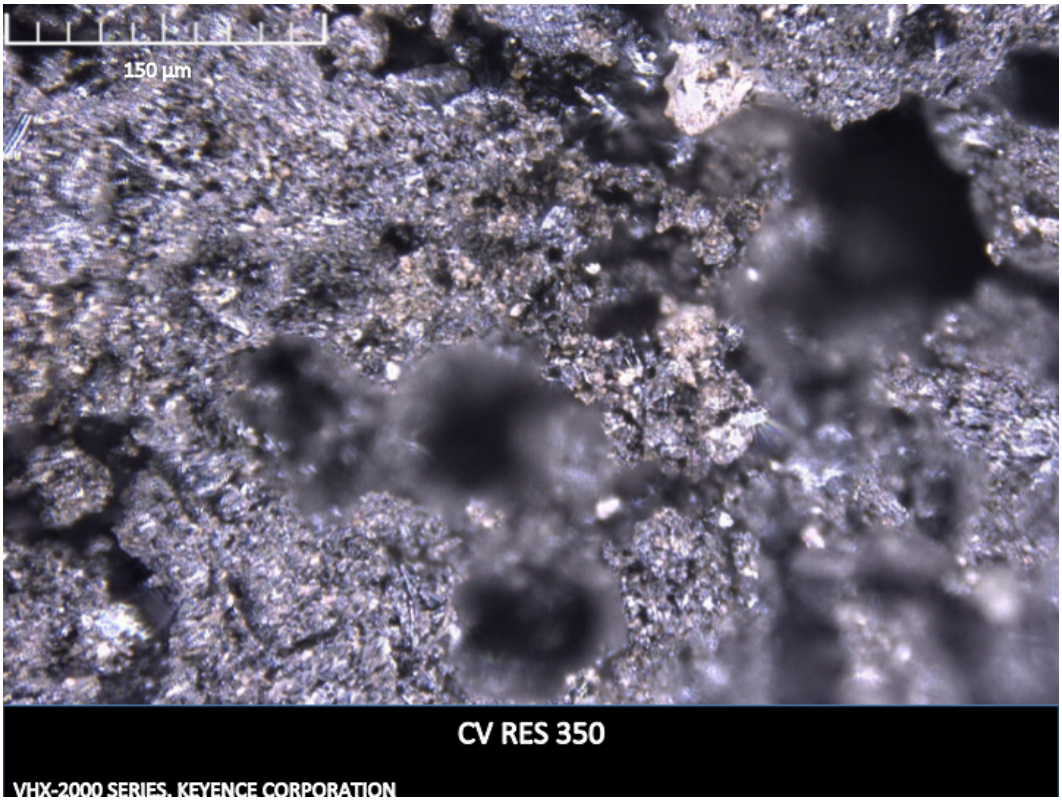

Figure 4.13: Pyrrohtite presence in Res 350

conversion liquefaction to the increasing content of iron pyrrhotite in the residues. The ratio of S/Fe from Table 4.14, however, suggests an increase in the sulphur content with respect to Fe. This is due to the contribution of organic sulphur since sulphur in the mineral matter does not participate in the reaction. These values cannot substantiate the presence of pyrrhotite as seen in Table 4.14, since higher sulphur content to iron may be due to the association of sulphur with other mineral elements in coal.

$$FeS_2 \rightarrow FeS_x \ + \ (1 - 0.5x)S_2 \tag{4.9}$$

$$FeS_x \rightarrow Fe \ + \ S_x \tag{4.10}$$

However,in presence of an hydrogen, these reactions are as follows [93], where at 450 °C liquefaction temperatures, pyrite was found to be in equilibrium with pyrrhotites.

$$FeS_2 + \ (x)H_2 \rightarrow FeS_{2-x} \ + \ (x)H_2S \tag{4.11}$$

Hence, XRD analysis of residues and raw coal was necessary to interpret this phenomena. They provide the structural information about the sample through Bragg's law by measuring the 2θ angle of diffraction. The hkl lattice values for pyrrhotite was compared to match with that for raw coal and residue's 2θ values using MDI Jade 9 software. The residual waste do show traces of pyrite formation and a structured carbon detected as graphite in the residues obtained from liquefaction at 300 °C, 350 °C, 400 °C and 450 °C as seen in Figs. 4.15, 4.16, 4.17 and 4.18 absent in Fig. 4.14 for XRD pattern of raw coal.

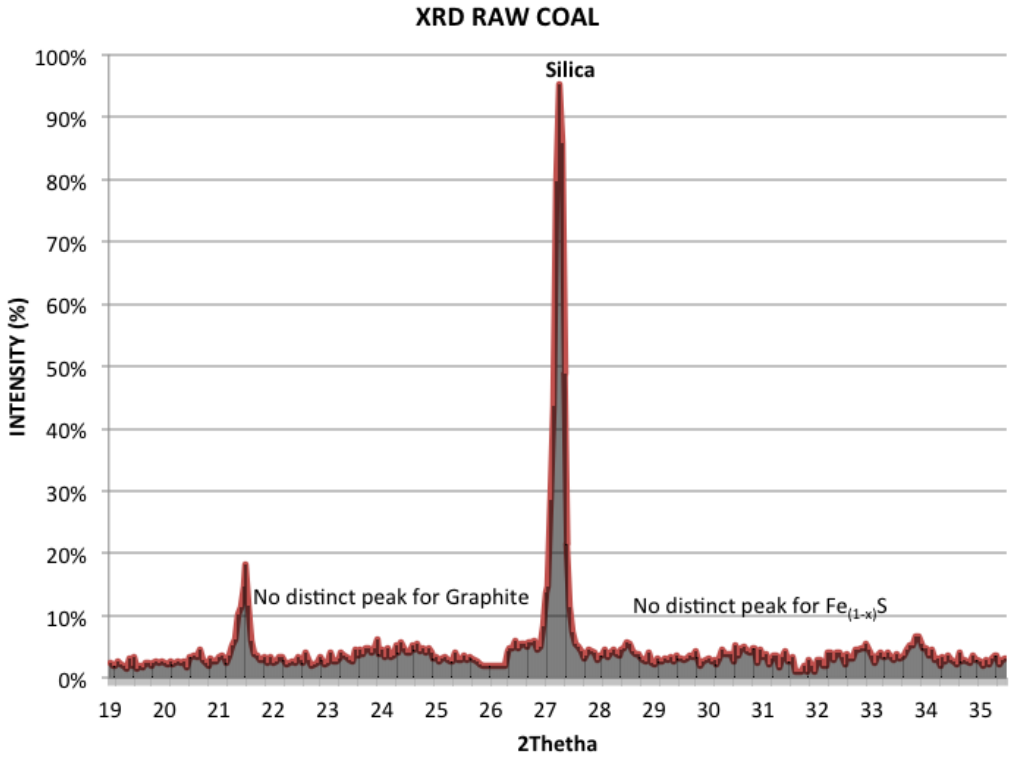

Figure 4.14: XRD for raw coal

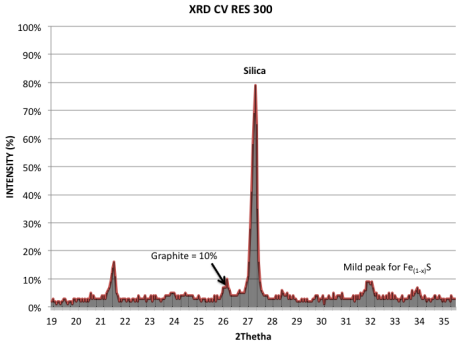

Figure 4.15: XRD for Res 300

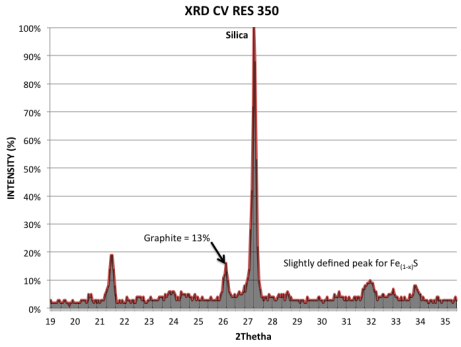

Figure 4.16: XRD for Res 350

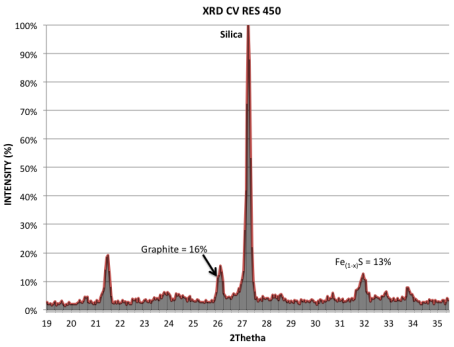

Figure 4.17: XRD for Res 400

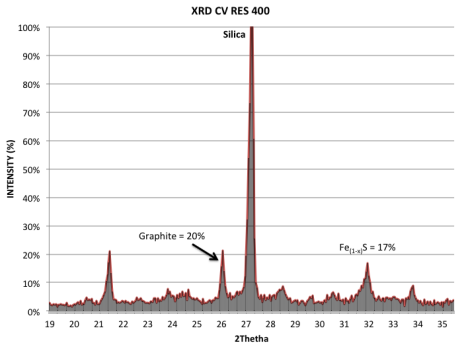

Figure 4.18: XRD for Res 450

4.5.5 FTIR CHARACTERIZATION

The infra-red spectra from 600 to 4000cm^{-1} and their semi-quantitative analysis for raw coal and the residues obtained from the direct coal liquefaction process are discussed here. Figs. 4.19, 4.20 and 4.21 represent the FTIR analysis for residues from HT solvent(under N_2), HT solvent (under H_2) and NHT solvents respectively. The baselines of the graphs have not been rectified and hence peaks do not appear in the linear frame for the sample under study. The infra-red spectroscopy provides necessary information about the various functional groups present in the raw coal and the modifications they undergo during the course of liquefaction giving us mineral rich residues. They rely on bonds with electric dipoles to be efficiently absorbed, generating the transmittance and/or absorbance data as the bond stretches and contracts [94]. FTIR analysis of coal to determine the structural functional groups and of the gasified chars have been carried out extensively [95] - [96].

The vibrations at 3600 cm^{-1} - 3700 cm^{-1} indicate the presence of mineral matter in the residue exhibited by the residues at higher intensities compared to that of raw coal [97]. Similar observations were made by Rahman et al. [67]. Precisely, the mineral matter at these wavenumbers are mainly associated with the hydroxyl groups, as Al-OH-Al or Al-OH-Mg and hence appear typically in the characteristic region of OH functional groups [98].

The peaks at 1050 cm^{-1} for all residues and coal structures are attributed to the presence of silicates. Peaks of CaO and FeO could be traced at 916 cm^{-1} and 870 - 790 cm^{-1} [99]. It is evident through Figs. 4.19, 4.20 and 4.21 the increasing intensity of ash content and mineral matter in the residue with increase in liquefaction residue and its direct co-relation with yield of coal liquid obtained at that particular process conditions. The intensity of ash peaks is however lower in residues from NHT liquefaction, which confirms the data from proximate analysis and substantiates the

lower conversion rates for NHT liquefaction under similar conditions as compared to that of HT solvent. The IR spectra do not show identifiable C=N, C-O, and C-S bonds because the bands corresponding to these functionalities overlapping [100].

A small asymmetric bend observed at 2890 cm^{-1} for residues from HT liquefaction under H_2 (at 350 °C, 400 °C and 450 °C) is clearly due to the aliphatic bending of CH directly bonded to the aromatic rings [101]. This proves the extent of solvent penetration at higher temperature associated with the coal's softening property, leading to opening of aromatic rings in case of liquefaction under H_2 [31]. Thus, lower yields at 300 °C were reported in Table 3.8 for HT liquefaction under H_2. However, in the case of HT and NHT liquefaction under N_2, the presence of aromatic CH stretching is evident from the peaks at 3040 cm^{-1}-3050 cm^{-1}, with comparatively very high intensity at the highest liquefaction temperature of 450 °C. This clearly proves the theory of the system dynamics due to insufficient hydrogen in accordance with the demand at higher liquefaction temperatures (as explained in Section 3.3.2), thus offering lower product yield and higher carbon content in waste (Section 4.5.3).

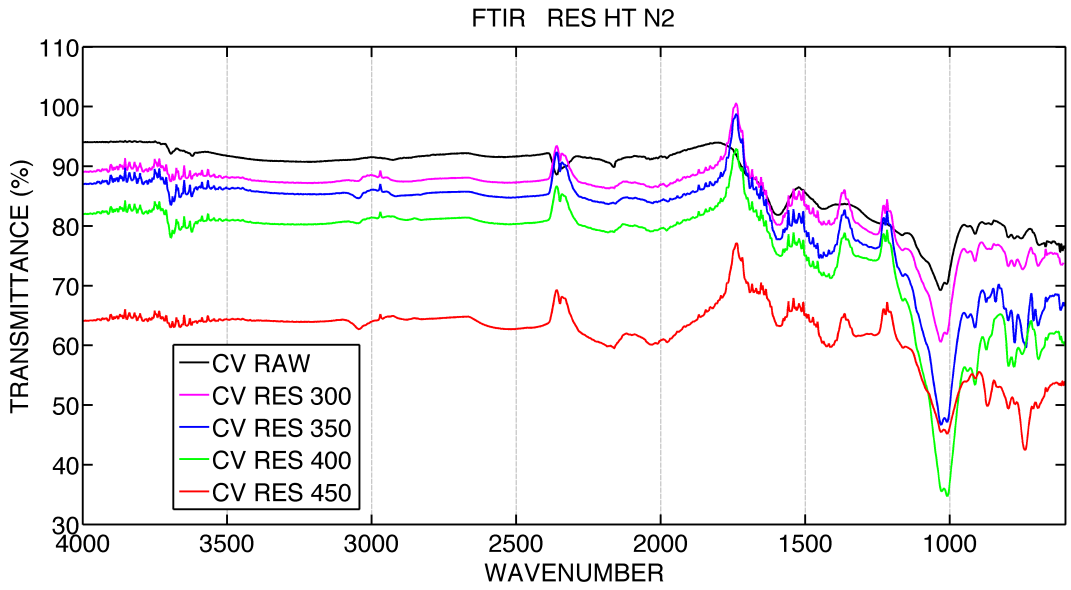

Figure 4.19: FTIR for residues from HT solvent

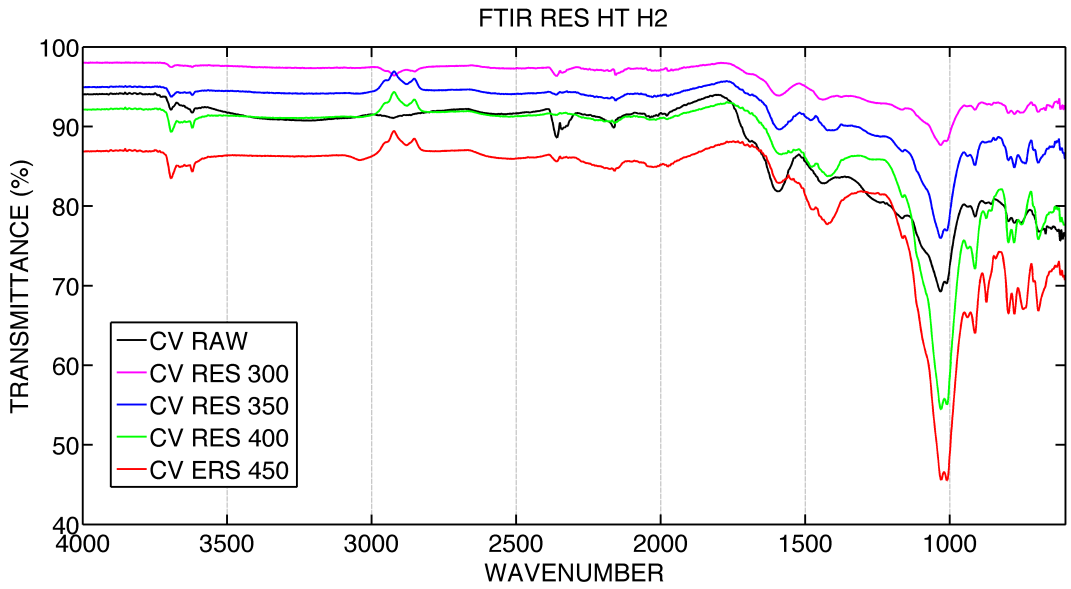

Figure 4.20: FTIR for residues from HT solvent in H_2

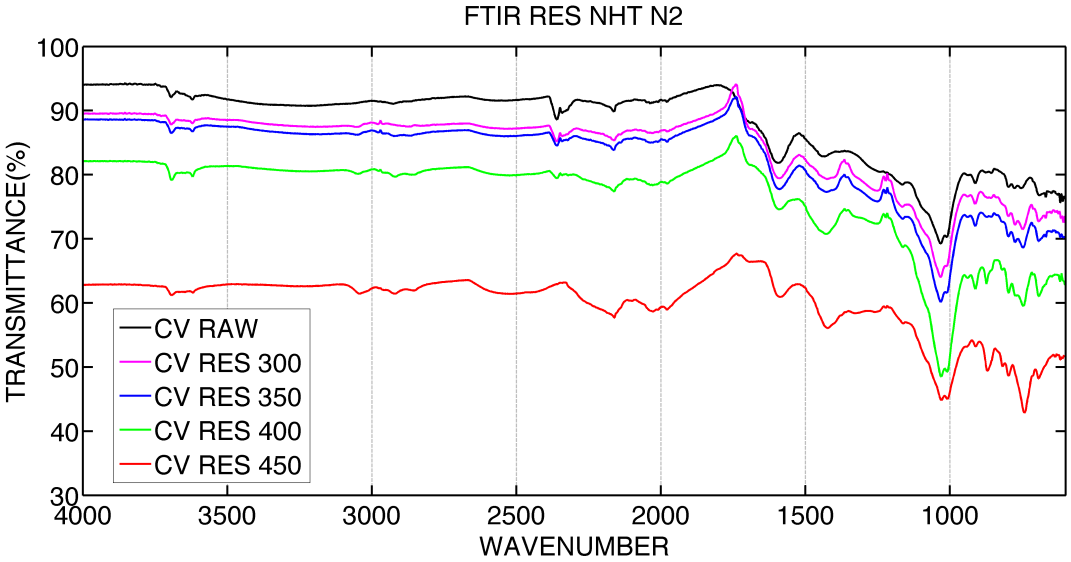

Figure 4.21: FTIR for residues from NHT solvent

4.5.6 PARTICLE SIZE ANALYSIS

Particle size of the waste has a great deal to convey about the attritions the feed particle undergoes from the time it is subjected to high pressure and temperature. Our experiments under different reaction conditions (variation of temperature and gas atmosphere) and solvents has been helpful in substantiating our previous con-

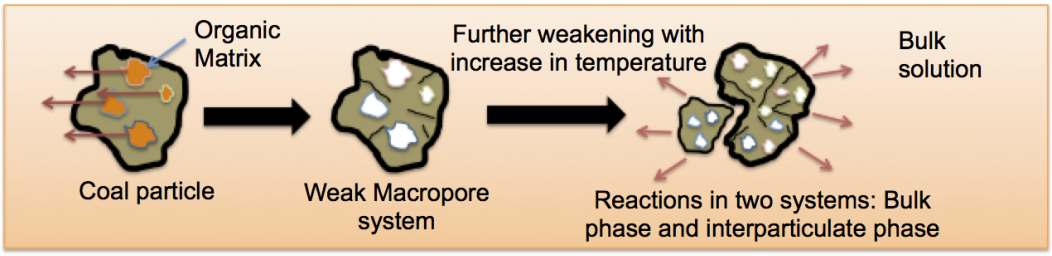

Figure 4.22: Existence of a Two-phase reaction system

clusions. A coal liquefaction process involves a number of physical processes towards particle distintegration and dissolution which have been related to the function of macerals [15], [102]. However, since a petrographic analysis of the residue was not carried out, it is difficult to correlate the particle size with respect to maceral content.

After the wet dispersion of the sample, a light sensor detects the particle. Light obscuration above 3% upto 12% was considered the most optimum range for effective particle size analysis. This method adopts Mie theory for calculation of the particle size distribution data, using the refractive index of the sample (taken as 1.5) and that of the dispersion medium(water).

Raw coal, sieved to $\leq$ 150 μm has a $d_x(50)$ of 61.9 μm 4.23 was our starting material. Solubility of the solvent and the softening temperature of the coal play a major role in the coal conversion. When introduced into the solvent material, the coal undergoes a volumetric increase associated with the swelling property of coals in organic solvents. Studies have proved upto 5% linear expansions of coal in organic solvents [103].

Also, the particle size distribution at 300 °C does not exhibit much variation with respect of that of the feed material, which proves that the particle integrity remains intact even at thermal contact with solvents and rapid quench. Further increase in temperature to 350 °C, where in the coal's softening temperature is reached, we observe a increase in the particle size. This could be associated with the phase where in the solvent penetration into the coal matrix occurs and the also factors contributing to the thermal expansion of the particle, as mentioned before. However, expansions more than 5% at 350 °C are due to particle agglomeration during measurements.

As the reaction progresses and organic matrix is removed, at temperatures above the softening temperature for coal, the particle is weakened and a macro-pore system extends into the bulk. This process is also accelerated at high temperatures by

the constant stirring of the slurry. The reactions thus occurring in the bulk solution and those within the particle contribute to the overall product composition and its distribution [15]. Thus, at liquefaction temperatures above the softening temperature of coal (i.e 400 °C and 450 °C), the particle size decreases for the residual waste and represents a bimodal particle size distribution for case of HT solvents (at 400 °C and 450 °C liquefaction residue) as depicted in Fig. 4.22.

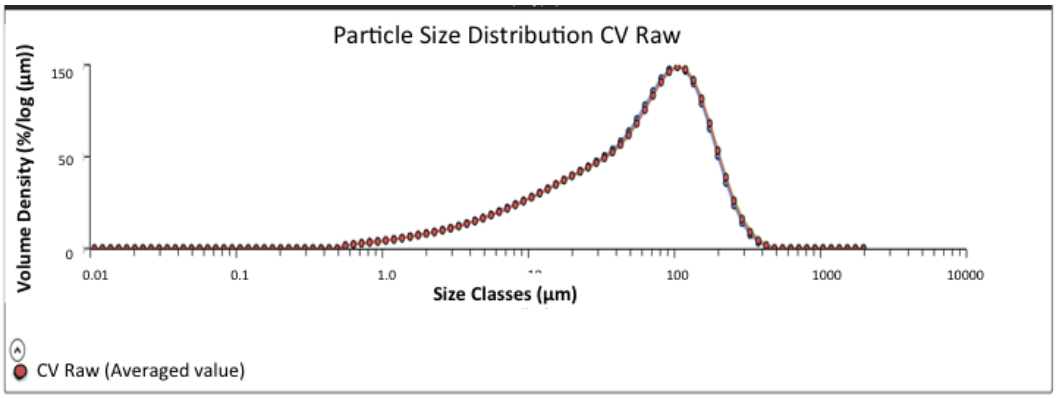

Sample Name	D_x (10) (µm)	D_x (50) (µm)	D_x (90) (µm)	Laser Obscuration (%)
CV Raw Run1	6.79	60.7	170	3.98
CV Raw Run 2	6.96	63.1	177	3.99
CV Raw Run 3	6.88	62.0	175	4.00
Mean	6.88	61.9	174	3.99
1X Std Dev.		1.21	3.59	0.01

Figure 4.23: Particle size distribution for CV raw

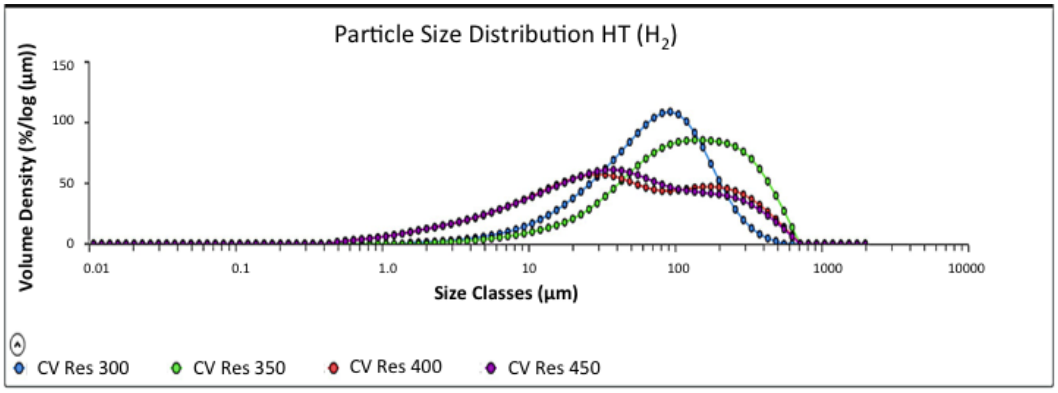

Sample Name	D_x (10) (µm)	D_x (50) (µm)	D_x (90) (µm)	Laser Obscuration (%)
CV Res 300	17.1	69.6	181	12.35
CV Res 350	26.2	116	362	6.87
CV Res 400	4.53	38.0	271	14.03
CV Res 450	4.53	37.4	251	19.06

Figure 4.24: Particle size distribution for residue HT in H_2

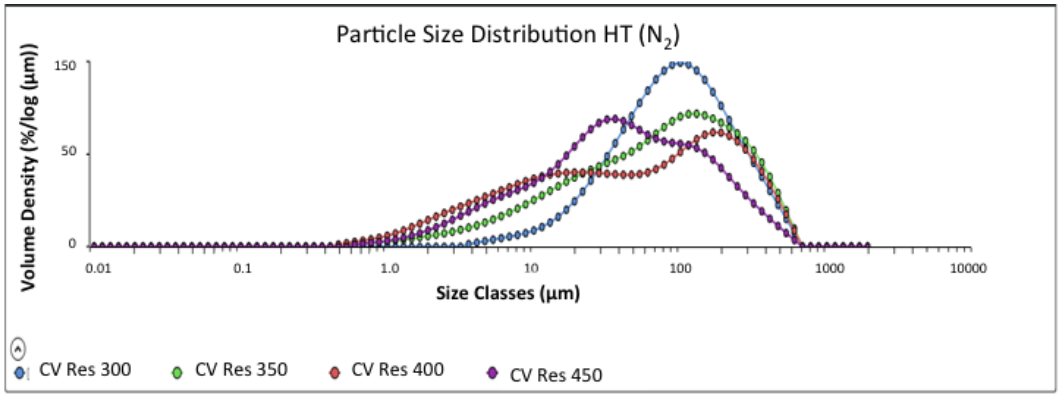

Sample Name	D_x (10) (µm)	D_x (50) (µm)	D_x (90) (µm)	Laser Obscuration (%)
CV Res 300	26.2	95.4	294	6.53
CV Res 350	9.13	80.5	320	7.27
CV Res 400	4.10	52.2	304	11.74
CV Res 450	5.77	40.9	210	11.94

Figure 4.25: Particle size distribution for residues HT in N_2

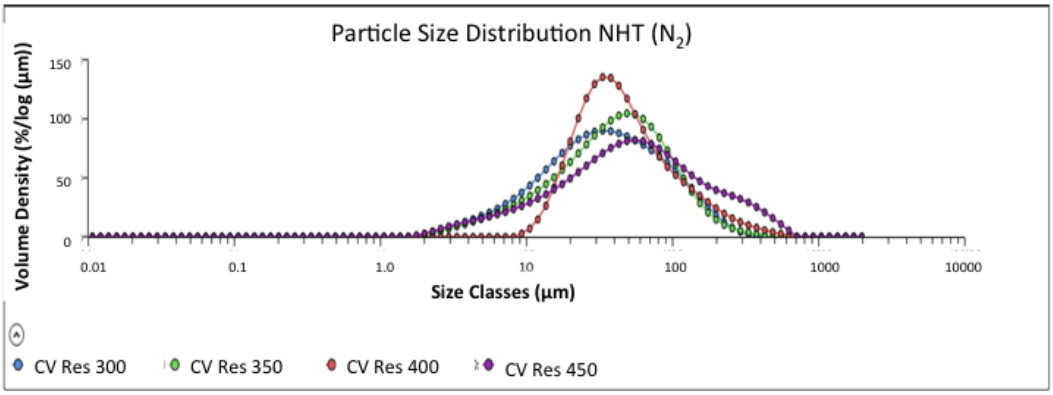

Sample Name	D_x (10) (µm)	D_x (50) (µm)	D_x (90) (µm)	Laser Obscuration (%)
CV Res 300	8.76	34.1	116	24.30
CV Res 350	9.78	40.3	112	22.14
CV Res 400	19.5	42.2	138	4.71
CV Res 450	9.69	51.7	235	11.66

Figure 4.26: Particle size distribution for residues for NHT in H_2

4.5.7 SURFACE AREA ANALYSIS

The surface area and porosity of raw coal have been compared with that of the residues. We see a trend of decreasing surface area for residues obtained from higher liquefaction temperatures. Many methods have been employed to study the surface area of coal. However, the traditional BrunauerEmmettTeller theory (BET) or the Barrett-Joyner-Halenda model (BJH) do not take into consideration the variations in the morphology of pore structures. Density functional theory (DFT) method has been critical in calculating pore size distribution from adsorption-desorption isotherm. Comparisons with various other models have proved that DFT method is a better model for estimation of parametric calculations and classification of pore sizes [104]. Also, at present DFT presents a realistic model for prediction of pore size distributions with improved accuracies [105].

The adsorptive used to characterize the porous solid structures depend on three main following criteria [106]:

1. Chemical Inertness
2. Large saturation pressure
3. Adsorption temperature (feasibility)

4. Molecular structure (spherical is ideal)

Use of N_2 as the adsorptive have posed problems due to the inability of the latter to diffuse into micro-pores at low temperatures [107]. Also, the permanent quadrapole moment of N_2 molecule at elevated temperatures do not adopt accuracy in results for fine micro-pores. Thus, CO_2 has been used here as the adsorptive, the critical dimensions of the N_2(30 nm) and CO_2(28 nm) being almost the same. The surface area classification using the DFT method is indicated in the Figs. 4.27 and 4.28. The micro-pores with pore size 5-20$\mathring{A}$ contribute largely to the surface area. The mesopores with pore sizes more than 20$\mathring{A}$ contribute less than 20% to the surface area [108]. The structure of the residues derived from the liquefaction were found to have similar contribution of micro-pores and mesopores towards the surface area. Hence, pore volume calculations were critical in determining the effect of the lower surface areas for the residues as shown in Table 4.15.

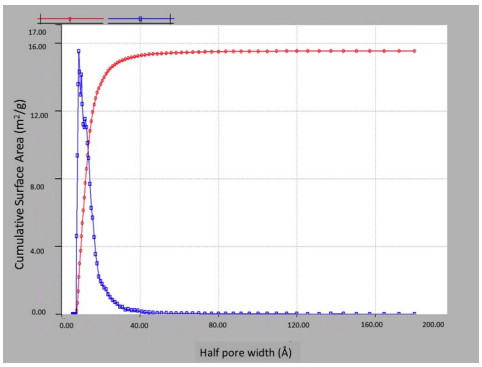

Figure 4.27: Surface area:CV raw coal

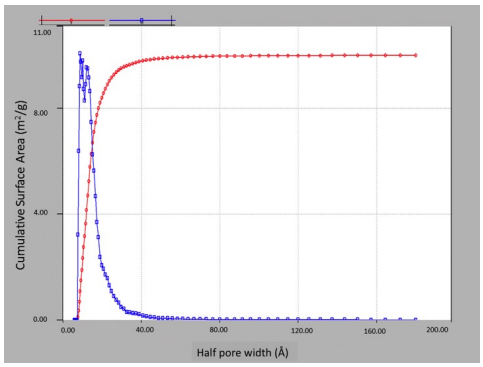

Figure 4.28: Surface area:Res 300

Now, sub-bituminous coals when heated at high temperatures, do not exhibit plasticity. However, during liquefaction under pressurized conditions, they tend to become plastic in nature. Here, the plasticity is related with the property associated with the enhanced solubility of the parent coal with the solvents thus encouraging reduction of molecular weight of the coal structure [109]. With increased plasticity, the reduction of the micro-porosity of the coals [72] is apparent with the generation of a closely bonded aromatized structure, with reduction in pore volume. The effect of these are observed from the Table. 4.15, thus, representing lower pore volumes and surface area for the residue obtained from 400 °C liquefaction temperature, which exhibited maximum conversion of volatiles, moisture and fixed carbon (Table 4.3).

Table 4.15: Surface area analysis of Raw Coal and Residues

Sample	Surface area (m^2/g)	Pore volume (cc/g)
Raw coal	15.540	0.023
RES 300	10.00	0.016
RES 350	5.90	0.010
RES 400	2.56	0.003
RES 450	6.25	0.010

4.6 GENERAL DISCUSSIONS

In order to understand any process dynamics, it is imperative to have a thorough knowledge of the properties of the raw materials in use. Thus, before we proceed towards upgrading of the residue or its utilization in any particular process stream, a knowledge or a basic awareness about its chemical and physical composition is critical.

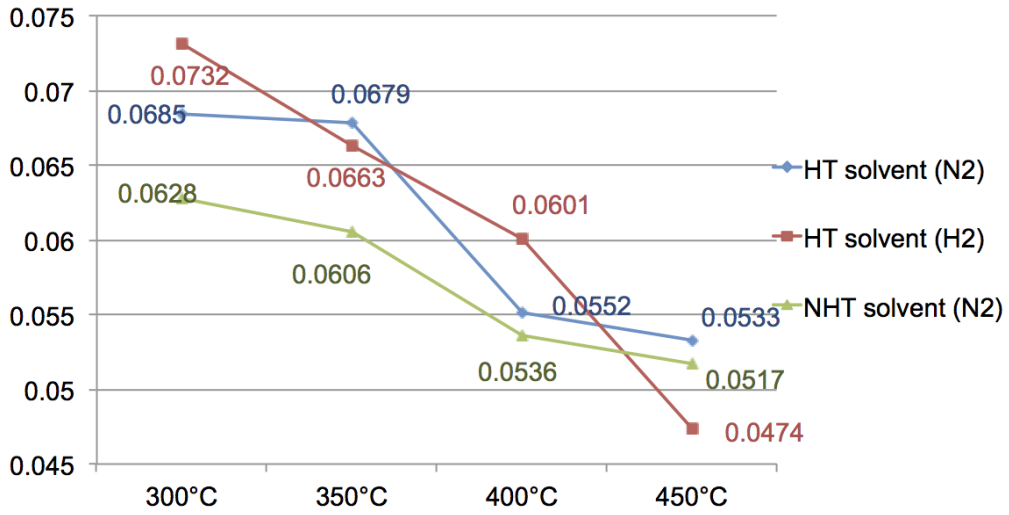

Figure 4.29: H/C ratio of the residues

As coal is a complex blend of organic and inorganic material, with the extraction of a large extent of organic matrix during liquefaction, the residual structure could be thought of an amalgamation of the unconverted organics and prevalent inorganic matrix. Hence, analytical techniques have been carefully chosen to investigate the nature of inorganic components and also understand better the structural transformations of the organic matrix of coal during liquefaction. Low conversions and high organics in the wastes, as seen in Chapter 3, initiated studies to determine elemental compositions of hydrogen, carbon and heteroatoms in the residue. Comparatively

slightly higher H/C ratios in residues obtained from liquefaction under H_2 proved the incorporation of hydrogen in the waste stream, seen in Fig. 4.29. The nature of this association was investigated with the help of FTIR, which provides information about the functional groups present in an sample.

Further, the proximate analysis aided in the calculation of conversion of the precursory tar material in coal during liquefaction, as seen in Fig. 4.11. An assumption that the ash remains unconverted during the process was confirmed with the help of XRF calculations. The ratio is calculated as follows:

$$\text{Mineral matter Ratio} = \frac{\frac{Si\ in\ residue}{Mineral\ component\ in\ residue}}{\frac{Si\ in\ raw\ coal}{Mineral\ component\ in\ raw\ coal}} \tag{4.12}$$

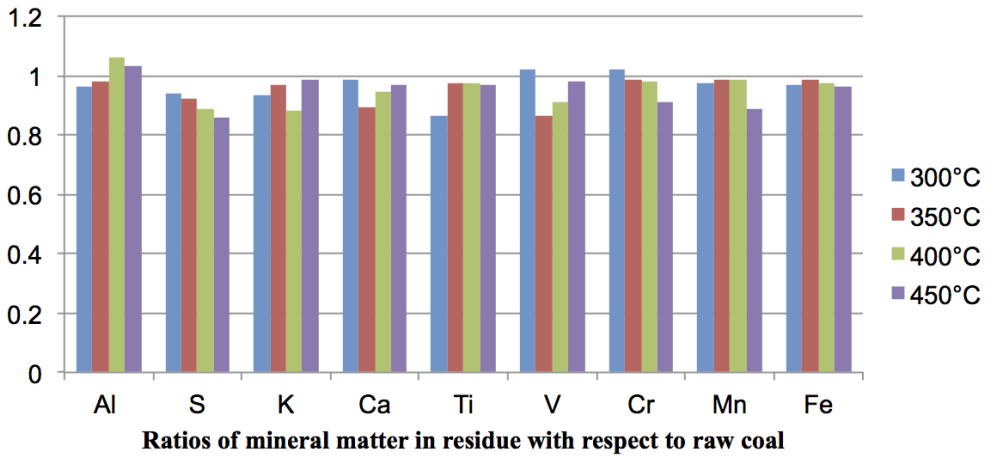

Figure 4.30: Ratio of silicates in residue and the mineral component in the residue to that of raw coal tends to unity

Any deviation from unity would indicate the loss of mineral matter in the product stream. However, since all values tend to unity, as shown in Fig. 4.30, our assumption is validated. XRD analysis showed presence of conversion of pyrite to pyrrhotite. Also, graphite carbon structure with increasing severity of liquefaction was studied. Laser diffraction technology was adopted for particle size analysis. An optimum laser obscuration was found to be in the range of 3-12%. The scattering due to the incident light on the particles are captured by a light sensor for particle size calculations. Lower obscuration lead to lower scattering of light particles. Thus, particle sizes corresponding to the obscuration values in the range specified are considered to be accurate. As the organic matrix of the coal is extracted during liquefaction, a macro-pore system extends into the bulk which under increasing

severity of liquefaction conditions, tends to undergo fragmentation. The bimodal particle size distribution at high liquefaction temperatures are a result of the competitive reactions occurring between the inter-particulate system and those with the particle and the bulk system.

Thus, characterization studies in conjugation with the study on effect of operating conditions was conducted to make future designers aware with regard to the potential trade-off between nature of residue to be handled and the relative process parameters to be accounted for, based on industrial policies, in order to achieve the desired efficiency in conversion to products.

4.7 CONCLUSIONS

In accordance to the analysis of chemical and physical properties of the residues derived from two different liquefaction solvents, namely NHT and HT at different parametric conditions, initial pressure of 20 bar and residence time of 60 minutes at four temperatures 300 °C, 350 °C, 400 °C and 450 °C, we derive the observations listed below:

1. SEM studies prove that the morphology of the residues do not undergo a major transition during the liquefaction process. However, higher percentage of mineral matter was evident from the backscattered electron images of the residues when compared with those of raw coal.

2. Solvent properties were found to highly dictate the composition of the liquid products, in comparison to that of the liquefaction atmosphere. Presence of H_2 atmosphere had a very little influence on the conversion of the tar precursors (fixed carbon), while high conversion values could be associated with the major hydrogen transfer dominated due to that from the solvents.

3. Efficient conversions of volatile material with increasing liquefaction temperature conditions is apparent.

4. The residues derived from liquefaction under NHT solvent represent very low ash values compared to that under HT solvent.

5. The H/C ratio decreased with increasing severity in liquefaction conditions, as desired. However, slightly higher H/C for the residues derived from liquefaction under H_2 proved the association of hydrogen in the waste stream.

6. Incorporation of the heteroatoms in the product stream was influenced to a large extent due to the solvent properties. Higher S/C and N/C ratios have been reported for residues from liquefaction under HT solvent, a recycle industrial solvent hydrotreated for heteroatom removal in comparison to NHT solvent that has a comparatively higher composition of heteroatoms.

7. For all conversion calculations, a basic assumption that ash remains unconverted during the liquefaction process was made. This was later confirmed from the XRF analysis which accounted for the ash properties in raw coal and the residue. Thus, a ratio of the silicates in the residue and each mineral component in the residue was compared to those in raw coal, yielded values close to unity.

8. FTIR characterization of the residues also represented the higher intensity of the aromatic matrix in the residues, thus proving the insatiability of the hydrogen demand at high temperatures, thus generating wastes with higher ratio of carbon to hydrogen content.

9. The particle size of the residues at first increase, at low liquefaction temperatures, suggesting solvent swelling effects and agglomeration, followed by a decrease in the particle size with increasing severity of liquefaction conditions. A two phase reaction system can be said to co-exist which leads to a bimodal particle size distribution at temperatures above the softening temperature of coal.

10. Density functional theory (DFT) method was employed to carry out classficiation of pore morphology for raw coal as well residues. CO_2 was chosen as the adsorptive since ineffective diffusion of N_2 into micro-pores at low temperature adsorption requirements.

11. A similar contribution towards the micro-porosity and mesopore distribution is evident in the residues as well in raw coal. However, the decrease in surface area is due to the reduction in the pore volume, suggesting agglomeration or closed pores developed during plasticity of sub-bituminous coal under pressurized liquefaction conditions.

Chapter 5

GASIFICATION CHARACTERISTICS OF RESIDUE FROM COAL LIQUEFACTION PROCESS IN PRESENCE OF CARBON DIOXIDE

5.1 INTRODUCTION

Gasification of coal residue is one of the ideas that was investigated. This process is comparatively insensitive to coal properties and can utilise it when other methods are unproductive [110]. Many definitions of gasification are available in literature. However, one of the simplest explanation is provided as gasification to be a technology useful in conversion of carbonaceous fuel to gaseous products encompassing reusable heating value [111].

Thus, generation of (syngas) from the refractory material rich in mineral and carbon material, residue, would be propitious towards optimization of the coal liquefaction process. However, given the intractable nature of carbon in the coal residue, a preliminary study to understand the behaviour of the material in presence of gasifying agents was perceived to be vital. In order to comment on the efficiency of this complex feed as a raw material in an entrained gasifier and thus determining

Table 5.1: Gas composition for raw materials, Gasification

Gas	Product Grade	MSDS reference	Inlet Pressure, atm
Nitrogen	5.0	P-4631	1.088
Carbon dioxide	4.8	P-4574	1.002
Air	Ultra zero Ambient Monitoring	P-4560	1.122

the design parameters for the same requires a vast study of the effect of various parameters such as feed particle size, thermoplasticity, system pressure, temperature constraints, reactivity, intrinsic and global kinetic parameters, coking behaviour of feed etc. on the gasification behaviour.

In this chapter, a kinetic study is carried out for the gasification of coal liquefaction residue in presence of carbon dioxide as the gasifying agent at 950 °C, 1000 °C and 1100 °C. An analysis of the type of model fitting the gasification data obtained from the TGA is undertaken to determine the intrinsic kinetic parameters of the process. Further, determination of the reactivity index for the residue and its comparison with coal is carried out.

Given the residue's elemental properties pertaining to a much lower H/C ratio compared to that of raw coal, it could be speculated that gasification of residue may require much higher temperatures for gasification i.e ease of gasification of refractory material in the residue would be difficult compared to raw coal. Hence, experiments have been undertaken to determine the gasification behaviour of residues.

5.2 EXPERIMENTAL METHOD

5.2.1 RAW MATERIALS

Coal liquefaction residue of approx. 5-6 mg was introduced in the analyser. Please refer Chapters 3 and 4 for further information on the preparation and properties of the residue.For the gasification run, nitrogen, carbon dioxide and air gas cylinders supplied by Praxair, Canada, were employed with the composition, as mentioned in Table 6.1. Gasification is insensitive to coal properties and can utilise coal where other methods are unproductive.

5.2.2 EQUIPMENT

Thermogravimetric analyzer (TGA) SDT Q600 from TA Instruments, USA featuring a horizontal balance (balance sensitivity of 0.1 μm) was extensively used to

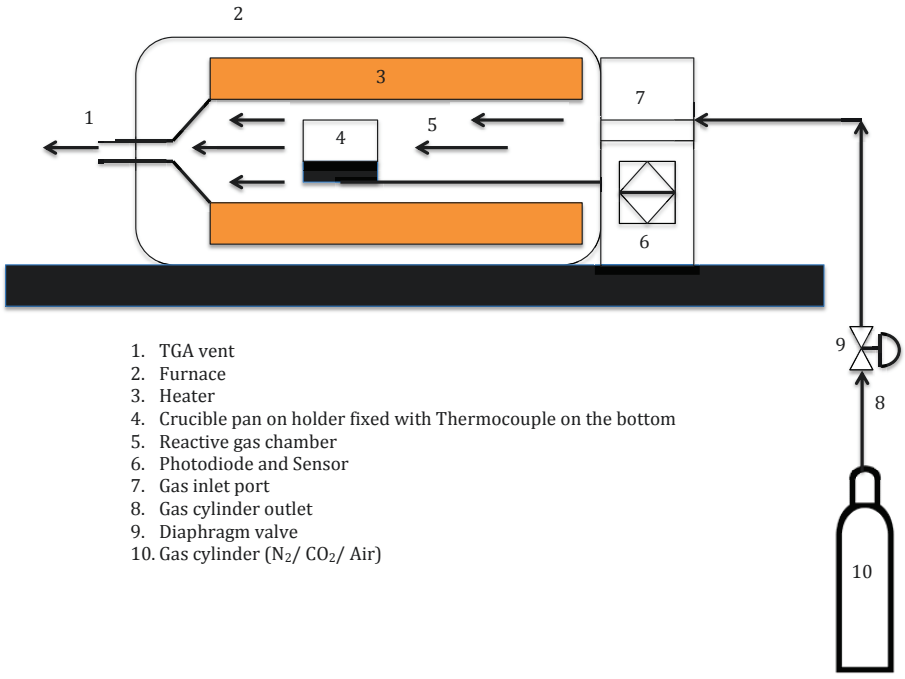

Figure 5.1: Thermogravimetric Analyzer set-up

investigate the gasification behaviour and nature of reactivity of the residues and compare it with raw coal. Two sample alumina crucibles each of 90 μL for a single run with provision for a reference crucible is featured in this device. The set-up has port 1 connected to nitrogen and port 2 to air and boasts of a separate internal port to introduce the desirable reactive gas. Mass flow controller with automatic gas switching feature was helpful during the experimental run. Type R platinum-rhodium thermocouples are inserted on the bottom of the thermo-balance or sample pan holder which are further connected to the temperature controller. The controls and sensor is hooked to a computer running the TA Universal Analysis interface which helps to maintain or modify the steps for the new as well as on going method. Differential Scanning Calorimetric measurements are also supported by the software. The weight signal thus displayed is the difference between the sample and reference

beams. The horizontal furnace incorporated in this model is a bifilar-wound type with a maximum heating rate upto 100 °C for temperatures between ambient to 1000 °C and 25 °C for ambient to 1500 °C. The maximum allowable temperature on the SDT Q600 is 1500 °C with a maximum sample capacity of 200 mg. The furnace uses a forced air with high flow rates to cool the system from 1500 °C to 50 °C in less than 30 minutes.

5.2.3 PROCEDURE

An empty reference crucible along with the sample crucible containing 5-6 μg of the residues and coal were placed in the sample holder plates. The samples were then treated through a 3-step procedure which incorporates the first two stages for volatile matter removal from ASTM D7582-12 [65] as follows:

1. Moisture removal: The sample was heated steadily upto 107 °C under inert atmosphere (N_2)and maintained isothermal for 10 minutes to remove moisture from the material.

2. Pyrolysis stage: The sample was further heated under inert atmosphere (N_2) until 950 °C and maintained at isothermal conditions for 30 minutes to ensure complete removal of volatile matter. This step is critical to the gasification process and has the potency to lead to undesirable by-products.

3. Gasification process: In the final step, the remaining char of the residue is now treated with CO_2 at the desired temperature for 60 minutes followed by a 15 minute exposure to air to confirm the carbon conversion in the process.

Note: Gas flow rates were maintained at 100 ml/min throughout for the experiment. All the steps were carried out in triplicates for all samples to confirm the accuracy of the results.

5.3 RESULTS & DISCUSSION

5.3.1 TEMPERATURE OF GASIFICATION

The gasification temperature is very crucial and plays an important role in design of gasifiers and the process economy. Non-isothermal gasification was carried out in presence of CO_2 for raw coal and residue samples. The temperature range which recorded the maximum change in the weight loss of the material, was taken into account for carrying out gasification of the residues.

From the figures, one can easily observe that the residues require higher gasification temperatures in comparison to raw coal. Also, residues obtained at higher liquefaction temperatures require higher temperatures for the onset of gasification reaction. Thus, a direct correlation between the H/C ratio of the feed to the required severity of the reaction conditions for gasification is proved. This is in agreement with the explanation by Best et al. [112], to be a function of hydrogen content in the sample during pyrolysis. With the loss of aromatic hydrogen during the devolatalization step, there is variation in the concentration of active sites. This could be accounted for, by the ring condensation reactions which in turn requires higher temperatures to achieve the desired activation energies for the exothermic gasification reaction to proceed. The reactivity index for the raw coal and residues are thus calculated in the next Section 5.3.2.

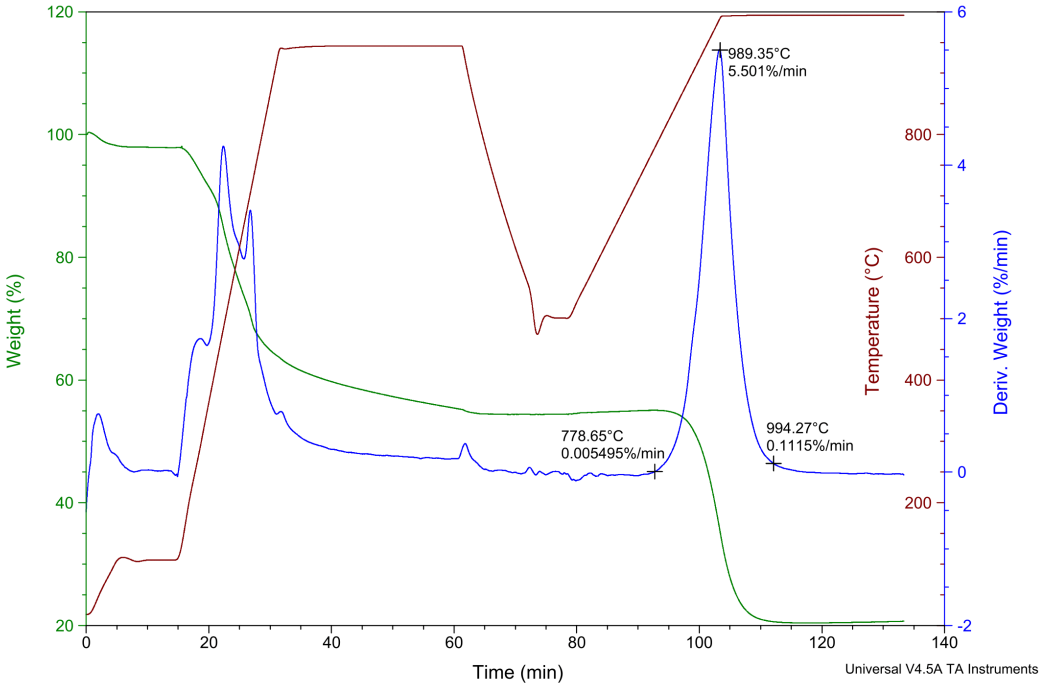

Figure 5.2: Non-isothermal gasification of Res 300

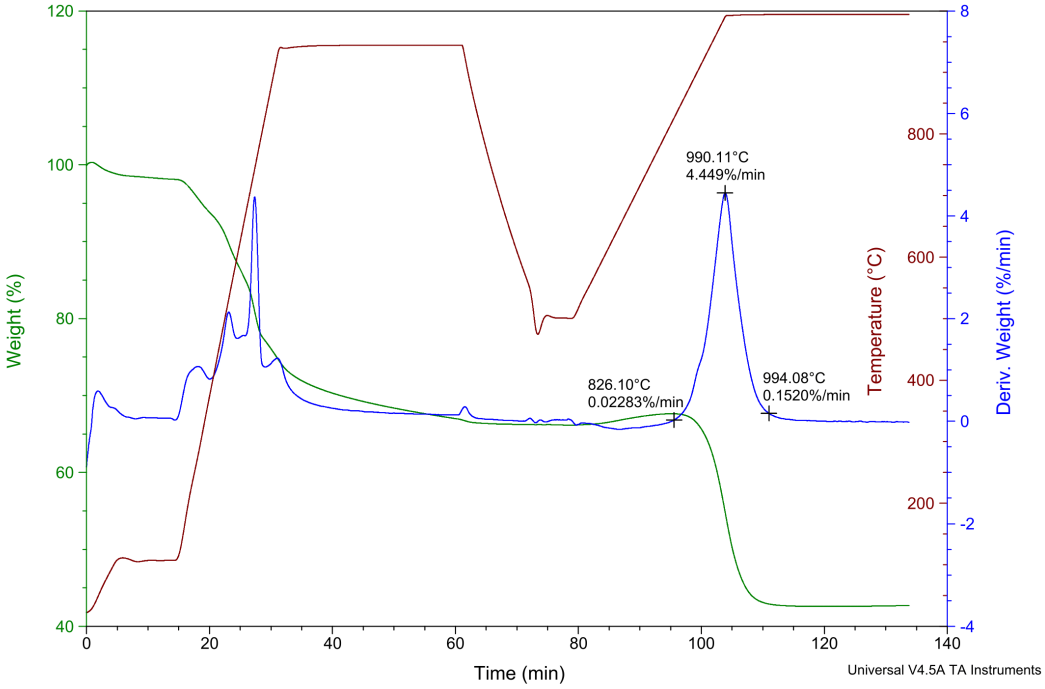

Figure 5.3: Non-isothermal gasification of Res 350

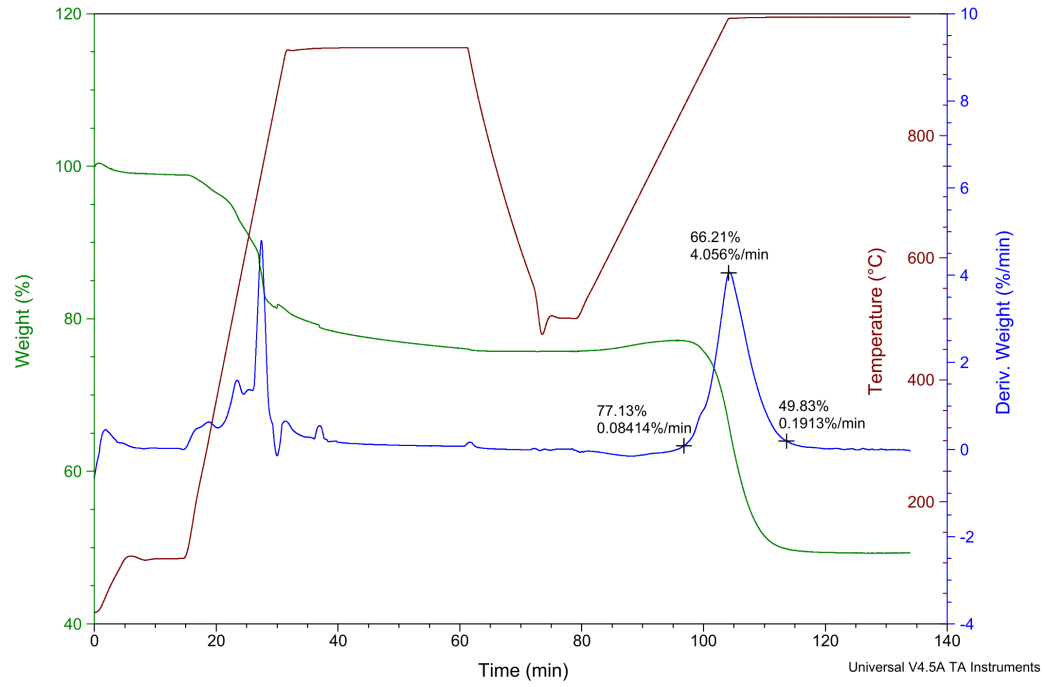

Figure 5.4: Non-isothermal gasification of Res 400

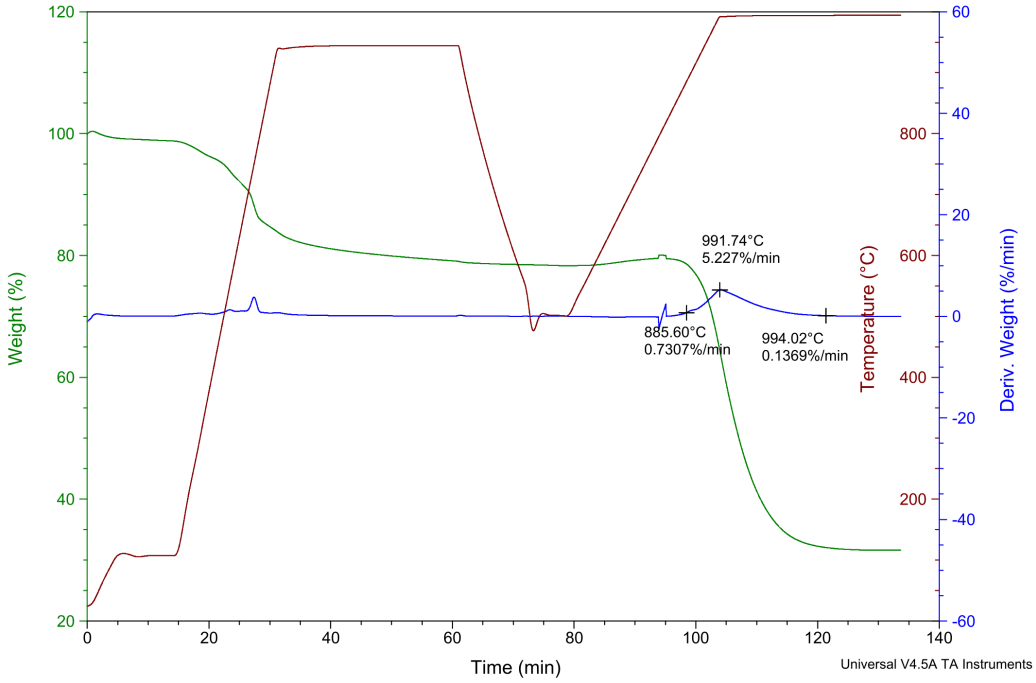

Figure 5.5: Non-isothermal gasification of Res 450

5.3.2 GASIFICATION REACTIVITY OF RESIDUE:COMPARISON WITH RAW COAL

Gasification is a two step process involving:

1. Rapid pyrolysis of the material to produce char (devolatalization) [113].
2. Gasification of the char in presence of CO_2.

The char after pyrolysis consists majorly of ash and carbonaceous material that contributes to the fixed carbon content. This is because the pyrolysis stage which starts at about 300 °C-400 °C is almost complete at around 950 °C, as per ASTM standards [65], [114]. Hydrogen and small amounts of heteroatoms such as nitrogen, sulphur and oxygen may also be present. Studies on char reactivity have proved improved reactivity with increased heating rates[115]. Hence,a maximum heating rate of 50 °C/min is maintained for this step. The second stage of gasification is not detectable below 800 °C - 900 °C [116] given the endothermic nature of the process. Also, as per our study in Section 5.3.1, temperatures in the range 950 °C - 1000 °C are most suitable for residue gasification.

We thus, assume that the total conversion on an ash free basis is equal to the carbon conversion of the residues. Various methods of calculating reactivity index

for raw coal have been stated in literature [117]-[118]. Raghunathan and Yang [119] have proposed that the average reactivity of coal was found to be inversely proportional to the half-life, $t_{0.5}$ as follows:

$$\mathrm{R_c} = \frac{\mathrm{R_u}}{\mathrm{t_{0.5}}} \tag{5.1}$$

where, R_c is the reactivity index, R_u is the proportionality factor = 0.38 (consistent with experiments) and $t_{0.5}$ is the time taken to reach 50% conversion of the material. This values is defined on the assumption of weight loss of carbon alone under isothermal conditions [119].

Similarly, reactivity index has also been calculated as,

$$\mathrm{R} = \frac{2}{\mathrm{t_{0.5}}} \tag{5.2}$$

Reactivity index is a indicator of reactivity for the feed material, being introduced into the gasifier. Reactivity of the feed depends on its chemical properties, volatile matter, oxygen content, aromatic ring condensation etc. [120], of which porosity and surface area being one of the most critical factors [121], [122]. At the onset of gasification, the pore volume of the existing pores increases,thus increasing the surface area. Also, there is opening of the closed pores, which contribute to the increase in the surface area. However, with the progress of the reaction, the pore walls collapse, thus, decreasing the surface area of the solid. Hence, reactivity index is calculated on the basis of conversion upto 50% for char with consideration of the structural parameters for char [123].

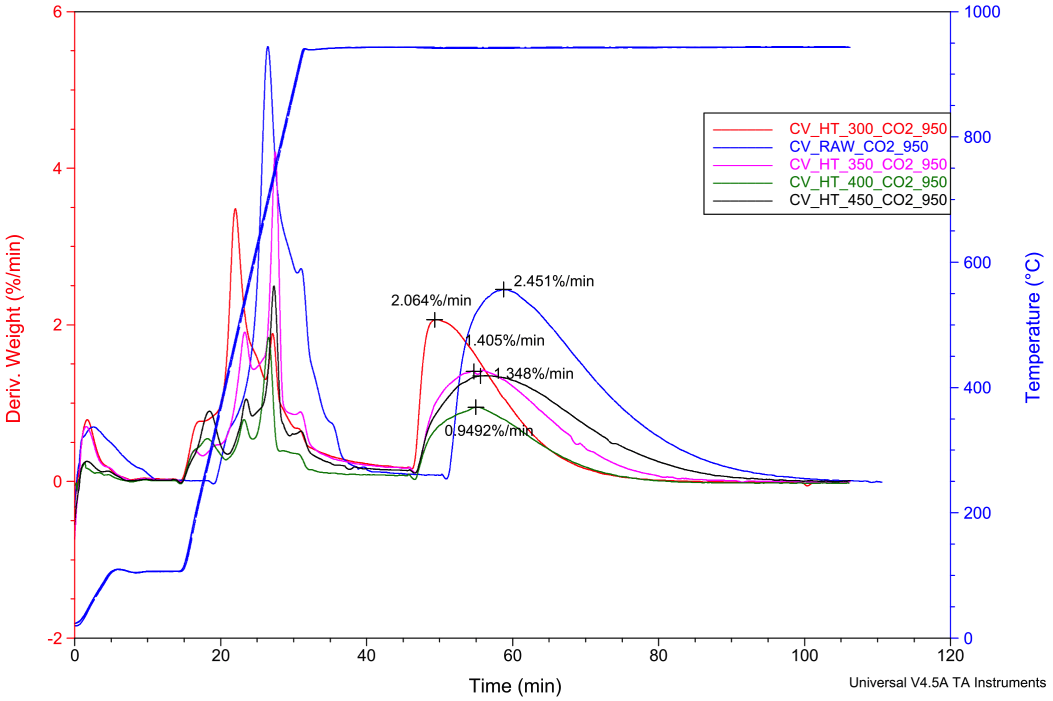

Figure 5.6: Reactivity of CV raw and residues in CO_2 at 950 °C

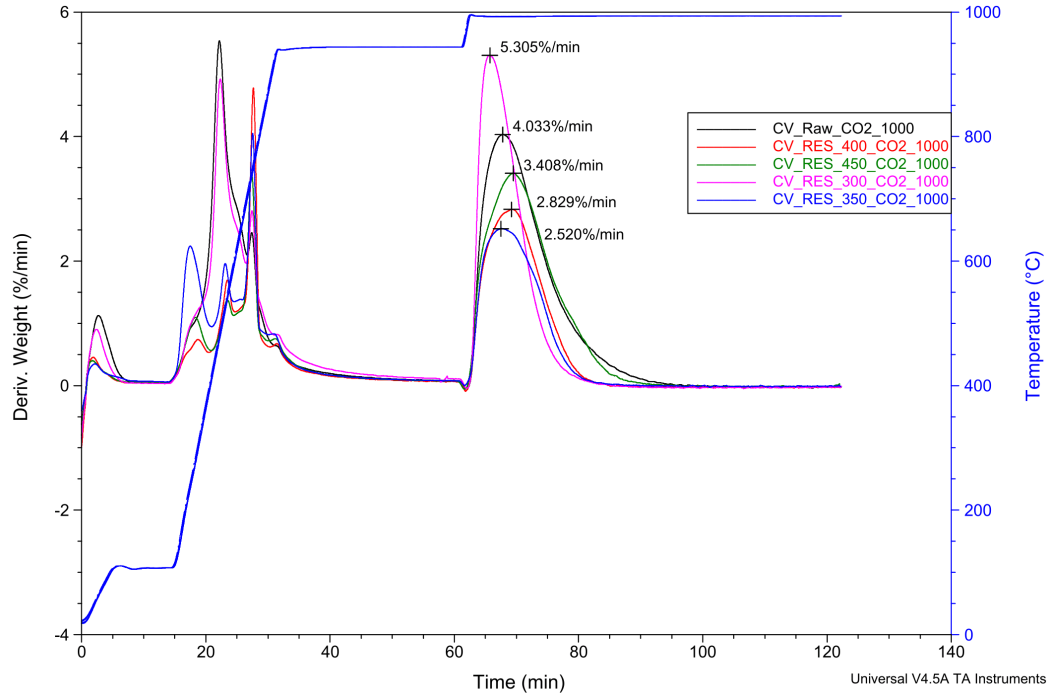

Figure 5.7: Reactivity of CV raw and residues in CO_2 at 1000 °C

Table 5.2: Reactivity of CV raw and Residues

Sample	R_c 950 °C	R_c 1000 °C	R_c 1100 °C
CV Raw	1.262	1.426	1.992
RES 300	0.646	2.774	4.057
RES 350	0.7914	1.359	2.950
RES 400	0.533	2.175	1.572
RES 450	0.329	1.803	2.424

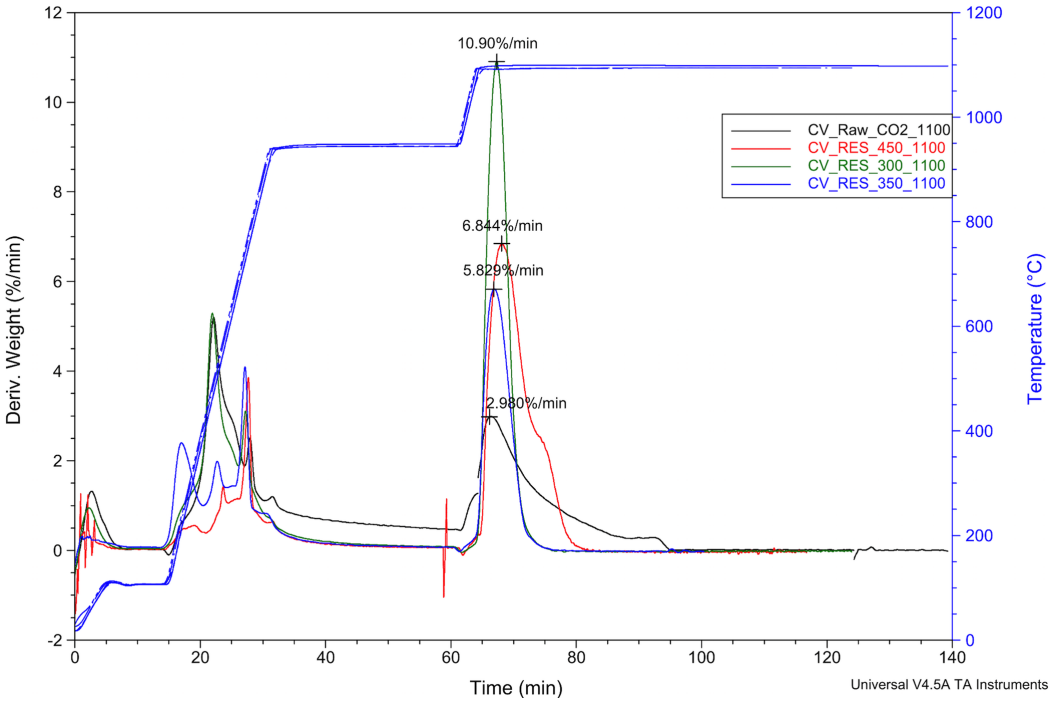

Figure 5.8: Reactivity of CV raw and residues in CO_2 at 1100 °C

However, in this study, the structural properties of coal char and those of residues are different4.15. Also, their chemical compositions differ. Hence, a difference in their gasification mechanism may be expected. A conversion of lesser than 50% is obtained for residues from 400 °C liquefaction temperature at lower gasification temperatures. Thus, comparison of the reactivity index based on the above method will not be the suited for our study. Hence, reactivity as calculated by equation 5.3, taking into account maximum rate of mass loss, forms the basis of comparison [123].

$$\mathrm{R} = \frac{1}{w_{daf}} \frac{\mathrm{dw}}{dt} \tag{5.3}$$

Here, w_{daf} is the weight of the feed on a dry and ash free basis

Table 5.3: Reactivity Index of CV raw and Residues based on 50% conversion

Sample	R_c 1000 °C	R_c 1100 °C
CV Raw	0.255	0.366
RES 300	0.382	0.562
RES 350	0.279	0.553
RES 400	0.269	0.526
RES 450	0.232	0.378

Table 5.4: Reactivity Index of CV raw and Residues based on 90% conversion

Sample	R_c 1000 °C	R_c 1100 °C
CV Raw	0.118	0.144
RES 300	0.190	0.346
RES 350	0.153	0.318
RES 400	0.150	0.204
RES 450	0.120	0.186

Thus, Tables 5.2, 5.3 and 5.4 indicate the competence of the residue as a potential feed for gasifiers. The values for reactivity index at 950 °C could not be measured since few residue samples did not undergo 50% conversion at that temperature. index at 90% conversion was essential to compare the reactivity of the gasification of the most aromatic portion of the char. Lower reactivity index with increasing liquefaction temperature, is reflective of the refractory material that has to be handled during gasification which is again directly related to the H/C contents in the sample material.

As described earlier, a number of factors contribute influence the reactivity or the gasification character of a feed. Improved reactivities with increase in temperature is evident and obvious, due to the increased molecular interactions at high temperature. Increasing reactivity index for residues obtained from lower liquefaction temperature suggest the ease of gasification with increasing H/C ratio affiliated with the sample property. The residues, though possessing lower initial surface area (Table 4.15), exhibit reactivities comparable to that of raw coal. During nitrogen pyrolysis, the surface area of the char was found to increase ten fold Wen and Dutta [124] for coal chars. A similar behaviour can be predicted for chars from residue, a derivative of coal.

Furthermore the residue's reactivity is influenced by the presence of higher mineral content which act as catalytically active sites for CO_2 adsoprtion, as was observed by Jenkins et al. [125] and Skodras and Sakellaropoulos [126]. Huang et al. [127] have related this behaviour to the property of alkali minerals to undergo in-

tercalation with carbon, increasing the interlayer distance and influences volume expansion, which further weakens the existing C-C bonds and improves gasification reaction. These reactions are predominantly surface reactions, which mainly occur in the the large pores, outside the microporous surface. The macropores appear in crystallite edges or sites that are in contact with inorganic impurities, that meliorate the gasification reactivity [122]. This is also in agreement with that of Hurt et al. [128], where it was observed that the gasification reactivity for sub-bituminous coals was insensitive to the large variations in the micro-pore area. This is largely due to the planar structure of char comprising of aromatic sheets [108] of crystallite form. Thus, porosity may not be the only structural character that could influence the gasification reactivity. The presence of these crystallite edges with mineral matter dispersed in the structure, can improve gasification rates largely as reported in Table 5.2.

5.3.3 KINETIC PARAMETER EVALUATION : MODEL FITTING UNDER LINEAR REGRESSION

The validity of the intrinsic kinetic parameters estimation for the reaction model in a TGA depends on the experimental conditions and initial surface area of the carbon [129]. The effect of chemisorption and its dynamics don't completely allow the temporal weight change profiles calibrated by the TGA be used to calculate the intrinsic parameters. Hence, the values reported in our study are apparent intrinsic kinetic parameters calculated for the initial stages of carbon conversion of the residues, where,

$$\mathrm{X} = \frac{(\mathrm{w_o} - \mathrm{w_{ash}}) - (\mathrm{w_t} - \mathrm{w_{ash}})}{w_o - w_{ash}}, where, 0 \leq \mathrm{X} \leq 0.8 \tag{5.4}$$

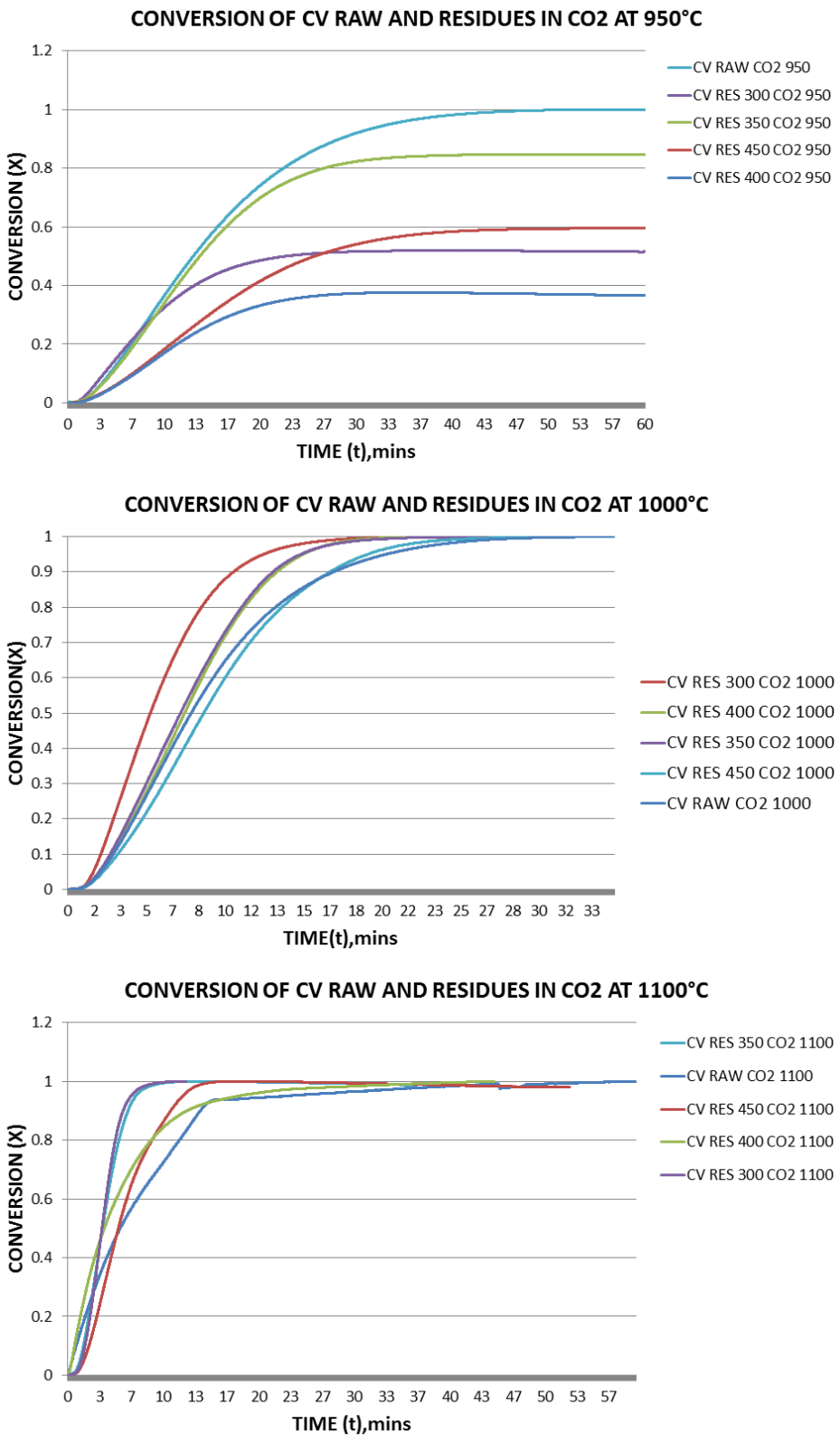

Figure 5.9: Conversion plot for CV raw and residues in CO_2

The Fig.5.10 represents the morphology of the residual material from the TGA for complete carbon conversion. There is evidence of enlarged and collapsed pore surfaces at almost all surfaces, visible in the magnified image. The particle may appear sintered due to compaction inside the TGA crucible.

Complete carbon conversions for coal residues was acquired experimentally for the gasification at 1000 °C and 1100 °C. Fig. 5.9 presents plots of the carbon conversion ratio (X) versus reaction time (t) under isothermal conditions for raw coal as well as residues, indicating faster reactivities for residues at higher temperatures than raw coal.

Gasification mechanism is governed by the endothermic Bouduard reaction, as follows [120]:

$$\mathrm{C} + \mathrm{CO_2} \rightarrow 2\mathrm{CO} \ \triangle\mathrm{H} \ = \ 172.5 \ kJ/mol \tag{5.5}$$

This occurs in two steps as proposed by Ergun [130],where Step 1 is the adsorption of carbon dioxide to the empty carbon site (C_f) and formation of carbon monoxide. The oxygen lost by CO_2 remains on the carbon surface (C_o).

$$\mathrm{CO_2} + \mathrm{C_f} \rightleftharpoons \mathrm{CO} + \mathrm{C_o} \tag{5.6}$$

Further, the transfer of carbon from solid to gas phase is the Step 2 given as,

$$\mathrm{C_o} \rightarrow \mathrm{CO} + n\mathrm{C_t} \tag{5.7}$$

n is any integer, when occupied sites are under individual consideration.

An overall rate equation considering that the reaction if of first order, can be given as,

$$\mathrm{r(X)} = \frac{dX}{dt} \ = \mathrm{kP_{CO_2}f(X)} \tag{5.8}$$

The term r(X) stands for the reaction rate, P_{CO_2} for the partial pressure of the reactant gas CO_2, f(X) accounts for the structural and chemical parameters that need to be accounted for during the reaction [131] and k is the kinetic rate constant, defined by Arrhenius law, given as [132],

$$\mathrm{k} = \mathrm{Ae}^{\frac{-\mathrm{E}}{\mathrm{RT}}} \tag{5.9}$$

Many models have been suggested for coal and char gasification in CO_2 [113], [122], [133], [134], [135]. A homogeneous model cannot represent the heterogeneity of the solid-gas reaction, hence, it was not considered. A modified volumetric model, proposed by Kasaoka et al. [134] was found to be the best fit for our data with linear

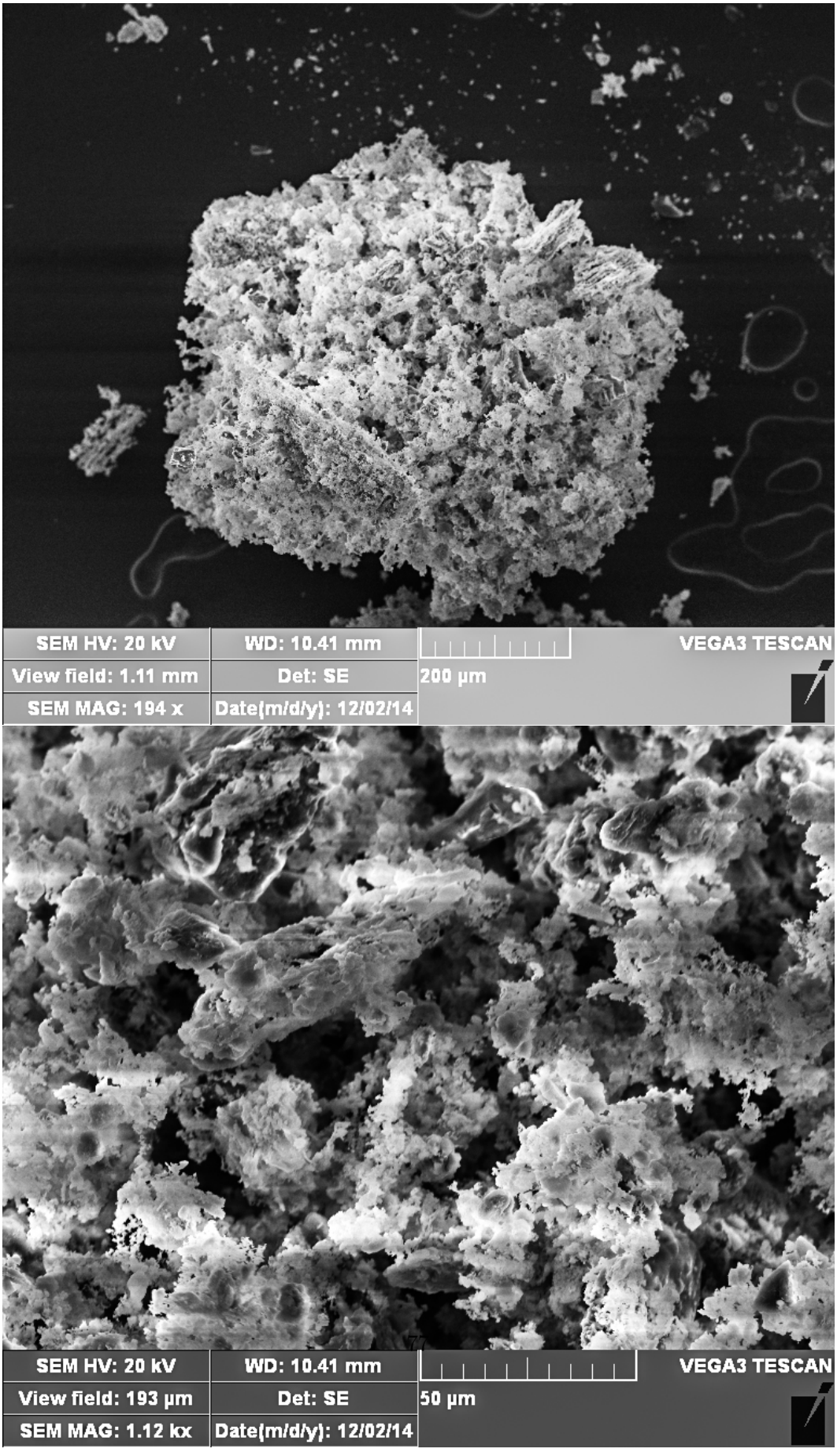

Figure 5.10: Char morphology after gasification in TGA

regression parameter of R^2 close to 0.99-1. It assumes uniform gas diffusion within the entire particle. A standard volumetric model defines reactivity as,

$$\mathrm{r(X)} = \frac{dX}{dt} = \mathrm{k(X)(1-X)} \tag{5.10}$$

Rearranging the above equation gives,

$$\frac{1}{(1-\mathrm{X})}\mathrm{dX} = \mathrm{k(X)dt} \tag{5.11}$$

Further, integrating both sides, we arrive at,

$$-\ln(1-\mathrm{X}) = \mathrm{k}t \tag{5.12}$$

However, in the case of a modified volumetric model, we account for the change in the reaction rate with conversion by introducing power law factor as,

$$\boxed{-\ln(1-\mathrm{X}) = \mathrm{at^b}} \tag{5.13}$$

Here, a and b are constants with no physical meaning.

Differentiating equation 5.13, we get,

$$\frac{1}{(1-\mathrm{X})}\frac{\mathrm{dX}}{\mathrm{dt}} = \mathrm{abt^{b-1}} \tag{5.14}$$

Thus substituting for k(X) from equation 5.10, we get,

$$\mathrm{k(X)} = \mathrm{abt^{b-1}} \tag{5.15}$$

Integrating further gives,

$$\mathrm{k(X)} = \int a^{\frac{1}{b}}\mathrm{b}{-}\ln(1-\mathrm{X})^{\frac{(\mathrm{b}-1)}{\mathrm{b}}}\mathrm{dX} \tag{5.16}$$

Further calculation of the kinetic parameters are obtained from linear regression of the data using the above equation 5.16 and substitution in the Arrhenius equation 5.9 to obtain A and E (activation energy) given in Table 5.5,

$$\ln(\mathrm{k}) = \ln(\mathrm{A}) - \frac{E}{R}(\frac{1}{T}) \tag{5.17}$$

Further kinetic constants are tabulated in the following Table 6.4

Thus, the rate equations can be given as,

Table 5.5: Kinetic parameters using linear regression

Feed	Gasification Temperature(K)	a	b	R^2
RES 300	1223.15	0.03196	1.849	0.9986
	1273.15	0.02002	1.252	0.9944
	1373.15	0.02564	2.594	0.9998
RES 350	1223.15	0.01093	1.580	0.9991
	1273.15	0.01565	1.939	0.9989
	1373.15	0.05522	1.962	0.9984
RES 400	1223.15	0.00769	1.476	0.9974
	1373.15	0.01181	2.115	0.9992
	1373.15	0.01226	1.057	0.9953
RES 450	1223.15	0.00948	1.339	0.9960
	1273.15	0.01112	1.808	0.9998
	1373.15	1.087e-06	5.243	0.9877

Table 5.6: Kinetic parameters using Arrhenius equation

Feed	E(kJ/mol)	A	R^2
RES 300	86.47	1.252e+03	0.9932
RES 350	166.11	2.403e+03	0.8021
RES 400	213.68	3.090e+03	0.6471
RES 450	196.55	2.843e+03	0.9997

RES 300,

$$\boxed{r(X) = [1.252e+03 - \frac{86.47}{R}](\frac{1}{T})\mathrm{P_{CO_2}f(X)}} \tag{5.18}$$

RES 350,

$$\boxed{r(X) = [2.403e+03 - \frac{166.11}{R}](\frac{1}{T})\mathrm{P_{CO_2}f(X)}} \tag{5.19}$$

RES 400,

$$\boxed{r(X) = [3.090e+03 - \frac{213.68}{R}](\frac{1}{T})\mathrm{P_{CO_2}f(X)}} \tag{5.20}$$

RES 450,

$$\boxed{r(X) = [2.843e+03 - \frac{196.55}{R}](\frac{1}{T})\mathrm{P_{CO_2}f(X)}} \tag{5.21}$$

Thus, the lower activation energies suggest the ease of gasification of residual chars, thus making them a potential source of gasifier feed.

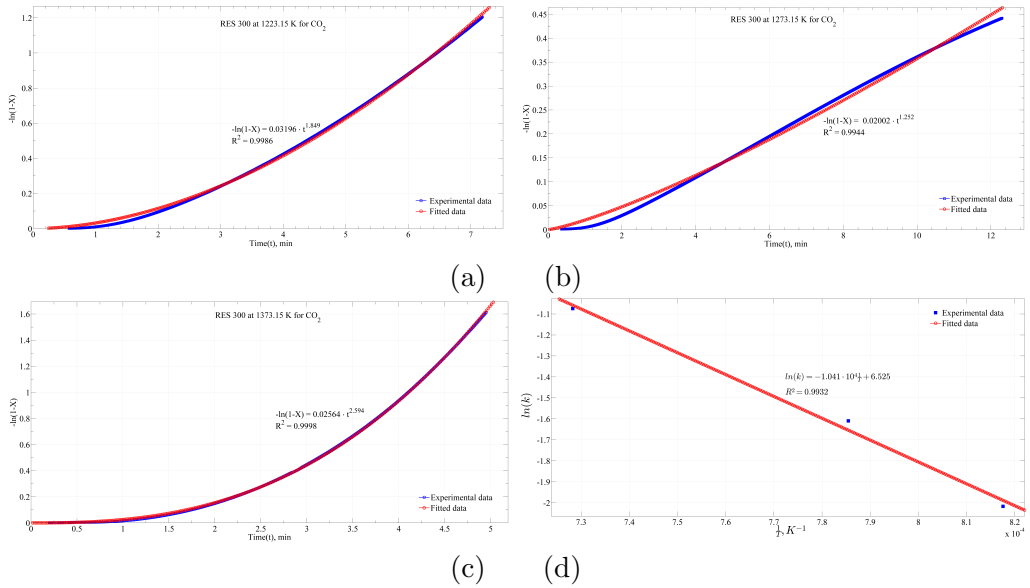

Figure 5.11: (a) Kinetics for CV Res 300 in CO_2 AT 950 °C, (b) Kinetics for CV Res 300 in CO_2 at 1000 °C, (c) Kinetics for CV Res 300 in CO_2 at 1100 °C, (d) Arrhenius plot for CV Res 300 in CO_2

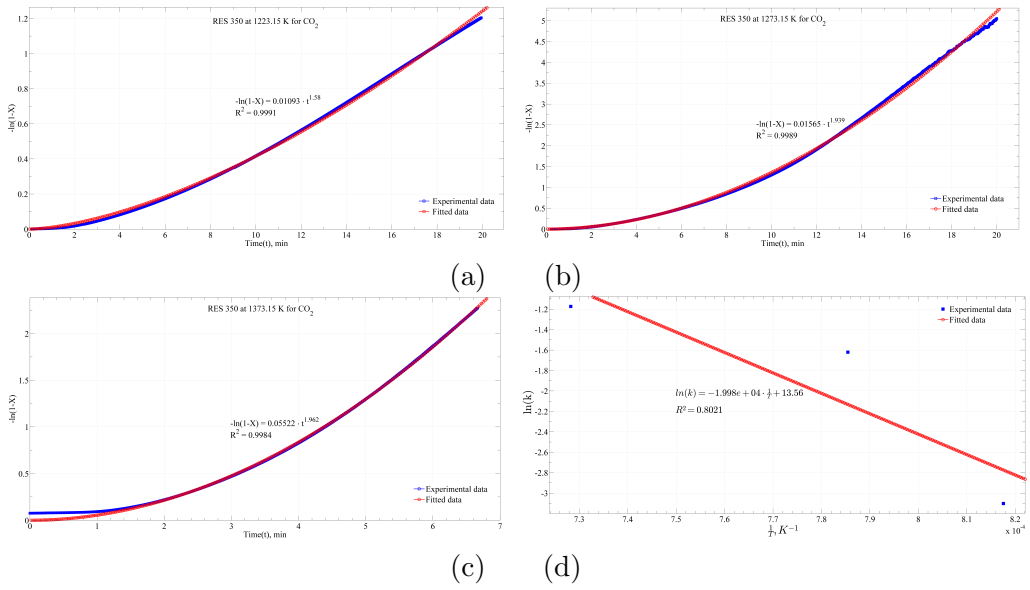

Figure 5.12: (a) Kinetics for CV Res 350 in CO_2 AT 950 °C, (b) Kinetics for CV Res 350 in CO_2 at 1000 °C, (c) Kinetics for CV Res 350 in CO_2 at 1100 °C, (d) Arrhenius plot for CV Res 350 in CO_2

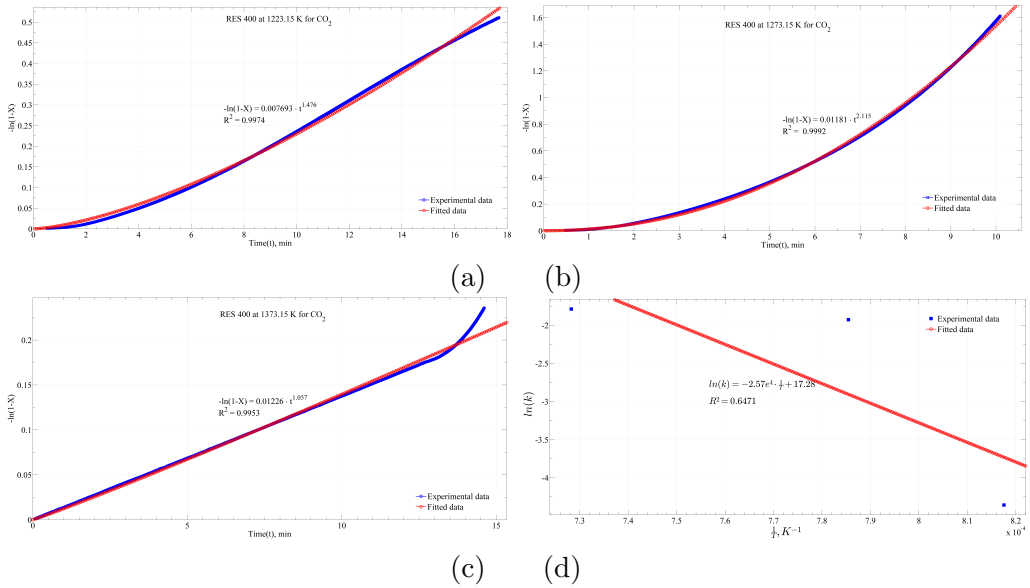

Figure 5.13: (a) Kinetics for CV Res 400 in CO_2 AT 950 °C, (b) Kinetics for CV Res 400 in CO_2 at 1000 °C, (c) Kinetics for CV Res 400 in CO_2 at 1100 °C, (d) Arrhenius plot for CV Res 400 in CO_2

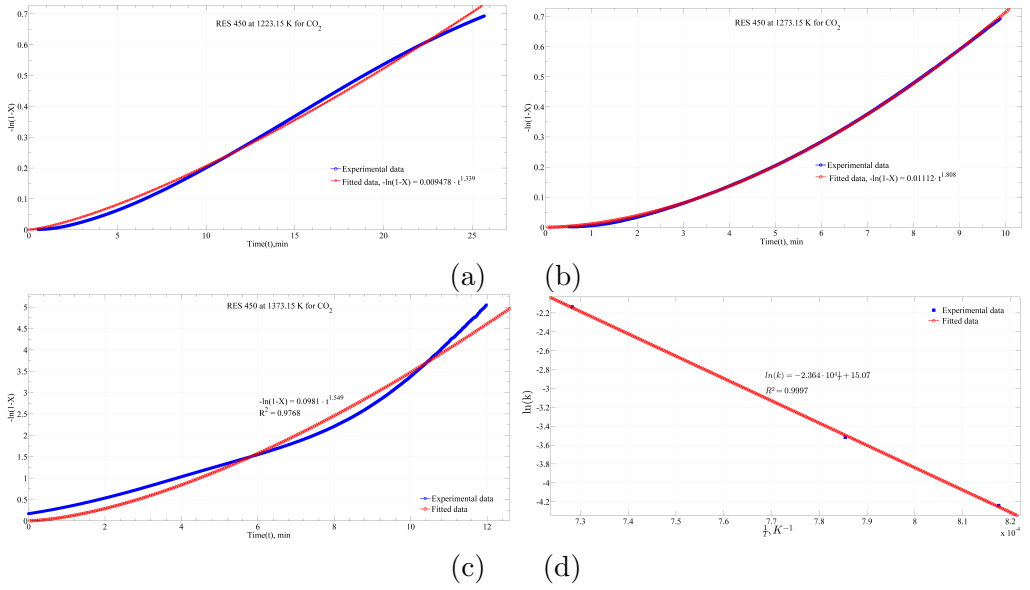

Figure 5.14: (a) Kinetics for CV Res 450 in CO_2 AT 950 °C, (b) Kinetics for CV Res 450 in CO_2 at 1000 °C, (c) Kinetics for CV Res 450 in CO_2 at 1100 °C, (d) Arrhenius plot for CV Res 450 in CO_2

5.4 GENERAL DISCUSSIONS

Universal gasifiers can be divided into 4 main zones, namely: Drying, Pyrolysis, Reduction and Combustion as depicted in Fig. 5.15. The zone directly in contact with oxygen is the combustion zone. Further depending on percentage of feed O_2, the zones are termed as gasification, pyrolysis and drying in the descending order of its availability. In a combustion zone, the feed material reacts with oxygen undergoing the following reactions [136]:

$$\mathrm{C} + \mathrm{O_2} \rightarrow \mathrm{CO_2} \triangle \mathrm{H_r} = -393.4 MJ/kmol \tag{5.22}$$

$$\mathrm{C} + 0.5\mathrm{O_2} \rightarrow \mathrm{CO} \ \triangle \mathrm{H_r} = -111.4 MJ/kmol \tag{5.23}$$

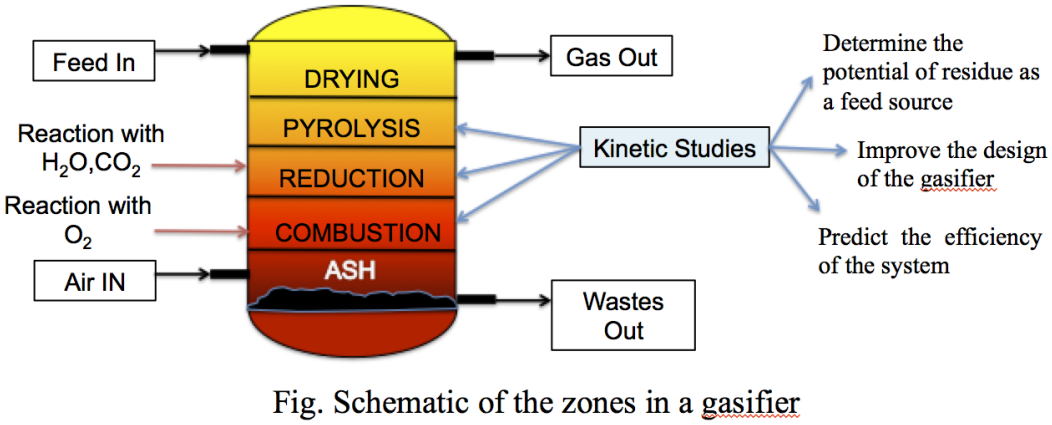

Figure 5.15: Schematic depicting zones in an Universal gasifier

The gasification zone has a comparatively lower O_2 availability and hence, reactions with CO_2 and H_2O are dominant this zone given as follows [136]:

$$\mathrm{C} + \mathrm{H_2O} \rightarrow \mathrm{H_2} + \mathrm{CO} \ \triangle \mathrm{H_r} = 130.5 MJ/kmol \tag{5.24}$$

$$\mathrm{C} + \mathrm{CO_2} \rightarrow 2\mathrm{CO} \ \triangle \mathrm{H_r} = -170.7 MJ/kmol \tag{5.25}$$

$$\mathrm{CO} + \mathrm{H_2O} \rightarrow \mathrm{H_2} + \mathrm{CO} \ \triangle \mathrm{H_r} = -40.2 MJ/kmol \tag{5.26}$$

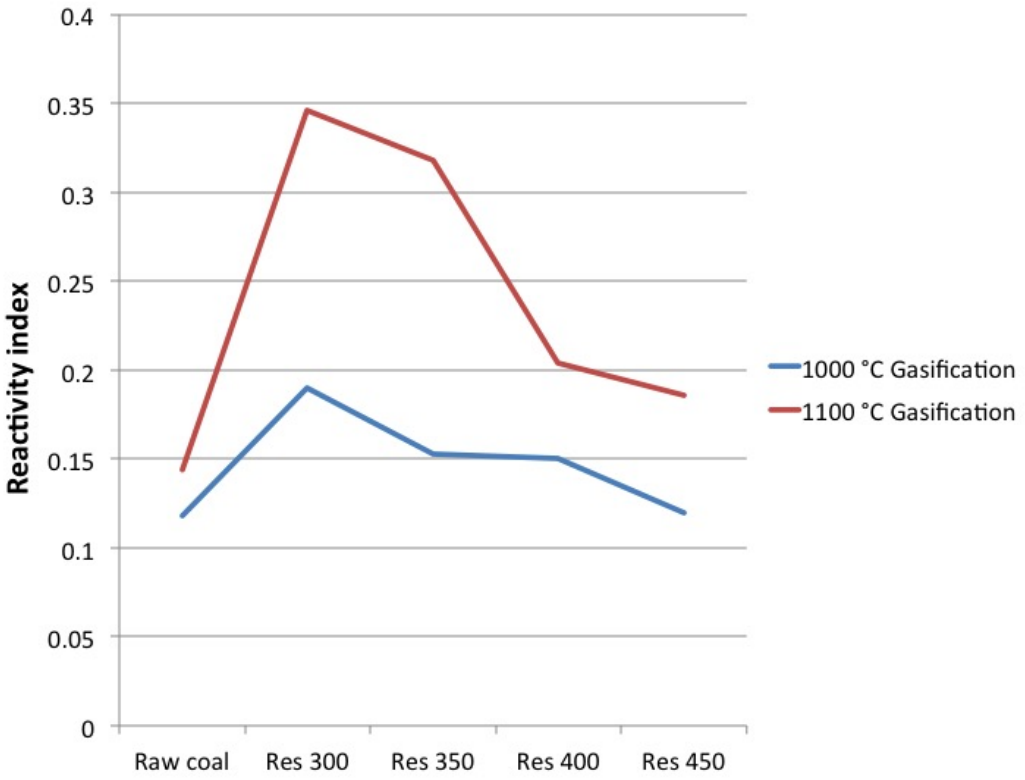

Figure 5.16: Reactivity index comparison of raw coal and residue based on 90% conversion

$$\mathrm{C} + \mathrm{H_2} \rightarrow \mathrm{CH_4} \ \triangle \mathrm{H_r} = -74.7 MJ/kmol \tag{5.27}$$

The exothermic heat released during the combustion process, provides the required heat to the gasification zones governed by endothermic reactions. Further, the pyrolysis zone is characterized by those sets of reactions which take place under inert atmospheric conditions. Majority of the reactions in this zone are dominated due to the release of the low molecular weight components in the system i.e volatile matter. A comparison of the reactivity index based on 90% conversion was undertaken, to evaluate the reactivity of the tar precursors or highly aromatic char of residues and raw coal. Decreasing reactivity index with increasing aromatic content was observed and is apparent, as shown in Fig. 5.16.

Thus, during kinetic evaluation of the residue under gasification, complete devolatilization of the material is ensured in presence of N_2, before introduction of the feed gas (CO_2). A kinetic study of these reaction zones and further evaluation of the kinetic parameters indicate the minimum energy to be overcome for product

formation. Thus, this study would aid in the determination of the potential of a residue as a feed source for gasifier plants under real-time conditions and predict system efficiency. Higher values of the corresponding Arrhenius constant indicate that mass transfer limitations are partially overcome. However, the values listed in Table 5.5 are apparent activation energy values since the calculations were based on assumptions as listed below:

1. The coal is considered to be a homogeneous entity consisting of carbon alone.
2. Reactions with mineral matter are taken into consideration.
3. Here, reactivity is associated to the mass loss of the material.
4. Since the sample quantity is very small (approx. 5 mg), rate of heating and mass loss of the sample is very small, hence time lag is considered negligible.

5.5 CONCLUSIONS

Based on the evaluation of the isothermal and non-isothermal gasification behaviour of residue at 950 °C, 1000 °C and 1100 °C in a TGA, the results can be stated as below:

1. The kinetic parameters reported in the study reflect the apparent values for rate of reaction of residues.
2. The improved reactivity with increase in temperature is apparent and was observed for both residues and parent coal gasification. Higher reactivity index were obtained for residues for measurements based on 90% conversion.
3. Higher reactivity indices were measured for residues in comparison to that of raw coal. This was associated with the higher content of mineral matter dispersion in the residues.
4. Further, reactivity of the residues was also found to be related to the aromaticity of the samples, suggesting requirement of higher activation energy for residues with lower H/C ratio.

Chapter 6

COMBUSTION BEHAVIOUR OF COAL LIQUEFACTION RESIDUE

6.1 INTRODUCTION

A popular, rapid and low energy demanding mechanism was explored to understand the potential of residue as a feed for real-time entrained flow reactors for combustion. Combustion can be perceived as gasification under oxidizing conditions, in lieu of, reduction in presence of carbon dioxide. Though NO_x, SO_x, CO and release of other harmful gases aka pollutants could be one of the downsides of this method, it is energy efficient compared to gasification and requires to be carried out under an optimal ratio of inert: O_2 to fulfil environmental standards for gas emissions.

The theory of combustion dates back to 19th century and has seen a steady growth since then. Combustion of coal for energy production has been a vital source of energy since 1880's in the US. However, residue's combustion characteristics for Western Canadian coals, have been barely investigated upon, until today. An insight towards its reactivity and a comparative study with raw coal would suggest its efficiency in applicability in the existing combustion reactors currently employed for coal. Also, the lower sulphur content in the residues, make it a potential feed for combustion process.

Combustion being a relatively faster reaction than gasification, due to its exothermic nature, the refractory residual material can be expected to undergo combustion with efficiency compared to that of raw coal. Thus, we have carried out a preliminary study on determination of the kinetic parameters and reactivity of the residue

Table 6.1: Gas composition for raw materials, Combustion

Gas	Product Grade	MSDS reference	Inlet Pressure, atm
Nitrogen	5.0	P-4631	1.088
Air	Ultra zero Ambient Monitoring	P-4560	1.122

in a TGA. Further a practical combustion unit such as an Entrained Flow Reactor was employed to determine the combustion efficiency of the residue in comparison to raw coal. These precursory investigations, we believe, would allow us to represent the conditions in a practical combustion system and thus help validate our conclusions effectively.

6.2 EXPERIMENTAL METHOD

6.2.1 RAW MATERIALS

The residues obtained from direct coal liquefaction process, of approx. 5-6 mg was introduced in the analyser. Please refer Chapters 3 and 4 for further information on the preparation and properties of the residue. For the combustion run, nitrogen and air gas cylinders supplied by Praxair, Canada, were employed with the composition, as mentioned in Table 6.1. Note: All samples are vacuum dried for a 12 hour period at 80 °C prior to its introduction into the experimental set-up.

6.2.2 EQUIPMENT

THERMOGRAVIMETRIC ANALYZER

For equipment details and specifications, please refer Chapter 5.

ENTRAINED FLOW GASIFIER

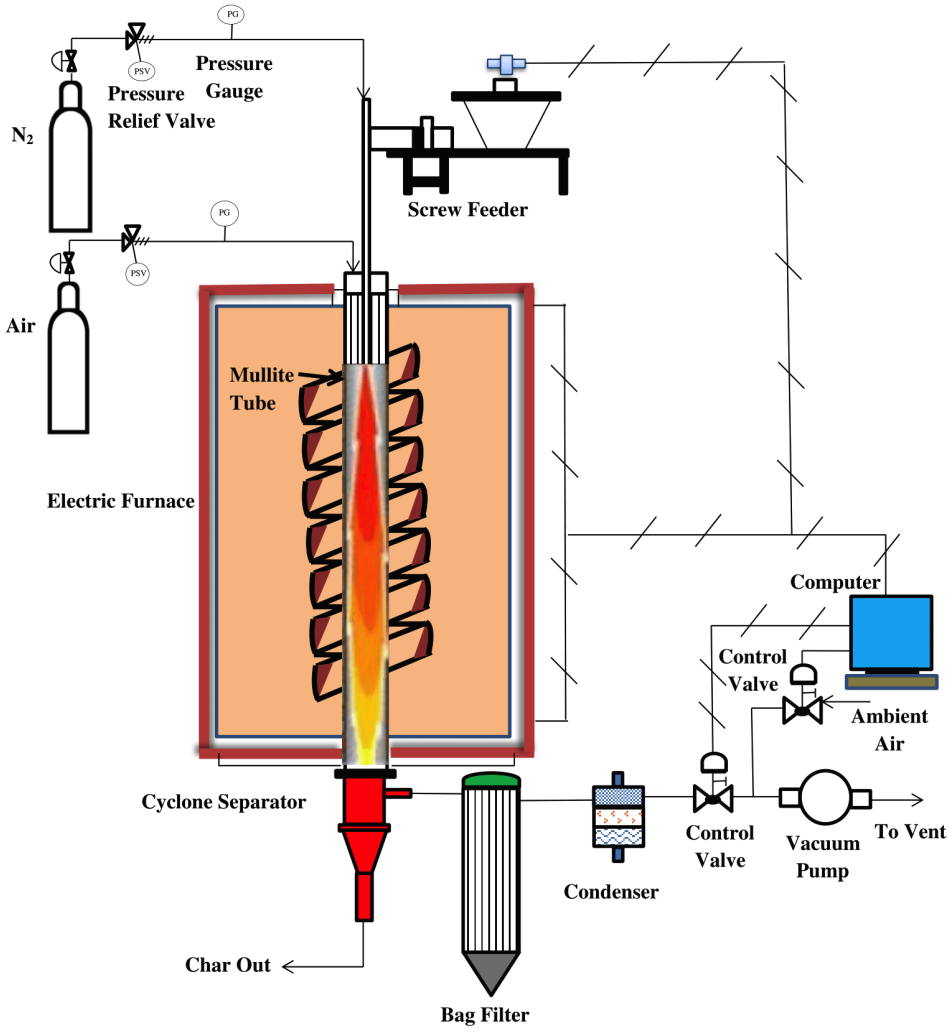

Figure 6.1: Schematic diagram of Entrained Flow Gasifier

Atmospheric pressure entrained flow gasifier (AEFG) with an electrically heated vertical core Mullite tube (MV-30, 2.56 inch ID, 60.24 inch height, maximum working temperature of 1500 °C) was employed to study the ash characteristics during combustion in a real-time boiler conditions for residues and raw coal. The furnace has a maximum working temperature of 1800 °C and is equipped with molybdenum disilicide heating elements (Moly D-33). PID temperature controllers (Omron E5CK) are fixed along the length of the reactor tube. The controllers are connected to a computer to remotely communicate with the system using Lab View interface. A Schenck AccuRate Tuf-flex series volumetric screw feeder capable of handling

feed-rates from 0.000017 to 280 cubic ft/hr, was fitted on the top of the tube system. It has a pulsating wall and flight free auger with stirring rod and polynozzle. Volumetric feeding deviations range from +/-0.5% to 3% for most materials. The feeder is weighed before and after the run to determine the real gravimetric rate of feed. To avoid particles to stick to the inner surface of the feeder probe,a preliminary N_2 flow is used to entrain the particles into the Mullite tube. The flow rates of Nitrogen and air are set to the desired value to prevent the effect of cooling gases. High precision mass flow controllers (AALBORG) are applied to adjust the gas flow rates. The pressure gauges at the inlet of the feeder system and the reactor tube is well-checked before the sample introduction. The bottom of the reactor tube is fitted with a cyclone separator where the char is separated from the flue gases and collected. The flue gases then pass through the bag filter to trap any sub-micron particles to a condenser for water vapour removal and further vented out through a vacuum pump. The vacuum pump thus helps in maintaining ambient (atmospheric) pressure conditions inside the gasifier.

6.2.3 PROCEDURE

THERMOGRAVIMETRIC ANALYZER

An empty reference crucible along with the sample crucible containing 5-6 μg of the direct coal liquefaction residues and raw coal were placed in the sample holder plates. The samples were then treated through a 3-step procedure which incorporates the first two stages for volatile matter removal from ASTM D7582-12 [65] as follows:

1. Moisture removal: The sample was heated steadily upto 107 °C under inert atmosphere (N_2) and maintained isothermal for 10 minutes to remove moisture from the material.

2. Pyrolysis stage: The sample was further heated under inert atmosphere (N_2) until 950°C and maintained at isothermal conditions for 30 minutes to ensure complete removal of volatile matter. This step is critical to the gasification process and has the potency to lead to undesirable by-products.

3. Combustion process: In the final step, the remaining char of the residue is now treated with air (O_2 flow rate = 19.9 - 21.9 ml/min) at the desired temperature for 60 minutes followed by a 15 minute exposure to air to confirm the carbon conversion in the process.

Note: Gas flow rates were maintained at 100 ml/min throughout for the experiment.

ENTRAINED FLOW GASIFIER

Raw coal and coal residue each were tested separately for the ash behaviour in the boiler. The furnace was heated upto 1000 °C incorporating a step wise ramp of 200 °C/hr overnight in order to achieve complete temperature stabilization. N_2 and Air flow rates were maintained at 1 and 4 litre/minute. A preheating time of a total of 15 minutes was maintained to avoid the effect due to cooling of gases. The sample was then introduced at a uniform gravimetric rate of 64 g/hr through the Schenck screw feeder into the reactor tube maintained at 1000 °C. After all of the sample had been introduced, the gas flow was shut off. The char collected from the bottom of the cyclone separator was further analysed using the TGA and SEM for ash content and morphology of the particles respectively.

6.3 RESULTS & DISCUSSION

6.3.1 COMBUSTION BEHAVIOUR OF RESIDUE DERIVED FROM DIRECT COAL LIQUEFACTION PROCESS

Similar assumptions as mentioned in Chapter 5 have been considered here to determine the combustion reactivity of residue and raw coal. An overall combustion reaction can be depicted as follows [137]:

$$(1+\lambda)C \ + \ O_2 \rightarrow 2\lambda CO \ + (1-\lambda)\mathrm{CO_2} \ \triangle \mathrm{H^{\circ}_{298K}} = 172.5\lambda \ - \ 393.5 \ kJ/mol \quad (6.1)$$

Various mechanistic pathways for determining combustion kinetic behaviour have been suggested in literature [138] - [139]. A three-step mechanism proposed by Hurt and Calo [138] is considered here.

$$2\mathrm{C_f} + \mathrm{O_2} \rightarrow 2\mathrm{C(O)} \quad (6.2)$$

$$\mathrm{C(O)} + \mathrm{O_2} \rightarrow \mathrm{CO_2} + \mathrm{C(O)} \quad (6.3)$$

$$\mathrm{C(O)} \rightarrow \mathrm{CO} + \mathrm{C_f} \quad (6.4)$$

The first step (equation 6.2) involves the chemisorption of the O_2 molecule from the bulk gas phase to the active carbon sites. Assuming uniform chemisorption, throughout the particle's surface, it is worth mentioning a peculiar observation

made by Yang and Wong et al. The oxygen chemisorbed on the basal plane of the particle's structure migrated to the edge sites for the combustion reaction to proceed. Major reactions, thus, suitably occur in the edge sites rather than the basal plane. Hence, as the reaction reached completion, the plane structures slowly fuse in due to Vanderwaals forces, suggesting the reaction site to be concentrated in the macro-pore region, as did Hurt et al. [128] [108]. The weakening of the adjacent $C-C$ and further oxidation of the $C(O)$ intermediate, leads to the formation of CO_2 and CO and leaves behind an empty carbon active site again as depicted in reactions (equation 6.3 and equation 6.4) respectively.

Combustion behaviour of residues was determined by non-isothermal heating to determine their temperature of oxidation. The onset, critical (corresponding to the highest reaction rate) and burn-off temperatures were recorded in the TGA as shown in Figs. 6.2, 6.3, 6.4 and 6.5. The reaction time recorded was much lesser than those for gasification under CO_2 atmospheres, given the exothermic nature of the reaction. The onset , critical and burn-off temperatures were found to be direct related to the H/C ratio of the residues, explained in Chapter5. Annealing of the chars have been found to have led the development of more ordered carbon structures, thus reducing the micro-porosity of the chars [140]. Hence, the residue chars obtained from residues at higher liquefaction temperatures require comparatively slightly higher onset temperatures for combustion.

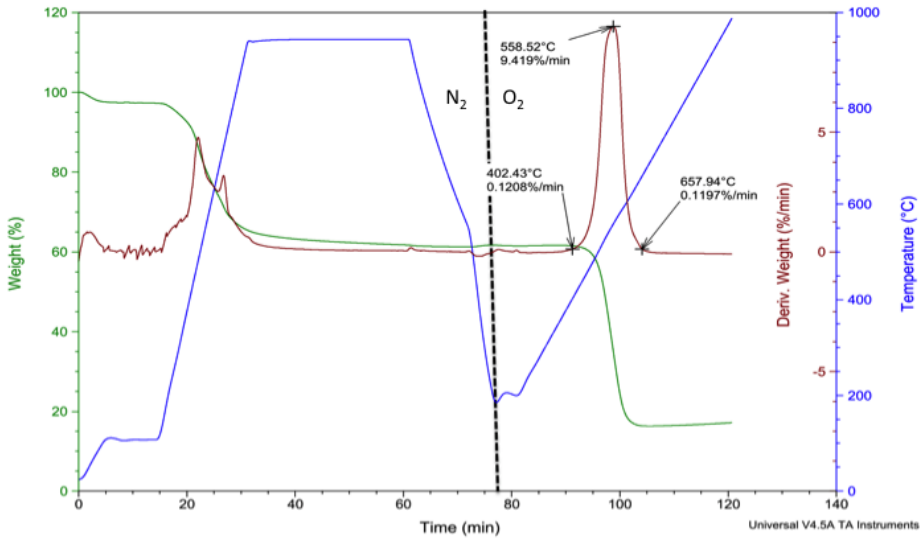

Figure 6.2: Non-isothermal oxidation of Res 300

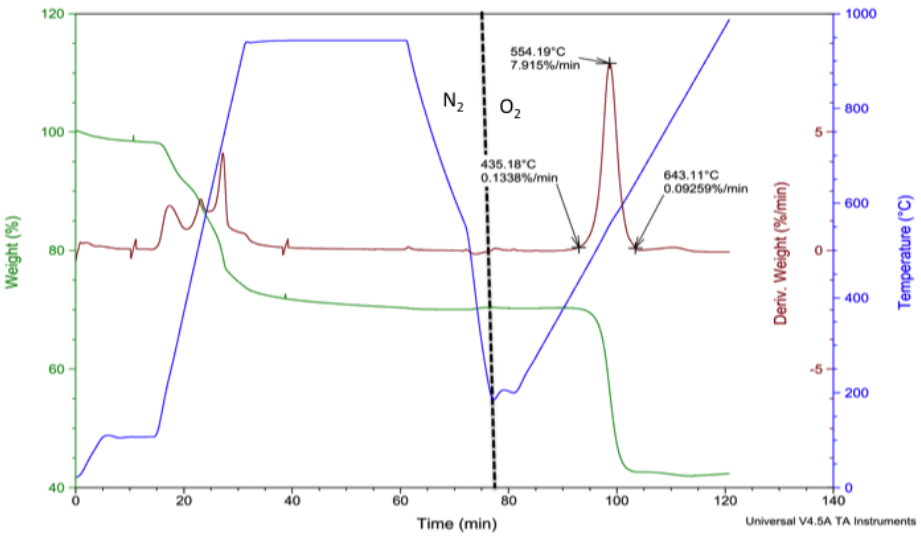

Figure 6.3: Non-isothermal oxidation of Res 350

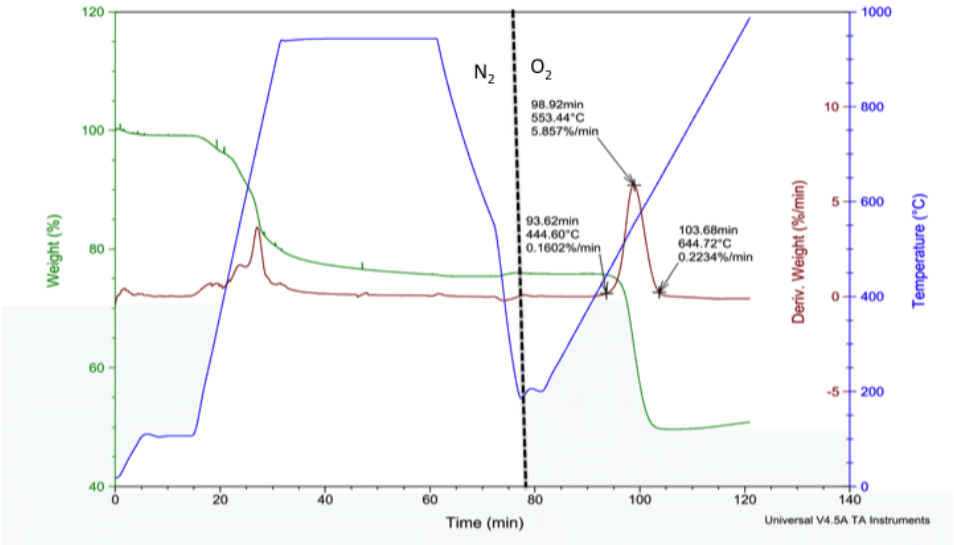

Figure 6.4: Non-isothermal oxidation of Res 400

Table 6.2: Reactivity index for Raw coal and residues based on 50% conversion

Sample	R_u 850 °C	R_u 950 °C	R_u 1000 °C
Raw coal	0.566	0.570	0.500
Res 300	0.484	0.553	0.863
Res 350	0.633	0.620	0.746
Res 400	0.603	0.692	0.709
Res 450	0.681	0.484	0.655

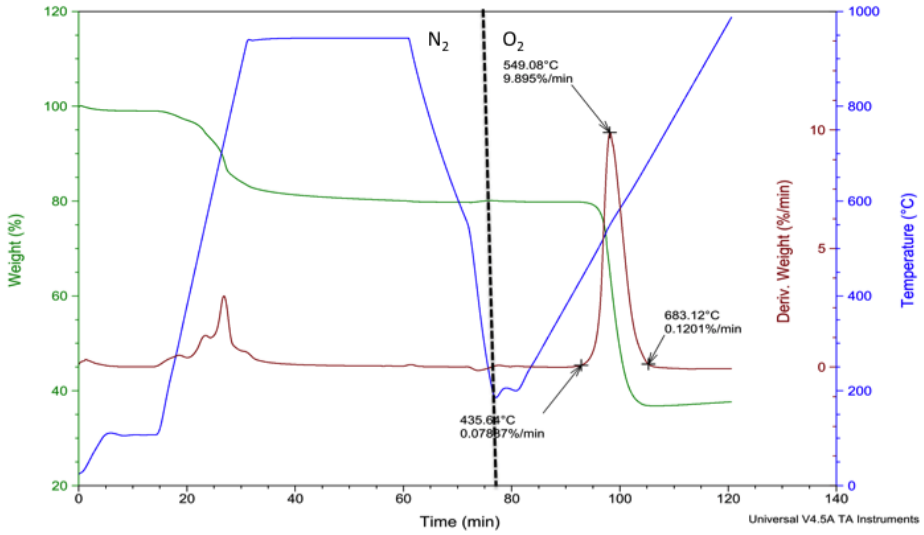

Figure 6.5: Non-isothermal oxidation of Res 450

Since the reactivity of the char-O_2 is much more rapid than in presence of pure CO_2, seen in Chapter 5, the reactivities show less dependence on the parent coal it is derived from [141]. Hence, the widely used reactivity index Yan et al. [52] could be applied to comment on the relative values of reactivity.

The Reactivity index can thus be defined as:

$$\mathrm{R_u} = \frac{2}{\tau_{0.5}} \tag{6.5}$$

Please refer Chapter 5 for explanation on the factors affecting reactivity in gasification. Similar factors dominate the reactivity in combustion reactions. However, the effect of pore surface area is highly influential in the latter. In our study, this effect is much more prominent given the sharp rise in the reactivity from the rate

Table 6.3: Reactivity index for Raw coal and residues based on 90% conversion

Sample	R_u 850 °C	R_u 950 °C	R_u 1000 °C
Raw coal	0.412	0.369	0.365
Res 300	0.355	0.396	0.650
Res 350	0.472	0.467	0.567
Res 400	0.445	0.510	0.524
Res 450	0.347	0.353	0.483

curves in Figs. 6.2, 6.3, 6.4 and 6.5. The increase in reactivity is largely related to the increase in the pore volume during combustion activity and as the reaction progress, reactivity decrease is due to the collapse of the pore walls explained earlier as the fusion of the plane structures [108]. During devolatilization, the char surface area is expected to rise upto 10 times its original (mentioned in Chapter 5) with the loss of volatile content and other functional groups. Thus, on the basis of the volatile content (Table 4.2) and initial surface area (Table 4.15) the char surface area increase could be in the order as mentioned:

$$\text{Res 400} \leq \text{Res 450} \leq \text{Res 350} \leq \text{Res 300} \leq \text{Raw coal}$$

However, the higher reactivity indices of the residues in Table 6.2 clearly proves that surface area alone is not the only factor at play. The reactivity index obtained from the above method is indicated in Table 6.2. A similar pattern of reactivity index was observed in presence of CO_2 by comparison of values on relative terms. At the lowest temperature of combustion, the reactivity for Res 350 was found to be the highest. This peak in the reactivity could be associated to the high mineral content per weight fixed carbon in the residue. Similar observations have been made by Yan et al. [52] and further investigation is required for conclusive result. Higher dispersion of mineral matter content in the char may be responsible for the catalytic combustion of the residues, thus providing us higher reactivities than raw coal. Since, the carbon at 90% conversions are usually difficult to burn due to their highly aromatic nature. A comparison of reactivity at 90% conversion is reported in Table 6.3. Though higher reactivity index with increasing temperature is apparent, the higher values can be reported for residues obtained at 350 °C and 400 °C. Since these values are related to the mass loss of carbon, lower carbon contents could be associated with the faster mass loss rate for these residues. Further, a comparatively higher H/C ratio for the residue derived at 350 °C explains the ease in mass loss of this sample compared to that of Res 400. However, an overall trend cannot be reported for oxidation reactivity of the residues in general.

The data thus generated in the TGA is a weight of the sample recorded with respect to time. This was helpful in obtaining the conversion degree (X) from the weight loss data as follows:

$$\mathrm{X} = \frac{(\mathrm{w_o} \ - \ \mathrm{w_{ash}}) \ - \ (\mathrm{w_t} \ - \ \mathrm{w_{ash}})}{w_o \ - \ w_{ash}} \tag{6.6}$$

The residue reactivity is a function of conversion which is given as is thus further calculated as:

$$\mathrm{r(X)} = \frac{1}{(\mathrm{w_t} \ - \ \mathrm{w_{ash}})} \frac{d(\mathrm{w_o} \ - \ \mathrm{w_t})}{dt} \tag{6.7}$$

Here, the terms w_o, w_t and $\mathrm{w}_a sh$ are defined as the weight present initially, during the time (t) and the final weight of the sample. Thus, the reaction rate equation can now be written, combining equations 6.6 and 6.7 in terms of conversion (X) as:

$$\mathrm{r(X)} = \frac{1}{(1 \ - \ \mathrm{X})} \frac{dX}{dt} \tag{6.8}$$

Complete conversion is derived from combustion under O_2. The plots 6.6, 6.7 and 6.8 represent the change in conversion with time and have been the basis for evaluation of the reactivity index 6.2 and kinetic parameters in the next section.

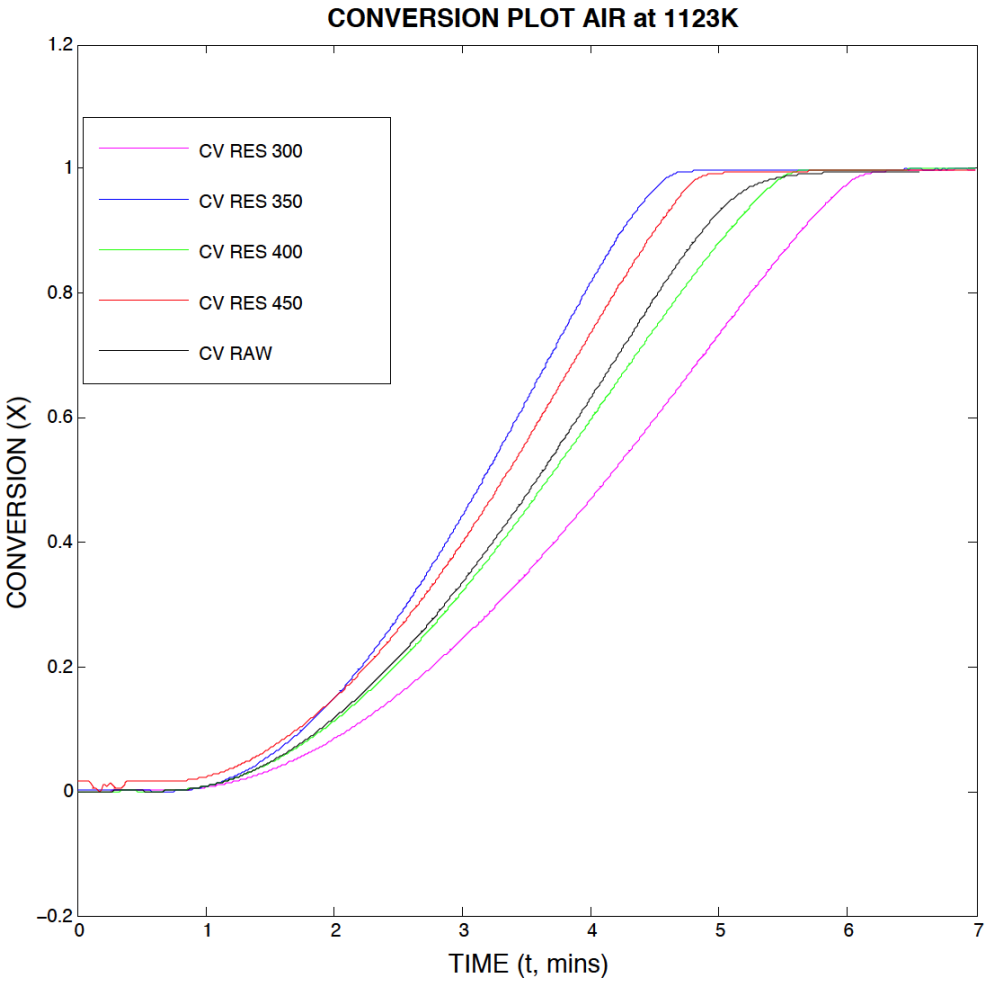

Figure 6.6: Conversion plot for CV raw and residues at 850 °C

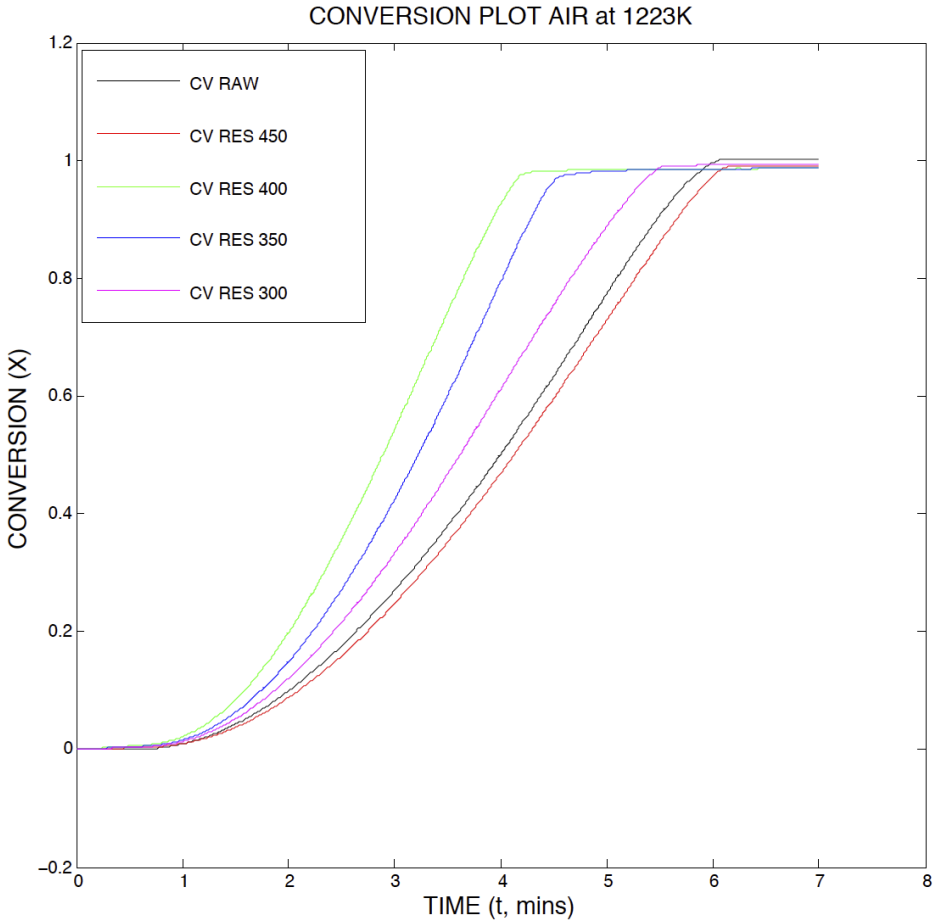

Figure 6.7: Conversion plot for CV raw and residues at 950 °C

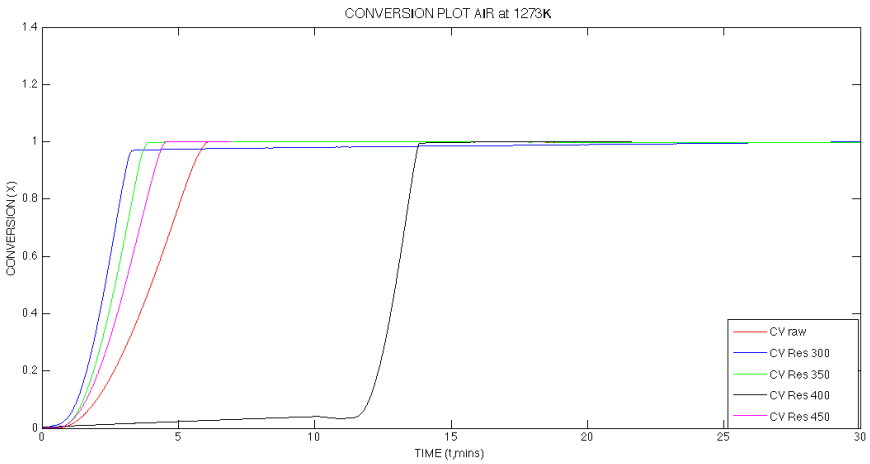

Figure 6.8: Conversion plot for CV raw and residues at 1000 °C

6.3.2 FORMULATION OF KINETIC PARAMETERS FOR COMBUSTION

Based on the validity study of TGA on the combustion activity, we may assume to operate on pseudo-steady conditions [129].This indicates that the inferences made on kinetic parametric analysis are almost free of the effects of chemisoprtion dynamics acting on the system.

Many model studies have been suggested for coal char combustion in O_2 [137], [142]-[143]. A homogeneous model was not considered, as mentioned in Chapter 5. A modified random pore model was found to be the best fit for our data with linear regression parameter of R^2 close to 0.9. It assumes that there is random overlapping of the surfaces of pores during the reaction [135]. A standard random pore model defines reactivity as,

$$\mathrm{r(X)} = \frac{dX}{dt} = \mathrm{k(X)e^{-E/RT}(1-X)(1-\psi ln(1-X))^{1/2}} \tag{6.9}$$

However, in the case of a modified random pore model, we account for the change in the reaction rate with conversion by introducing power law factor as [144],

$$\boxed{\mathrm{r(X)} = \frac{dX}{dt} = \mathrm{k(X)e^{-E/RT}(1-X)^{n}(1-\psi ln(1-X))^{1/2}}} \tag{6.10}$$

Here, n is a constant with no physical meaning. The value of ψ is considered to be close to 60.

Further calculation of the kinetic parameters are obtained from linear regression

Table 6.4: Kinetic parameters using Arrhenius Equation

Feed	E(kJ/mol)	A	R^2
RES 300	45.96	68.03	0.9932
RES 350	21.06	79.26	0.8021
RES 400	77.78	91.53	0.6471
RES 450	22.48	1.67e02	0.9997

of the data using the above equation 6.10 and substitution in the Arrhenius equation 6.11 to obtain A and E (activation energy) given in Table 6.4,

$$\ln(\mathrm{k}) = \ln(\mathrm{A}) - \frac{E}{R}(\frac{1}{T}) \tag{6.11}$$

Further kinetic constants are tabulated in the following Table6.4

Thus, the rate equations can be given as,

RES 300,

$$\boxed{r(X) = [68.03 - \frac{45.96}{R}](\frac{1}{T})(\ln \mathrm{P_{O_2}})\mathrm{f(X)}} \tag{6.12}$$

RES 350,

$$\boxed{r(X) = [79.26 - \frac{21.06}{R}](\frac{1}{T})(\ln \mathrm{P_{O_2}})\mathrm{f(X)}} \tag{6.13}$$

RES 400,

$$\boxed{r(X) = [91.53 - \frac{77.78}{R}](\frac{1}{T})(\ln \mathrm{P_{O_2}})\mathrm{f(X)}} \tag{6.14}$$

RES 450,

$$\boxed{r(X) = [1.67e02 - \frac{22.48}{R}](\frac{1}{T})(\ln \mathrm{P_{O_2}})\mathrm{f(X)}} \tag{6.15}$$

Low activation energies represent the ease of combustion activity of the residues. The values above represent the apparent kinetic parameters. However, in order to confirm the values to be true values of activation energy, comparison of results with those at lower temperatures of combustion is necessary. A sample fitting for residue derived at 300 °C liquefaction is represented by Fig. 6.9. Similar fittings were obtained for residues obtained at liquefaction at 350 °C, 400 °C and 450 °C.

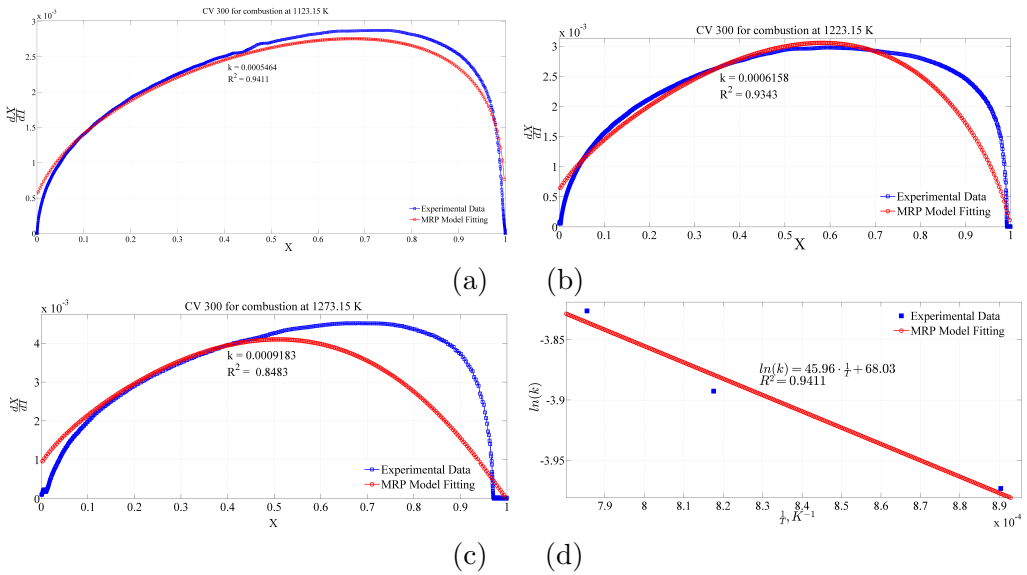

Figure 6.9: (a) Kinetics for CV Res 300 in O_2 AT 850 °C, (b) Kinetics for CV Res 300 in O_2 at 950 °C, (c) Kinetics for CV Res 300 in O_2 at 1000 °C, (d) Arrhenius plot for CV Res 300 in O_2

6.3.3 DETERMINING THE ASH CHARACTERISTICS OF LIQUEFACTION RESIDUE AND ITS COMPARISON WITH RAW COAL IN A REAL-TIME BOILER

As mentioned in Chapter 2, residues from the coal liquefaction process have been used as a boiler fuel much before 1960's. However, the environmental concerns raised due to the pollutant gaseous release and the ash slagging behaviour [53] of the feedstock are major concerns which have the dimed the applicability of the residues as a fuel source. In order to partially overcome the effects of SO_x release, blended feedstock consisting low sulphur coal and high calorific value coal have been utilized [145]. Thus, taking these factors into consideration, combustion of coal and residue was carried out in a real-time entrained flow reactor.

The Figs. 6.10 and 6.11 represent the char obtained from the entrained flow reactor for combustion of residue and raw at the same reaction conditions. Firstly, the temperatures inside the reactor system was maintained at 1000°C, well below the general ash slagging temperature for coals. Further, the residue and coals characterized for S/C ratio of 0.076 e-02 and 0.109 e-02, respectively were employed as the feedstock for the process.

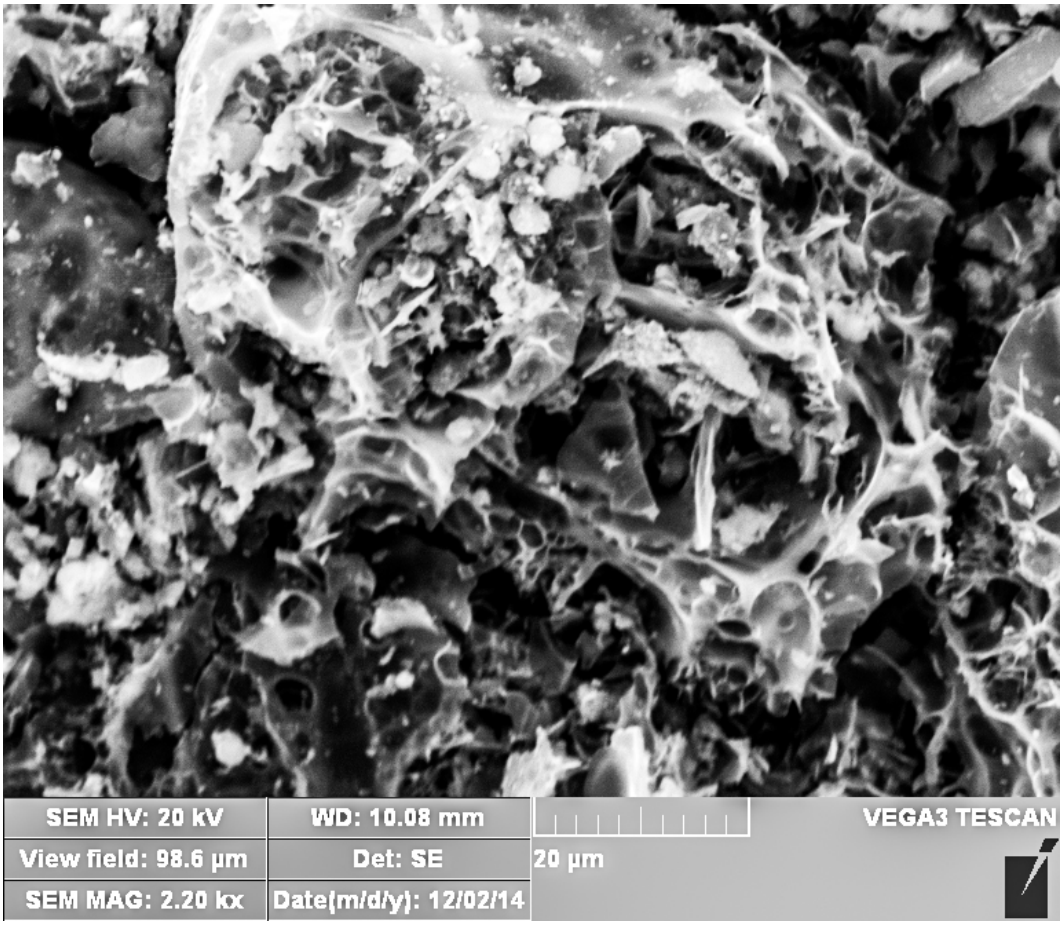

Figure 6.10: Residue char after combustion in an Entrained flow reactor

Considering the reaction mechanism of combustion, the oxygen diffuses rapidly into the porous surface of the char. As the reaction progress and the conversion approaches completion, the pore walls collapse slowly (evident from the rate curves) and seen in the Figs. 6.10 and 6.11. The residue chars are much more fragmented, while the raw coal char are granular. This was further confirmed from the particle size analysis of the chars (Figs. 6.12 and 6.13). This was further validated through a proximate analysis in a TGA, to calculate the left over ash in the chars derived from each of the two process materials (Table 6.5).

Table 6.5: Ash content in the char of residue and raw coal from Entrained flow reactor

Sample	Ash wt.% (A_f)	Ash wt.% (A_o)	E %
Char from Residue combustion	62.23	25.89	78.83
Char from Raw coal combustion	41.81	21.33	62.26

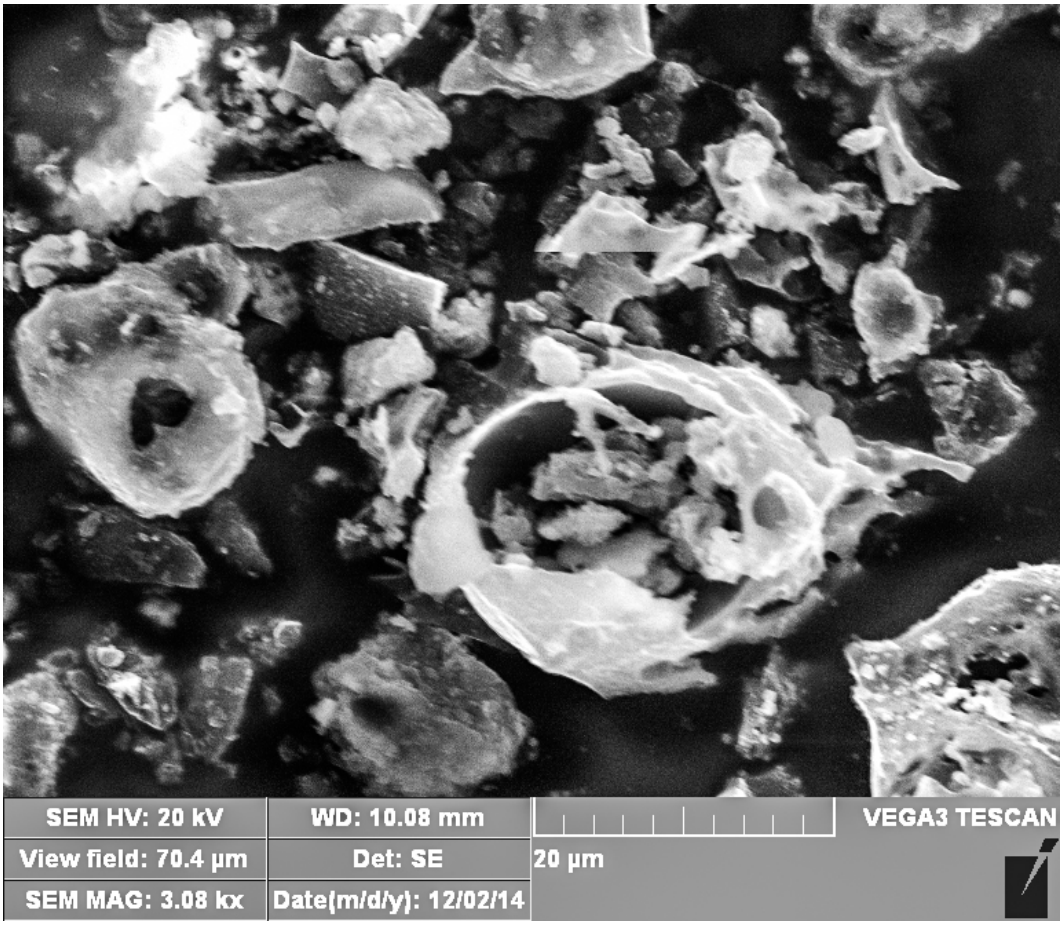

Figure 6.11: Raw coal char after combustion in an Entrained Flow reactor

The ash content of the chars determined with the TGA was used to calculate the efficiency in an entrained flow reactor by equation 6.16. An ash-tracer technique assuming the inertness of mineral matter during the combustion, is employed to calculate the efficiency of residual and raw coal combustion as follows [145]:

$$\mathrm{E} = [1 - \frac{\mathrm{A_o} \ * \ (100 - \mathrm{A_f})}{\mathrm{A_f} \ * \ (100 - \mathrm{A_o})} \ X \ 100 \tag{6.16}$$

Here, A_f and A_o are the final and initial ash contents of the samples.

Thus, combustion efficiency calculated above yields better results for residue combustion than that of raw coal (Table 6.5). This justifies our previous results and inferences with regard to higher reactivity of the residues, evident from the kinetic parametric calculations proving lower activation energy requirement for residues than raw coal.

The adiabatic temperature have been calculated by equating equations 6.17 and

6.18 as follows:

$$\mathrm{Q} = \triangle\mathrm{H} * \mathrm{m}_{\mathrm{organics}} * \mathrm{Efficiency} \tag{6.17}$$

$$\mathrm{Q} = \sum \mathrm{m_i Cp_i} * (T_{adiabatic} \ - \ T_o) \tag{6.18}$$

where the values are considered as stated below:

1. $\triangle$H = 32790 kJ/kg of carbon
2. $m_{organics}$ = mass of the sample * (% of organics remaining on an ash and moisture free basis/100)
3. Efficiency%, is as calculated from Table 6.5
4. i = components in the samples. Here, we account for mineral matter (since silicates are present in large amounts in raw coal as well residues, we account mainly for silicates, for calculation purposes), carbon content and CO_2 formed.
5. The m_i values of the above components are calculated from the results derived from proximate analysis of the residue (Table 4.2) and raw coal (Table 3.1). Further, m_{CO_2} is computed on the basis of 5.22.
6. The values of specific heat are taken from Perry's Handbook [146] as, Cp_{Si} = 0.703 kJ/kgK, Cp_{carbon} = 0.71 kJ/kgK and Cp_{CO_2} = 0.893 kJ/kgK. Since, the combustion was undertaken under isothermal conditions, constant values, independent of temperature, have been under consideration for comparison purposes only. These do not represent the true values of specific heat capacity for the samples.

Residue was more efficient than raw coal. Despite higher mineral content, the residue also resulted in a higher calculated adiabatic temperature increase during combustion (Table 6.6). Thus, residue was overall a better feed material than raw coal under the conditions evaluated.

Table 6.6: Calculated adiabatic temperatures of residue and raw coal combustion in the entrained flow reactor

Sample	$T_{adiabatic}$ (K)
Char from Residue combustion	2022
Char from Raw coal combustion	1904

Thus, effective utilization of the residue by accounting for the precursory steps to reduce the pollutant emission in a similar fashion, as being undertaken for raw coal, would prove to be a constructive step towards tapping the valuable energy from the coal liquefaction solid wastes.

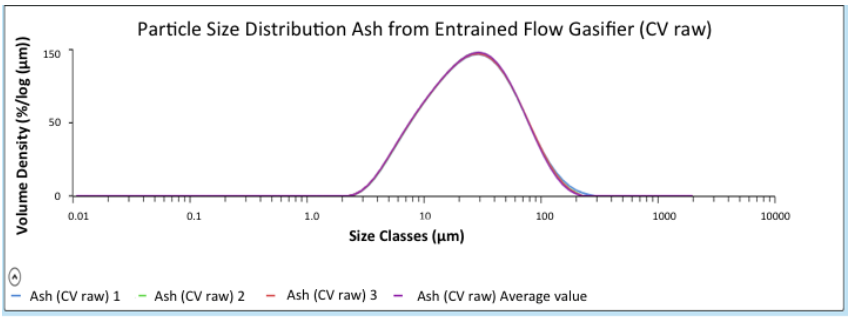

Sample Name	D_x (10) (µm)	D_x (50) (µm)	D_x (90) (µm)	Laser Obscuration (%)
CV Raw Run1	6.79	60.7	170	3.98
CV Raw Run 2	6.96	63.1	177	3.99
CV Raw Run 3	6.88	62.0	175	4.00
Mean	6.88	61.9	174	3.99
1X Std Dev.		1.21	3.59	0.01

Figure 6.12: Particle size distribution for Ash from CV Raw Partial Oxidation

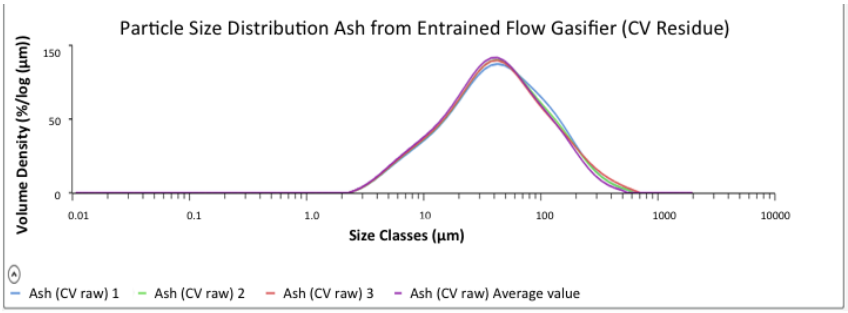

Sample Name	D_x (10) (µm)	D_x (50) (µm)	D_x (90) (µm)	Laser Obscuration (%)
CV Res Run1	9.93	42.5	156	2.26
CV Res Run 2	9.73	41.2	153	2.58
CV Res Run 3	9.66	40.9	160	2.72
Mean	9.68	41.0	153	2.59
1X Std Dev.		0.217	8.15	0.24

Figure 6.13: Particle size distribution for Ash from Residue Partial Oxidation

6.4 GENERAL DISCUSSIONS

Ash wastes of the boiler bottoms generally form the raw material for cement industries. Presence of unburnt carbon in these bottom wastes are detrimental towards ash utilisation. Thus, complete conversion of carbon as boiler feed is preferred for effective utilisation of waste. This forms the basis of execution of experiments in an entrained flow reactor. The efficiency of the boiler feed for an entrained flow reactor system is compared based on an ash-tracer technique using equation 6.16. In order to overcome discrepancies due to different distribution of ash and carbon content in the residue as well raw coal, a comparison of the temperature the combustion products reach theoretically, assuming no loss of heat to the surroundings, is undertaken. Thus, though residue is efficient than raw coal, but if one considers the higher mineral content, the adiabatic temperatures of the residue and raw coal are found to be in a similar temperature range. These values indicate the temperature of the products, assuming there is no loss of heat to the surroundings.

A comparison of reactivity at 90% conversion is reported in Fig. 6.14. Though higher reactivity index with increasing temperature is apparent, the higher values can be reported for residues obtained at 350 °C and 400 °C. Though reasons for higher reactivity index for residue derived at 350 °C have been explained in Section 6.3.1, an overall trend cannot be reported for oxidation reactivity of the residues alone.

Further, the data on mass low rate obtained from the TGA have been accounted for the determination of activation energy and Arrhenius constant for the residues. The reactivity is related to mass loss rate alone. Also, since coal is assumed to be a homogeneous entity representing carbon particle only, side reactions associated with those of mineral matter are ignored. These values indicate the minimum energy barrier to be overcome for a reaction to proceed towards completion with desired product formation. This would, in turn, aid in estimation of the minimum energy values that need to be supplied to the reactor, employing residue as the feed, for almost complete combustion of feed carbon. Again, note the low values of 'A' in Table 6.4. Very low values indicate the existence of mass transfer limitations. Thus, the activation energy values reported here represent the apparent activation energy values of the residues.

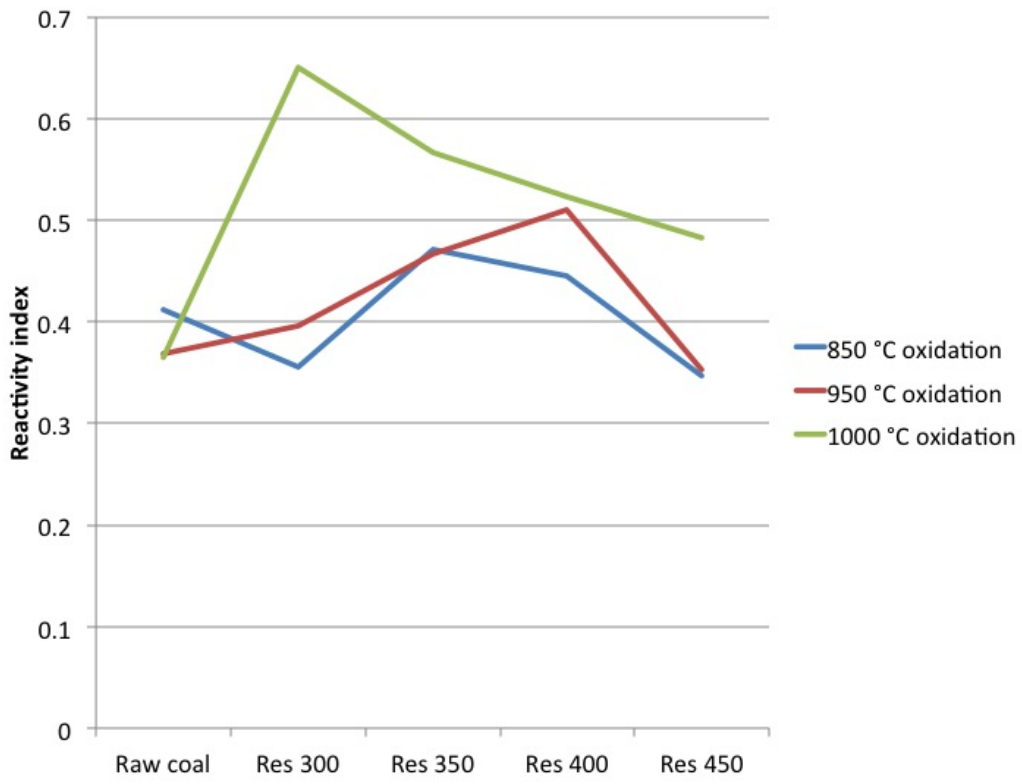

Figure 6.14: Reactivity index comparison of raw coal and residue based on 90% conversion

6.5 CONCLUSIONS

Based on the evaluation of the isothermal and non-isothermal combustion behaviour of residue at 850 °C, 950 °C and 1000 °C in a TGA and in a real-time boiler using an Entrained flow reactor, the results can be stated as below:

1. Increase in temperature tends to accelerate the mass loss and thus the reactivity index (associated with the mass loss rate). Much larger mass loss rates are reported for the residues in comparison to that of raw coal. Similar contributing factors, as seen in Chapter 5, were found to enhance the combustion reactivity of residues.

2. Efficiency of the boiler feed was calculated based on an ash-tracer method given by equation 5.9. Utilization of the residue as a boiler feed yields higher efficiency of 79% as against 62% efficiency of raw coal.

3. A comparison of the adiabatic temperatures of the residues and the raw coal

was conducted. Thus, though residue is efficient than raw coal, but if one considers the higher mineral content, the adiabatic temperatures of the residue and raw coal are found to be in a similar temperature range. These values are indicative of the maximum temperature that can be obtained for a given composition of reactants, assuming there is no loss of heat to the surroundings.

Chapter 7

CONCLUSIONS

Industrial recycle solvents and pulverized coal from Sherritt Intl. Ltd. were the raw materials employed under conditions that resembled a real-time liquefaction process. Increasing the severity of the liquefaction conditions is speculated to yield larger coal liquid yields, which may in turn be effective in reduction of residue formation. Also, since a coal liquefaction process is considered to proceed through a radical formation mechanism, where the fate of the product stream is dictated by hydrogen capping, liquefaction under H_2 using hydrotreated solvent may be expected to curb residue formation. Liquefaction experiments were conducted on Canadian sub-bituminous coal valley (CV) coal by employing non-hydrotreated under N_2 and hydrotreated solvents under H_2 and N_2 at four different temperature conditions (300 °C, 350 °C, 400 °C and 450 °C) to study the effect of these parametric variations on the coal liquefaction residue generated during the process. The conclusions can be summarized as follows:

1. Better yields of liquid products were derived from the HT solvent (83%) compared to nonhydrotreated solvent (68%) owing to improved dissolution and H-donor ability of the solvent.

2. Liquefaction at 300 °C generated a major reject stream with residues upto 78 wt.% organic (daf basis). Further increase in the liquefaction temperature increased the organic conversion of the coal upto 400 °C. However, due to conditions leading to unavailability of hydrogen at very high liquefaction temperatures (450 °C), the organic conversion reduces to yield upto 44 wt.% C (daf basis) in the waste stream.

3. Comparatively higher coal liquid yields (83%) were observed for liquefaction under HT solvent under N_2. The highest value of liquid yield for liquefaction

under NHT solvent was 68%.

4. Liquefaction under H_2 at induction/residence time of 60 min, had a negative impact on the yield of the liquid products. It is speculated that this could be due to adduction reactions generating upto 55 wt.% residual stream at low temperatures (300 °C). Further increase in temperature, increases the conversion percentage and reduces the percentage of organic in the residual stream to 30 wt.% C at 350 °C and 400 °C. Further increase in temperature to 450 °C, results in very slight increase (about 1 wt.%) in the yield of coal liquid products.

In order to understand any process dynamics, it is imperative to have a thorough knowledge of the properties of the raw materials in use. Thus, before we proceed towards upgrading of the residue or its utilization in any particular process stream, a knowledge or a basic awareness about its chemical and physical composition is critical. A solvent with lower heteroatoms is expected to yield liquid products of superior quality which do not require extensive hydro-processing towards heteroatom removal. Increasing severity of liquefaction could in turn reduce the particle size of the coal particles during the process. Also, with increasing conversion of the organic matrix of coal, a large chunk of the bulky mineral material could be suspected in the residual waste stream. Thus, analysis of the residues have been conducted to determine the morphology, mineral composition, particle size distribution, surface area, elemental composition and presence of the type of functional groups to yield the following results:

1. SEM studies prove that the morphology of the residues do not undergo a major transition during the liquefaction process. However, higher percentage of mineral matter was evident from the backscattered electron images of the residues when compared with those of raw coal.

2. Solvent properties were found to highly dictate the composition of the liquid products, in comparison to that of the liquefaction atmosphere. Presence of H_2 atmosphere had a very little influence on the conversion of the tar precursors (fixed carbon), while high conversion values could be associated with the major hydrogen transfer dominated due to that from the solvents.

3. Efficient conversions of volatile material with increasing liquefaction temperature conditions is apparent.

4. The residues derived from liquefaction under NHT solvent represent very low ash values compared to that under HT solvent.

5. The H/C ratio decreased with increasing severity in liquefaction conditions, as desired. However, slightly higher H/C for the residues derived from liquefaction under H_2 proved the association of hydrogen in the waste stream.

6. Incorporation of the heteroatoms in the product stream was influenced to a large extent due to the solvent properties. Higher S/C and N/C ratios have been reported for residues from liquefaction under HT solvent, a recycle industrial solvent hydrotreated for heteroatom removal in comparison to NHT solvent that has a comparatively higher composition of heteroatoms.

7. For all conversion calculations, a basic assumption that ash remains unconverted during the liquefaction process was made. This was later confirmed from the XRF analysis which accounted for the ash properties in raw coal and the residue. Thus, a ratio of the silicates in the residue and each mineral component in the residue was compared to those in raw coal, yielded values close to unity.

8. FTIR characterization of the residues also represented the higher intensity of the aromatic matrix in the residues, thus proving the insatiability of the hydrogen demand at high temperatures, thus generating wastes with higher ratio of carbon to hydrogen content.

9. The particle size of the residues at first increase, at low liquefaction temperatures, suggesting solvent swelling effects and agglomeration, followed by a decrease in the particle size with increasing severity of liquefaction conditions. A two phase reaction system can be said to co-exist which leads to a bimodal particle size distribution at temperatures above the softening temperature of coal.

10. Density functional theory (DFT) method was employed to carry out classification of pore morphology for raw coal as well residues. CO_2 was chosen as the adsorptive since ineffective diffusion of N_2 into micro-pores at low temperature adsorption requirements.

11. A similar contribution towards the micro-porosity and mesopore distribution is evident in the residues as well in raw coal. However, the decrease in surface area is due to the reduction in the pore volume, suggesting agglomeration or closed pores developed during plasticity of sub-bituminous coal under pressurized liquefaction conditions.

A kinetic study of combustion and gasification zones and further evaluation of the kinetic parameters indicate the minimum energy to be overcome for product formation. Thus, this study would aid in the determination of the potential of a residue as a feed source for gasifier plants under real-time conditions and predict system efficiency. Given the residue's elemental properties pertaining to a much lower H/C ratio compared to that of raw coal, it could be speculated that gasification of residue may require much higher temperatures for gasification i.e ease of gasification of refractory material in the residue would be difficult compared to raw coal. Hence, experiments have been undertaken to determine the gasification behaviour of residues. Based on the evaluation of the isothermal and non-isothermal gasification behaviour of residue at 950 °C, 1000 °C and 1100 °C in a TGA, the results can be stated as below:

1. The kinetic parameters reported in the study reflect the apparent values for rate of reaction of residues.

2. The reactivity of the residues were found to be higher than that of the raw coal at high temperatures of gasification. This phenomena was associated with the catalytic activity of the mineral matter in the residues which served as an enhancing medium for the gasification reactions.

3. The residues obtained from higher temperatures of liquefaction, demanded much severe conditions of gasification depending upon their H/C ratio.

4. Further, determination of the kinetic parameters have been carried out using line fitting techniques and linear regression in suitable models.

Combustion being a relatively faster reaction than gasification, due to its exothermic nature, the refractory residual material can be expected to undergo combustion with efficiency compared to that of raw coal. Thus, we have carried out a preliminary study on determination of the kinetic parameters and reactivity of the residue in a TGA. Further a practical combustion unit such as an Entrained Flow Reactor was employed to determine the combustion efficiency of the residue in comparison to raw coal. These precursory investigations, we believe, would allow us to represent the conditions in a practical combustion system and thus help validate our conclusions effectively. Based on the evaluation of the isothermal and non-isothermal combustion behaviour of residue at 850 °C, 950 °C and 1000 °C in a TGA and in a real-time boiler using an Entrained flow reactor, the results can be stated as below:

1. Increase in temperature tends to accelerate the mass loss and thus the reactivity index (associated with the mass loss rate). Much larger mass loss rates

are reported for the residues in comparison to that of raw coal. Similar contributing factors, as seen in Chapter 5, were found to enhance the combustion reactivity of residues.

2. Efficiency of the boiler feed was calculated based on an ash-tracer method given by equation 5.9. Utilization of the residue as a boiler feed yields higher efficiency of 79% as against 62% efficiency of raw coal.

3. A comparison of the adiabatic temperatures of the residues and the raw coal was conducted. Thus, though residue is efficient than raw coal, but if one considers the higher mineral content, the adiabatic temperatures of the residue and raw coal are found to be in a similar temperature range. These values are indicative of the maximum temperature that can be obtained for a given composition of reactants, assuming there is no loss of heat to the surroundings.

Attempts to conduct oxidative hydrothermal dissolution of residues was also undertaken. It was realized that liquefaction residues would require much severe conditions for dissolution and do not comply with the parametric condition requirements of that of raw coal. A safety note is included in the Appendix.

Bibliography

[1] Sivakumar Vasireddy, Bryan Morreale, Anthony Cugini, Chunshan Song, and James J Spivey. Clean liquid fuels from direct coal liquefaction: chemistry, catalysis, technological status and challenges. *Energy & Environmental Science*, 4(2):311–345, 2011.

[2] AS Al-Jarri, RA Startzman, et al. Worldwide Petroleum-Liquid Supply and Demand (includes associated papers 52597 and 52598). *Journal of Petroleum Technology*, 49(12):1–329, 1997.

[3] Mikael Höök and Kjell Aleklett. A review on coal-to-liquid fuels and its coal consumption. *International Journal of Energy Research*, 34(10):848–864, 2010.

[4] Sunggyu Lee, James G Speight, and Sudarshan K Loyalka. *Alternative Fuel Technologies*. CRC Press, Boca Raton, FL, 2007.

[5] Rakesh Agrawal, Navneet R Singh, Fabio H Ribeiro, and W Nicholas Delgass. Sustainable fuel for the transportation sector. *Proceedings of the National Academy of Sciences*, 104(12):4828–4833, 2007.

[6] Isao Mochida, Osamu Okuma, and Seong-Ho Yoon. Chemicals from direct coal liquefaction. *Chemical reviews*, 114(3):1637–1672, 2013.

[7] Alfred G. Comolli, Theo L.K. Lee, Gabriel A. Popper, and Peizheng Zhou. The Shenhua coal direct liquefaction plant. *Fuel Processing Technology*, 59 (23):207 – 215, 1999. ISSN 0378-3820. doi: http://dx.doi.org/10.1016/S0378-3820(99)00016-8. URL `http://www.sciencedirect.com/science/article/pii/S0378382099000168`.

[8] Motoyuki Sugano, Taku Tamaru, Katsumi Hirano, and Kiyoshi Mashimo. Additive effect of tyre constituents on the hydrogenolyses of coal liquefaction residue. *Fuel*, 84(17):2248–2255, 2005.

[9] Katsumi Hirano. Outline of NEDOL coal liquefaction process development (pilot plant program). *Fuel processing technology*, 62(2):109–118, 2000.

[10] S Khare and M Dell'Amico. An overview of conversion of residues from coal liquefaction processes. *The Canadian Journal of Chemical Engineering*, 91 (10):1660–1670, 2013.

[11] Anthony N Stranges. Friedrich Bergius and the transformation of coal liquefaction from empiricism to a science-based technology. *Journal of Chemical Education*, 65(9):749, 1988.

[12] Martin L Gorbaty. Prominent frontiers of coal science: past, present and future. *Fuel*, 73(12):1819–1828, 1994.

[13] John H Shinn. From coal to single-stage and two-stage products: a reactive model of coal structure. *Fuel*, 63(9):1187–1196, 1984.

[14] Marielle R Narkiewicz and Jonathan P Mathews. Improved low-volatile bituminous coal representation: Incorporating the molecular-weight distribution. *Energy & Fuels*, 22(5):3104–3111, 2008.

[15] Darrell Duayne Whitehurst, Thomas O Mitchell, and Malvina Farcasiu. *Coal liquefaction: the chemistry and technology of thermal processes*, volume 1. New York, Academic Press, Inc., 1980.

[16] He Huang, Shaojie Wang, Keyu Wang, Michael T Klein, and William H Calkins. Effect of solvent characteristics on coal liquefaction. *Preprints of Papers- American Chemical Society Division Fuel Chemistry*, 41:961–966, 1996.

[17] Jean P Teas. Graphic analysis of resin solubilities. *Journal of paint technology*, 40(516):19–25, 1968.

[18] Hans-Peter Hombach. General aspects of coal solubility. *Fuel*, 59(7):465–470, 1980.

[19] Chunshan Song, Ajay K Saini, and Harold H Schobert. Effects of drying and oxidation of Wyodak subbituminous coal on its thermal and catalytic liquefaction. Spectroscopic characterization and products distribution. *Energy & fuels*, 8(2):301–312, 1994.

[20] Michael A Wilson, Ronald J Pugmire, AM Vassallo, DM Grant, PJ Collin, and KW Zilm. Changes in aromaticity during coal liquefaction. *Industrial*

& Engineering Chemistry Product Research and Development, 21(3):477–483, 1982.

[21] Natsuko Cyr and Nosa O Egiebor. Characterization of coal-liquefaction residues by solid-state C-13 NMR-spectroscopy. *Advances in Chemistry Series*, 229:281–294, 1993.

[22] Peter F Barron, John F Stephens, and Michael A Wilson. Aromatic and aliphatic composition of the solid and liquid products from hydrogenation of liddell coal. *Fuel*, 60(6):547–549, 1981.

[23] B Granoff and PA Montano. Mineral matter effects in coal conversion. In *Chemistry and Physics of Coal Utilization-1980*, volume 70, pages 291–308. AIP Publishing, 1981.

[24] Dilip K Mukherjee and Priya B Chowdhury. Catalytic effect of mineral matter constituents in a North Assam coal on hydrogenation. *Fuel*, 55(1):4–8, 1976.

[25] Peter H Given, Donald C Cronauer, William Spackman, Harold L Lovell, Alan Davis, and Bimal Biswas. Dependence of coal liquefaction behaviour on coal characteristics. 2. Role of petrographic composition. *Fuel*, 54(1):40–49, 1975.

[26] SJ Russel. Characterization by scanning microscopy of mineral matter in residues of coal liquefaction. *Scanning Electron Microscopy*, 1:95–100, 1977.

[27] RG Jenkins and PL Walker Jr. Analysis of mineral matter in coal. *Analytical methods for coal and coal products*, 2:265–292, 1978.

[28] Frank Derbyshire, Alan Davis, Mike Epstein, and Peter Stansberry. Temperature-staged catalytic coal liquefaction. *Fuel*, 65(9):1233–1239, 1986.

[29] B Cornils, J Hibbel, P Ruprecht, J Langhoff, and R Dürrfeld. Gasification of hydrogenation residues using the Texaco coal gasification process. *Fuel processing technology*, 9(3):251–264, 1984.

[30] Long Xu, Mingchen Tang, Line Duan, Baolin Liu, Xiaoxun Ma, Yulong Zhang, Morris D. Argyle, and Maohong Fan. Pyrolysis characteristics and kinetics of residue from china Shenhua industrial direct coal liquefaction plant. *Thermochimica Acta*, 589(0):1 – 10, 2014. ISSN 0040-6031. doi: http://dx.doi.org/10.1016/j.tca.2014.05.005. URL `http://www.sciencedirect.com/science/article/pii/S0040603114002020`.

[31] Jun Li, Jianli Yang, and Zhenyu Liu. Hydro-treatment of a direct coal liquefaction residue and its components. *Catalysis Today*, 130(2):389–394, 2008.

[32] Peng Li, Zhi-Min Zong, Fang-Jing Liu, Yu-Gao Wang, Xian-Yong Wei, Xing Fan, Yun-Peng Zhao, and Wei Zhao. Sequential extraction and characterization of liquefaction residue from Shenmu–Fugu subbituminous coal. *Fuel Processing Technology*, 2014.

[33] Ren Ying-jie, An-ling Wei, De-xiang Zhang, Jin-chao Zhao, Chun-dai Lin, and Jin-sheng Gao. Rheological characteristics of coal hydro-liquefaction residue. *Journal of Fuel Chemistry and Technology*, 35(3):262–267, 2007.

[34] Tao-Xia Wang, Zhi-Min Zong, Jia-Wei Zhang, Yan-Bin Wei, Wei Zhao, Bao-Min Li, and Xian-Yong Wei. Microwave-assisted hydroconversions of demineralized coal liquefaction residues from Shenfu and Shengli coals. *Fuel*, 87 (45):498 – 507, 2008. ISSN 0016-2361. doi: http://dx.doi.org/10.1016/j.fuel.2007.04.016. URL `http://www.sciencedirect.com/science/article/pii/S0016236107002025`. The 9th ChinaJapan Symposium on Coal and {C1} Chemistry.

[35] Xi-jie Chu, Wen Li, Bao-qing Li, and Hao-kan Chen. Gasification property of direct coal liquefaction residue with steam. *Process safety and environmental protection*, 84(6):440–445, 2006.

[36] Motoyuki Sugano, Rieko Ikemizu, and Kiyoshi Mashimo. Effects of the oxidation pretreatment with hydrogen peroxide on the hydrogenolysis reactivity of coal liquefaction residue. *Fuel processing technology*, 77:67–73, 2002.

[37] Ying Zhou, Nan Xiao, Jieshan Qiu, Yufeng Sun, Tianjun Sun, Zongbin Zhao, Yi Zhang, and Noritatsu Tsubaki. Preparation of carbon microfibers from coal liquefaction residue. *Fuel*, 87(1516):3474 – 3476, 2008. ISSN 0016-2361. doi: http://dx.doi.org/10.1016/j.fuel.2008.05.017. URL `http://www.sciencedirect.com/science/article/pii/S0016236108002184`.

[38] Yi Li, Xiangping Zhang, Shiyao Lai, Haifeng Dong, Xuelian Chen, Xiaoliang Wang, Yi Nie, Ying Sheng, and Suojiang Zhang. Ionic liquids to extract valuable components from direct coal liquefaction residues. *Fuel*, 94:617–619, 2012.

[39] James C. Hower, Robert A. Keogh, Darrell N. Taulbee, and Robert F. Rathbone. Petrography of liquefaction residues: semifusinite concentrates from

a Peach Orchard coal lithotype, Magoffin County, Kentucky. *Organic Geochemistry*, 20(2):167 – 176, 1993. ISSN 0146-6380. doi: http://dx.doi.org/10.1016/0146-6380(93)90035-A. URL `http://www.sciencedirect.com/science/article/pii/014663809390035A`.

[40] James C. Hower, Ken B. Anderson, Glenda Mackay, Henrique Pinheiro, Deolinda Flores, and Manuel J. Lemos de Sousa. Interlaboratory comparisons of petrography of liquefaction residues from three Argonne premium coals. *Organic Geochemistry*, 22(1):27 – 32, 1995. ISSN 0146-6380. doi: http://dx.doi.org/10.1016/0146-6380(95)90005-5. URL `http://www.sciencedirect.com/science/article/pii/0146638095900055`.

[41] N Tomoyuki, S Isao, and S Mitsuhiro. Fluidity of coal liquefaction residue. *Nippon Enerugi Gakkaishi*, 72(10):977–984, 1993.

[42] I Masumi, I Kunihiro, O Yasunari, and I Kenji. Characteristics of coal liquefaction residue produced at the 1 ton/day PDU. *Sekitan Kagaku Kaigi Happyo Ronbunshu*, 32:49–52, 1995.

[43] Z Liu and J Yang. Some thoughts on the strategy of direct coal liquefaction–Partial liquefaction and utilization of heavy liquefaction products, 1998.

[44] Hisashi Ochihai, Wataru Ohki, Isao Tateno, Mashimo Kiyoshi, and Wainai Tohru. Pyrolysis of 1 t/d PSU coal liquefaction residue with supercritical fluids. *Fuel and Energy Abstracts*, 43(1):61, 2002. ISSN 0140-6701. doi: http://dx.doi.org/10.1016/S0140-6701(02)80602-6. URL `http://www.sciencedirect.com/science/article/pii/S0140670102806026`.

[45] Yi Nie, Lu Bai, Yi Li, Haifeng Dong, Xiangping Zhang, and Suojiang Zhang. Study on extraction asphaltenes from direct coal liquefaction residue with ionic liquids. *Industrial & Engineering Chemistry Research*, 50(17):10278–10282, 2011.

[46] Jieli Wang, Hongwei Yao, Yi Nie, Lu Bai, Xiangping Zhang, and Jianwei Li. Application of iron-containing magnetic ionic liquids in extraction process of coal direct liquefaction residues. *Industrial & Engineering Chemistry Research*, 51(9):3776–3782, 2012.

[47] Yi Li, Xiangping Zhang, Heifeng Dong, Xiaoliang Wang, Yi Nie, and Suojiang Zhang. Efficient extraction of direct coal liquefaction residue with the [bmim] Cl/NMP mixed solvent. *RSC Adv.*, 1(8):1579–1584, 2011.

[48] BG Silbernagel, LA Gebhard, RA Flowers, and JW Larsen. Demineralization effects on the EPR properties of Argonne premium coals. *Energy & fuels*, 5 (4):561–568, 1991.

[49] Chen Chong, Gao Jinsheng, and Yan Yongjie. Change of coal organics during chemical demineralization [J]. *Journal of East China University of Science and Technology*, 3, 1997.

[50] Nan Xiao, Ying Zhou, JieShan Qiu, and Zonghua Wang. Preparation of carbon nanofibers/carbon foam monolithic composite from coal liquefaction residue. *Fuel*, 89(5):1169–1171, 2010.

[51] Jun-hu Zhou, Lei Fang, Jun Chen, Jian-zhong Liu, Zhi-jun Zhou, and Ke-fa Cen. Dynamic sulfur emission from combustion of blends of coal liquefaction residue and biomass. *Journal of Fuel Chemistry and Technology*, 33(5):626, 2005.

[52] Jingchong Yan, Zonqing Bai, Wen Li, and Jin Bai. Direct liquefaction of a chinese brown coal and CO_2 gasification of the residues. *Fuel*, 136(0): 280 – 286, 2014. ISSN 0016-2361. doi: http://dx.doi.org/10.1016/j.fuel.2014.07.054. URL `http://www.sciencedirect.com/science/article/pii/S0016236114007054`.

[53] J.S. Harrison. M - The Utilization or Disposal of Coal Processing Residues. In *Oils and Gases from Coal*, pages 253 – 264. Pergamon, 1980. ISBN 978-0-08-025678-8. doi: http://dx.doi.org/10.1016/B978-0-08-025678-8.50020-8. URL `http://www.sciencedirect.com/science/article/pii/B9780080256788500208`.

[54] Production of hydrogen-enriched hydrocarbonaceous liquids, January 23 1962. US Patent 3,018,242.

[55] CY Wen and TZ Chaung. Entrainment coal gasification modeling. *Industrial & Engineering Chemistry Process Design and Development*, 18(4):684–695, 1979.

[56] Rakesh Govind and Jogen Shah. Modeling and simulation of an entrained flow coal gasifier. *AIChE Journal*, 30(1):79–92, 1984.

[57] Norman L Carr and Bruce K Schmid. Integrated coal liquefaction-gasification process, October 28 1980. US Patent 4,230,556.

[58] Reginald D Richardson. Process utilizing pyrolyzation and gasification for the synergistic co-processing of a combined feedstock of coal and heavy oil to produce a synthetic crude oil, February 13 1990. US Patent 4,900,429.

[59] Y. Taki, M. Maemura, S. Kawai, Y. Nakako, and H. Narita. Gasification test of coal liquefaction residue from pilot plant. In International Energy Agency Coal Research Ltd, editor, *1991 International Conference on Coal Science Proceedings*, pages 408 – 411. Butterworth-Heinemann, 1991. ISBN 978-0-7506-0387-4. doi: http://dx.doi.org/10.1016/B978-0-7506-0387-4.50104-2. URL `http://www.sciencedirect.com/science/article/pii/B9780750603874501042`.

[60] Cui Hong, Yang Jianli, Liu Zhenyu, and Bi Jicheng. Coal liquefaction residue and its gasification for hydrogen [J]. *Coal Conversion*, 1:003, 2001.

[61] Jun-hu Zhou, Lei Fang, Jun Cheng, Jian-zhong Liu, Zhen-yu Huang, and Ke-fa Cen. Influence of heating-up rate on combustion property and kinetic parameters of Shenhua coal liquefaction residuals [J]. *Power Engineering*, 4: 027, 2005.

[62] Xijie Chu, Wen Li, Baoqing Li, and Haokan Chen. Sulfur transfers from pyrolysis and gasification of direct liquefaction residue of Shenhua coal. *Fuel*, 87(2):211–215, 2008.

[63] Wang Peng, Bu Xue-peng, Xin Shi-he, and Deng Yi-ying. Study on the pyrolysis characteristics of coal liquefaction residues. *Coal Chemical Industry*, 2: 20–23, 2005.

[64] Xin Liu, Zhi-jie Zhou, Qi-jing Hu, Zheng-hua Dai, and Fu-chen Wang. Experimental study on co-gasification of coal liquefaction residue and petroleum coke. *Energy & Fuels*, 25(8):3377–3381, 2011.

[65] ASTM D7582-12:Standard Test Methods for Proximate Analysis of Coal and Coke by Macro Thermogravimetric Analysis, 2012.

[66] ASTM D3176-09:Standard Practice for Ultimate Analysis of Coal and Coke, 2009.

[67] Moshfiqur Rahman, Arunkumar Samanta, and Rajender Gupta. Production and characterization of ash-free coal from low-rank Canadian coal by solvent extraction. *Fuel Processing Technology*, 115:88–98, 2013.

[68] ASTM D2887:Standard Test Method for Boiling Range Distribution of Petroleum Fractions by Gas Chromatography, 2013.

[69] Bilal A Akash. Thermochemical liquefaction of coal. *Int. J. of Thermal & Environmental Engineering*, 5(1):51–60, 2013.

[70] James A Franz, Tom Autrey, Donald M Camaioni, John D Watts, and Rodney J Bartlett. Role of aromatic structure in pathways of hydrogen transfer and bond cleavage in coal liquefaction: Theoretical studies. *Coal Science and Technology*, 24:1411–1414, 1995.

[71] Testuo Aida Motohiko Satoh Yasuhumi Shimoura and Masayuki Fujii. Coal gel chemistry 2. Coal liquefaction by binary solvent system, 1988.

[72] Amir Attar and Robert Allen Meyers. *Coal Structure*. Academic Press, 1982.

[73] Hengfu Shui, Zhenyi Cai, and Chunbao Charles Xu. Recent advances in direct coal liquefaction. *Energies*, 3(2):155–170, 2010.

[74] Donald C. Cronauer, Robert I. McNeil, Donald C. Young, and Raffaele G. Ruberto. Hydrogen/deuterium transfer in coal liquefaction. *Fuel*, 61(7):610 – 619, 1982. ISSN 0016-2361. doi: http://dx.doi.org/10.1016/0016-2361(82)90005-9. URL `http://www.sciencedirect.com/science/article/pii/0016236182900059`.

[75] Peter R Solomon, Michael A Serio, Girish V Despande, and Erik Kroo. Cross-linking reactions during coal conversion. *Energy & Fuels*, 4(1):42–54, 1990.

[76] Kouichi Miura, Kazuhiro Mae, Wen Li, Takumi Kusakawa, Fumiaki Morozumi, and Akiko Kumano. Estimation of hydrogen bond distribution in coal through the analysis of OH stretching bands in diffuse reflectance infrared spectrum measured by in-situ technique. *Energy & Fuels*, 15(3):599–610, 2001. doi: 10.1021/ef0001787. URL `http://dx.doi.org/10.1021/ef0001787`.

[77] Mariangel Rivolta Hernandez, Carolina Figueroa Murcia, Rajender Gupta, and Arno de Klerk. Solvent–coal–mineral interaction during solvent extraction of coal. *Energy & Fuels*, 26(11):6834–6842, 2012.

[78] Joseph I Goldstein, Dale E Newbury, Patrick Echlin, David C Joy, Charles Fiori, Eric Lifshin, et al. *Scanning electron microscopy and X-ray microanalysis. A text for biologists, materials scientists, and geologists*. Plenum Publishing Corporation, 1981.

[79] R Joseph, JT & Fischer. Moisture removal from and liquefaction of Beulah Zap lignite. *Am. Chem. Soc. Div. Fuel Chem. Prepr*, pages 853–860, 1990.

[80] KS Vorres, R Kolman, and T Griswold. Kinetics of vacuum drying and rehydration of Illinois No. 6 coal samples: Implications for pore structure. Technical report, Argonne National Lab., IL (USA), 1988.

[81] Eric M. Suuberg, Yoshinobu Otake, Yongseung Yun, and Seetharama C. Deevi. Role of moisture in coal structure and the effects of drying upon the accessibility of coal structure. *Energy & Fuels*, 7(3):384–392, 1993. doi: 10.1021/ef00039a009. URL `http://dx.doi.org/10.1021/ef00039a009`.

[82] JA Pajares and Juan MD Tascón. *Coal Science*. Elsevier, 1995.

[83] GA Norton, WE Straszheim, KA Younkin, and R Markuszewski. Direct determination of organic oxygen in coal using scanning electron microscopy with wavelength-dispersive X-ray analysis. *Am. Chem. Soc., Div. Gas Fuel Chem., Prepr.*, 31(CONF-860425-), 1986.

[84] Alexis Volborth, GE Miller, PA Jerabek, and CK Garner. Oxygen determination and stoichiometry of some coals. In *Division of Fuel Chemistry, American Chemical Society Meeting, Chicago, Illinois*, 1977.

[85] Norbert Berkowitz. The chemistry of coal. *Elsevier Science Pub. Inc., New York, NY*, 1985.

[86] Martin L Gorbaty, John W Larsen, and Irving Wender. *Coal science*, volume 2. Academic Press, 1984.

[87] Zhigang Wu, Ryan P Rodgers, and Alan G Marshall. ESI FT-ICR mass spectral analysis of coal liquefaction products. *Fuel*, 84(14):1790–1797, 2005.

[88] David W Staubs, Ronald L Miller, Howard F Silver, and Robert J Hurtubise. The effect of solvent on solvent refined coal denitrification. *Industrial & Engineering Chemistry Process Design and Development*, 18(4):667–671, 1979.

[89] GF Morrison. Chemical desulfurization of coal. *IEA Coal Research, London*, pages 43–45, 1981.

[90] ME Fleet. Structurat aspects of tfie marcasite-pyrite transfortvtation. *The Canadian Mineralogist*, 10, 1970.

[91] SK Bhargava, A Garg, and ND Subasinghe. In situ high-temperature phase transformation studies on pyrite. *Fuel*, 88(6):988–993, 2009.

[92] Pedro A Montano, Arun S Bommannavar, and Vipul Shah. Mössbauer study of transformations of pyrite under conditions of coal liquefaction. *Fuel*, 60(8): 703–711, 1981.

[93] JM Lambert Jr, PL Walker Jr, AJ Perrotta, JP McCullough, and H Beuther. Physical characterization and pressure−temperature microscopy of the pyritepyrrhotite transformation. *Fuel*, 62(12):1474–1480, 1983.

[94] George W Gokel. *Dean's handbook of organic chemistry*, volume 71375937. McGraw-Hill New York, 2004.

[95] JoséV Ibarra, Edgar Munoz, and Rafael Moliner. FTIR study of the evolution of coal structure during the coalification process. *Organic Geochemistry*, 24 (6):725–735, 1996.

[96] M Cloke, A Gilfillan, and E Lester. The characterization of coals and density separated coal fractions using FTIR and manual and automated petrographic analysis. *Fuel*, 76(13):1289–1296, 1997.

[97] T Yoshida, T Takanohashi, K Sakanishi, I Saito, M Fujita, and K Mashimo. The effect of extraction condition on HyperCoal production (1)under room-temperature filtration. *Fuel*, 81(11):1463–1469, 2002.

[98] Christian Menno Müller, Bobby Pejcic, Lionel Esteban, Claudio Delle Piane, Mark Raven, and Boris Mizaikoff. Infrared attenuated total reflectance spectroscopy: An innovative strategy for analyzing mineral components in energy relevant systems. *Scientific reports*, 4, 2014.

[99] DK Sharma and SK Singh. Advanced process for the production of clean coal by chemical leaching technique. *Energy sources*, 17(4):485–493, 1995.

[100] MD Guillén, MJ Iglesias, A Dominguez, and CG Blanco. Semi-quantitative FTIR analysis of a coal tar pitch and its extracts and residues in several organic solvents. *Energy & Fuels*, 6(4):518–525, 1992.

[101] O Ruau, P Landais, R Michels, and E Langlois. Evaluation of organic matter reactivity during pyrolysis by Micro-FTIR techniques. In *Preprints of Symposia-Divison of Fuel Chemistry American Chemical Society*, volume 42, pages 164–167, 1997.

[102] Isabel Suárez-Ruiz and John C Crelling. *Applied coal petrology: the role of petrology in coal utilization*. Academic Press, 2008.

[103] Wilfrid Francis. *Coal: its formation and composition*. E. Arnold, 1961.

[104] John Landers, Gennady Yu Gor, and Alexander V Neimark. Density functional theory methods for characterization of porous materials. *Colloids and Surfaces A: Physicochemical and Engineering Aspects*, 437:3–32, 2013.

[105] Christian M Lastoskie and Keith E Gubbins. Characterization of porous materials using density functional theory and molecular simulation. *Studies in Surface Science and Catalysis*, 128:41–50, 2000.

[106] J Garrido, A Linares-Solano, JM Martin-Martinez, M Molina-Sabio, Francisco Rodriguez-Reinoso, and R Torregrosa. Use of nitrogen vs. carbon dioxide in the characterization of activated carbons. *Langmuir*, 3(1):76–81, 1987.

[107] K Lee Smith. *The structure and reaction processes of coal*. Springer, 1994.

[108] SK Bhatia. Reactivity of chars and carbons: New insights through molecular modeling. *AIChE journal*, 44(11):2478–2493, 1998.

[109] Richard C. Neavel. Liquefaction of coal in hydrogen-donor and non-donor vehicles. *Fuel*, 55(3):237 – 242, 1976. ISSN 0016-2361. doi: http://dx.doi.org/10.1016/0016-2361(76)90095-8. URL `http://www.sciencedirect.com/science/article/pii/0016236176900958`.

[110] Larry Thomas. *Coal geology*. John Wiley & Sons, 2012.

[111] Christopher Higman and Maarten Van der Burgt. *Gasification*. Gulf professional publishing, 2011.

[112] PE Best, PR Solomon, MA Serio, EM Suuberg, WR Mott Jr, and R Bassilakis. Relationship between char reactivity and physical and chemical structural features. *Prepr. Pap., Am. Chem. Soc., Div. Fuel Chem.;(United States)*, 32 (CONF-870802-), 1987.

[113] Kouichi Miura, Kenji Hashimoto, and Peter L Silveston. Factors affecting the reactivity of coal chars during gasification, and indices representing reactivity. *Fuel*, 68(11):1461–1475, 1989.

[114] Robert H Essenhigh and Ann M Mescher. Influence of pressure on the combustion rate of carbon. In *Symposium (International) on Combustion*, volume 26, pages 3085–3094. Elsevier, 1996.

[115] James T Ashu, Nsakala Ya Nsakala, Om P Mahajan, and Philip L Walker Jr. Enhancement of char reactivity by rapid heating of precursor coal. *Fuel*, 57 (4):250–251, 1978.

[116] S Dutta, CY Wen, and RJ Belt. Reactivity of coal and char. 1. in carbon dioxide atmosphere. *Industrial & Engineering Chemistry Process Design and Development*, 16(1):20–30, 1977.

[117] André D Engelbrecht, Brian C North, and Trevor D Hadley. Clean coal technology: Gasification of South African coals. In *Science Real and Relevant: 2nd CSIR Biennial Conference*, 2008.

[118] Supaporn Sawettaporn, Kunchana Bunyakiat, and Boonyarach Kitiyanan. CO_2 gasification of Thai coal chars: Kinetics and reactivity studies. *Korean journal of chemical engineering*, 26(4):1009–1015, 2009.

[119] K Raghunathan and Ray YK Yang. Unification of coal gasification data and its applications. *Industrial & Engineering Chemistry Research*, 28(5):518–523, 1989.

[120] Lawrence J Shadle, David A Berry, and Madhava Syamlal. Coal conversion processes, gasification. *Kirk-Othmer Encyclopedia of Chemical Technology*, 2002.

[121] Raymond C Everson, Hein WJP Neomagus, Henry Kasaini, and Delani Njapha. Reaction kinetics of pulverized coal-chars derived from inertinite-rich coal discards: gasification with carbon dioxide and steam. *Fuel*, 85(7): 1076–1082, 2006.

[122] Alejandro Molina and Fanor Mondragon. Reactivity of coal gasification with steam and CO_2. *Fuel*, 77:1831–1839, 1998.

[123] PL Walker Jr, OP Mahajan, and Richard Yarzab. Unification of coal char gasification reactions. *Am. Chem. Soc., Div. Fuel Chem., Prepr.;(United States)*, 22(CONF-770301-P2), 1977.

[124] CY Wen and S Dutta. Rates of coal pyrolysis and gasification reactions. *In: Coal conversion technology.(A79-53776 24-44) Reading, Mass., Addison-Wesley Publishing Co., Inc., 1979, p. 57-170.*, 1:57–170, 1979.

[125] Robert G Jenkins, Satyendra P Nandi, and Philip L Walker Jr. Reactivity of heat-treated coals in air at 500 c. *Fuel*, 52(4):288–293, 1973.

[126] G Skodras and GP Sakellaropoulos. Mineral matter effects in lignite gasification. *Fuel processing technology*, 77:151–158, 2002.

[127] Yanqin Huang, Xiuli Yin, Chuangzhi Wu, Congwei Wang, Jianjun Xie, Zhaoqiu Zhou, Longlong Ma, and Haibin Li. Effects of metal catalysts on CO_2 gasification reactivity of biomass char. *Biotechnology advances*, 27(5):568–572, 2009.

[128] RH Hurt, AF Sarofim, and JP Longwell. The role of microporous surface area in the gasification of chars from a sub-bituminous coal. *Fuel*, 70(9):1079–1082, 1991.

[129] Bo Feng and Suresh K Bhatia. On the validity of thermogravimetric determination of carbon gasification kinetics. *Chemical engineering science*, 57(15): 2907–2920, 2002.

[130] Sabri Ergun. Kinetics of the reaction of carbon with carbon dioxide. *The Journal of Physical Chemistry*, 60(4):480–485, 1956.

[131] MV Gil, J Riaza, L Álvarez, C Pevida, JJ Pis, and F Rubiera. Oxy-fuel combustion kinetics and morphology of coal chars obtained in N_2 and CO_2 atmospheres in an entrained flow reactor. *Applied Energy*, 91(1):67–74, 2012.

[132] S.A. Arrhenius. Über die dissoziationswärme und den einfluss der temperatur auf den dissociationsgrad der elektrolyte. *Zeitschrift für anorganische und allgemeine Chemie*, 4:96–116, 1889.

[133] SK Bhatia and DD Perlmutter. A random pore model for fluid-solid reactions: I. Isothermal, kinetic control. *AIChE Journal*, 26(3):379–386, 1980.

[134] S Kasaoka, Y Sakata, and C Tong. Kinetic evaluation of the reactivity of various coal chars for gasification with carbon dioxide in comparison with steam. *Int. Chem. Eng.;(United States)*, 25(1), 1985.

[135] Martyna Tomaszewicz, Grzegorz Łabojko, Grzegorz Tomaszewicz, and Michalina Kotyczka-Morańska. The kinetics of CO_2 gasification of coal chars. *Journal of Thermal Analysis and Calorimetry*, 113(3):1327–1335, 2013.

[136] James G Speight. *Coal-fired power generation handbook*. John Wiley & Sons, 2013.

[137] Stephen R Turns et al. *An introduction to combustion*, volume 287. McGraw-hill New York, 1996.

[138] Robert H Hurt and Joseph M Calo. Semi-global intrinsic kinetics for char combustion modeling. *Combustion and flame*, 125(3):1138–1149, 2001.

[139] SG Chen, RT Yang, F Kapteijn, and JA Moulijn. A new surface oxygen complex on carbon: toward a unified mechanism for carbon gasification reactions. *Industrial & Engineering Chemistry Research*, 32(11):2835–2840, 1993.

[140] H-Y Cai, AJ Güell, I Netal Chatzakis, J-Y Lim, DR Dugwell, and R Kandiyoti. Combustion reactivity and morphological change in coal chars: Effect of pyrolysis temperature, heating rate and pressure. *Fuel*, 75(1):15–24, 1996.

[141] S Dutta and CY Wen. Reactivity of coal and char. 2. In oxygen-nitrogen atmosphere. *Industrial & Engineering Chemistry Process Design and Development*, 16(1):31–37, 1977.

[142] Maryam Gharebaghi, Robin M. Irons, Mohamed Pourkashanian, and Alan Williams. An investigation into a carbon burnout kinetic model for oxycoal combustion. *Fuel Processing Technology*, 92(12):2455 – 2464, 2011. ISSN 0378-3820. doi: http://dx.doi.org/10.1016/j.fuproc.2011.08.015. URL `http://www.sciencedirect.com/science/article/pii/S0378382011003092`.

[143] G Liu, P Benyon, KE Benfell, GW Bryant, AG Tate, RK Boyd, DJ Harris, and TF Wall. The porous structure of bituminous coal chars and its influence on combustion and gasification under chemically controlled conditions. *Fuel*, 79(6):617–626, 2000.

[144] Jian-Liang Zhang, Guang-Wei Wang, Jiu-Gang Shao, and Hai-Bin Zuo. A modified random pore model for the kinetics of char gasification. *BioResources*, 9(2):3497–3507, 2014.

[145] Violeta Artos and Alan W Scaroni. Tga and drop-tube reactor studies of the combustion of coal blends. *Fuel*, 72(7):927–933, 1993.

[146] Robert H Perry, DW Green, and JO Maloney. Perry's handbook of chemical engineering. *Perry's Handbook of Chemical Engineering*, 1997.

[147] Ken B Anderson, John C Crelling, Willianm W Hugget, Derek Perry, Tom Fullinghim, Patrick McGill, and Paul Kaelin. Oxidative hydrothermal dissolution (OHD) of coal and biomass. *Fuel*, 2(2), 2011.

Appendix A

OXIDATIVE HYDROTHERMAL TREATMENT OF COAL LIQUEFACTION RESIDUE

1.1 INTRODUCTION

Coal residue is a complex network comprising organic and inorganic matrix. The organic matrix is mainly composed of an ordered aromatic carbon structure. Thus rupture of the aromatic network will yield lighter compounds. Solubilization of organic matrix under high temperature and pressure conditions in sub-critical water was the outcome on reaction of coal with molecular oxygen [147]. Thus, a similar mechanism was tested to investigate the fate of the residue in an oxidative hydrothermal dissolution reaction.

The residues had poor solubilization in oxygen at lower temperatures. An attempt to conduct the reaction at higher temperatures was unsuccessful due to the failure of one of the reactors which further led to injury of the student. Various reasons for the failure which were speculated have been discussed. Future experiments of this kind should be conducted on the completion of the steps necessary to avoid any catastrophic incident.

1.2 EXPERIMENTAL METHOD

1.2.1 RAW MATERIALS

Two major raw materials for the process were RES 450 and dil. H_2O_2 solution. Please refer Chapter 4 for Res 450 material properties. A 30 wt.% H_2O_2 solution received from Sigma Aldrich diluted to 0.5 M solution was employed for the process.

1.2.2 EQUIPMENT

A micro-reactor setting held in a square-plate holder was fixed to the motor shaft extension and placed in a sand bath. Four of each micro-reactor were high-quality, fully annealed Type 316-Stainless Steel(SS) tubing from Swagelok, EN ISO 1127 or equivalent. The tubing had 3/4th inch outer diameter with a wall thickness of about 0.049 inch. The maximum allowable working pressure for these tubes were reported to be close to 7000 psig. A 1/8th tubing of Type 316-SS tubing was connected to the head of the micro-reactor tube sealed with Swagelok fittings and ball valve. A K-type thermocouple was connected to one of the micro-reactors to measure the temperature of the reactor. A fluidized sandbath SBS-4 from Techne connected with a TCS (temperature control system) was employed. Air with a maximum pressure of upto 5 atm was used as the fluidization medium.

1.2.3 PROCEDURE

Three micro-reactors were filled with 5-10 ml of 0.5 M H_2O_2 and 100-500 mg of residue. After manually sealing the micro-reactors, a leak test using N_2 was carried out to ensure a leak-free operating system. The N_2 was then released through the outlet valve connected to the head of the 1/8th tubing of the reactor system. The fourth micro-reactor was connected to the thermocouple and kept blank throughout the run. It was also checked for leaks. A square-plate holder was employed which held the four micro-reactors securely. The desired temperature of the reaction is set using the TCS. The air flow for fluidization is turned on. The square plate is tightly secured to the motor shaft and the micro-reactors are inserted into the sandbath. The motor is turned on and the temperature is noted.

1.3 INCIDENT REPORT

The temperature of the reaction was set at 260 °C [147]. Since no dissolution of the residual material was observed at this temperature, the temperature was raised

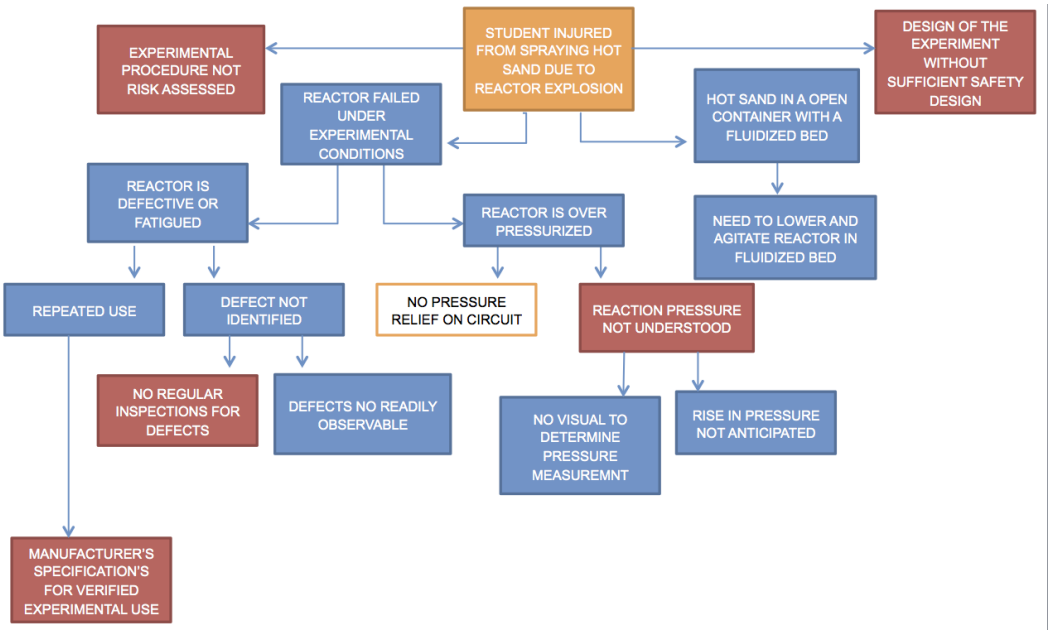

Figure 1.1: HAZOP study undertaken for the OHD process

to 350 °C. The reactors were used 4-5 times prior to the run upto 200 °C - 250 °C. A fluidized sand bath was at temperature close to 350 °C when the sealed and leak proof micro-reactors were placed inside the bath using a square plate holder. After placing the reactor, one of the screws of the square plate was secured. An attempt to tighten the other screw of the square plate was made, when one of the reactors cracked open. This caused a major spill of hot sand on the hands of the student working on it. The student was rushed to the hospital. Second degree burns were reported on the left and right wrist of the student. The sand bath collar was deformed. The safety slash, safety goggles and other necessary basic PPE saved the student from further injury.

1.4 SAFETY NOTE

An incident report had been filed with Environment, Health and Safety - University of Alberta. A HAZOP study (Hazard and Operability study) was carried out. The outcome of the study pointed out four major areas which required further work and assessment for future work to be continued in this area as shown in Fig. 1.1. The following steps have been undertaken addressing the issues involved with the process:

1. SOP has been documented for a reactor system handling organic solvents

(higher boiling point).

2. Preparation of a risk assessment on reactor system capable of handling aqueous system, in which, each step would be assessed prior to operation of experiment of this kind is in progress.

3. Set-up is placed in the walk-in fume hood with slashes provided at the top and bottom for safety. Fume hood is periodically tested for proper airflow.

4. Accommodation of pressure gauge for multiple reactor systems was difficult due to space restraints. However, pressure gauge has been installed in the single reactor systems.

5. For more precise and safety purposes, efforts are being made to attach a safety valve to the micro-reactor systems in the near future.

6. Current plans to install sand baths with enclosures at the top is in progress. However, since the commercial sand bath systems currently in manufacture, come in an open setting, attempts would be made to contact the manufacturer to discuss newer closed systems for safety concerns.

7. In previous experimental studies, employing organic solvents, vapour pressure at desired temperatures were observed (from literature).

8. For aqueous reaction systems (water), vapour pressure was calculated for water alone. Rise in pressure due to side reactions in presence of hydrogen peroxide was not understood properly.

9. Recently, a similar experiment was carried out at the Swagelok facility using hydrogen peroxide to understand the overall reaction pressure for the system and thus understand the necessary precursors to be considered in order for such an experiment to be carried out at our laboratory facility.

10. Since, the reactor set-ups employing organic solvents (used previously) were working efficiently for 5-6 runs, no defects were noticed on observation. No reactor testing facility is available in the department.

11. Now on, to assess the defects, we would visually inspect the reactors for cracks or deformations, if any (Given that was noticed in the reactor after the incident).

12. The estimated vapour pressure for the aqueous system was 2400 psi at 350 °C, which was much lower than the pressure limit for the reactors ($\sim$7600 psi).

13. Since the complex reaction mixture (water, hydrogen peroxide, coal residue containing mineral matter) was not completely understood, thus, the reaction pressure for the system was completely unknown.

14. Also, developing an experimental set-up with the employment of thicker walled reactor tubing is in progress.